Supporting Information

Mechanistic Studies of the TRIP Catalyzed Allylation With Organozinc Reagents

Peter E. Hartmann,[a,b] Mattia Lazzarotto,[a] Jakob Pletz,[a] Stefan Tanda,[c] Philipp Neu,[a] Walter Goessler,[c] Wolfgang Kroutil,[a] A. Daniel Boese*[b] and Michael Fuchs*[a]

[a] Msc. Peter E. Hartmann, Msc. Mattia Lazzarotto, Dr. Jakob Pletz, Dr. Philipp M. Neu, Prof. Wolfgang Kroutil, Dr. Michael Fuchs
Institute of Chemistry, Bioorganic and Organic Chemistry
University of Graz
Heinrichstrasse 28/II, 8010 Graz, Austria, Europe.
E-mail: michael.fuchs@uni-graz.at

[b] Msc. Peter E. Hartmann, Prof. A. Daniel Boese
Institute of Chemistry, Quantum Chemistry
University of Graz
Heinrichstrasse 28/II, 8010 Graz, Austria, Europe.
E-mail: adrian_daniel.boese@uni-graz.at

[c] Msc. Stefan Tanda, Prof. Walter Gössler,
Institute of Chemistry, Analytical Chemistry
University of Graz
Heinrichstrasse 28/II, 8010 Graz, Austria, Europe.

1. Table of contents

2. Experimental Part – Instrumentation, Spectra and Additional Tables

2.1. Instrumentation

^{1}H-, ^{13}C-, ^{31}P- and ^{11}B-NMR spectra were recorded on a Bruker AVANCE III 300 spectrometer (^{1}H: 300.13 MHz; ^{13}C: 75.47 MHz; ^{31}P: 121.49 MHz; ^{11}B: 96.29) with an autosampler. Chemical shifts were referenced to the residual proton and carbon signal of the deuterated solvent [$CDCl_3$: δ = 7.26 ppm (^{1}H), 77.16 ppm (^{13}C)]. Chemical shifts δ are given in ppm (parts per million) and coupling constants *J* in Hz (Hertz). Deuterated solvents for nuclear resonance spectroscopy were purchased from Roth.

Melting points were determined on a Gallenkamp MPD350.BM2.5 apparatus with an integrated microscopical support. They were measured in open capillary tubes with a mercury-in-glass thermometer and were not corrected.

IR-spectra were recorded neat on a Bruker Alpha-P (ATR) instrument.

The specific optical rotation was determined on a Perkin Elmer Polarimeter 341 with an integrated sodium vapor lamp. All samples were measured in $CHCl_3$ and CH_2Cl_2 (both were purchased from Sigma Aldrich, ACS specrophotometric grade, ≥99.8%) at the D-line of the sodium light (λ = 589 nm) under non-tempered conditions between 22 °C and 27 °C.

High resolution mass spectra were recorded on an Agilent 6230 TOF LC/MS using ESI (positive mode, capillary voltage 3.5 kV) or APCI (negative mode, 5.0 kV) methods.

Chiral HPLC analysis was performed on a Shimadzu HPLC system [DGU-20A (degasser), LC-20A (pump), SIL-20A (autosampler), CTO-20AC (column oven), SPD-M20A (detector), CBM-20AC (controller)] with *n*-heptane/2-PrOH as eluent using Daicel columns [dimension: 4.6 x 250 mm, 5 µm particle size, except Chiralpak AD (10 µm) and Chiralcel OJ (10 µm)] and conditions as specified below.

All GC-MS measurements were carried out with an Agilent 7890A GC system, equipped with an Agilent 5975C mass-selective detector (electron impact, 70 eV), a HP-5-MS column (30m x 0.25 mm x 0.25 µm film) and an Agilent 7697A headspace autosampler using He as carrier gas at a flow of 0.7 mL/min. The following temperature program was used in all GC-MS headspace measurements: initial temperature 40°C, hold for 5 min, 10 °C/min, to 200 °C. Headspace parameters: vial pressurization gas: He; loop size: 1 mL; transfer line: DB-ProSteel (0.53 mm diameter); oven temperature: 50°C; loop temperature: 55°C; transfer line: 60°C; vial equilibration time: 4 min; Injection duration: 0.5 min; vial size: 20 mL; vial shaking: level 5, 71 shakes per min with acceleration of 260 cm/s^2; fill pressure: 15 psi. Propene: t_{ret} = 1.78 min.

All GC-FID measurements were carried out on an Agilent 7890A GC system equipped with an Agilent HP-5 column (30m x 0.25 mm x 0.25 µm film) using He as carrier gas at a flow of 0.63 mL/min with following parameters: initial temperature 40°C, hold for 2 min, ramp 1: 10 °C/min, to 180°C, hold for 1 min, ramp 2: 20 °C/min, to 300°C, hold for 2 min.

2.2. Mechanistic Studies – NMR Spectra

*2.2.1. Studies of the reaction with zinc organyl reagents derived from **3** and **4**:*

As a substantial part of the NMR was obtained during the revision process, two different batches of dimethyl methylphosphonate (reference compound for the ^{31}P-NMR spectra) were used. The two batches only differ in the trace impurities of the ^{31}P-NMR spectra. In order to avoid misunderstandings, the NMR spectra of both batches are presented and the used batch is marked below the NMR spectra of the conducted experiments.

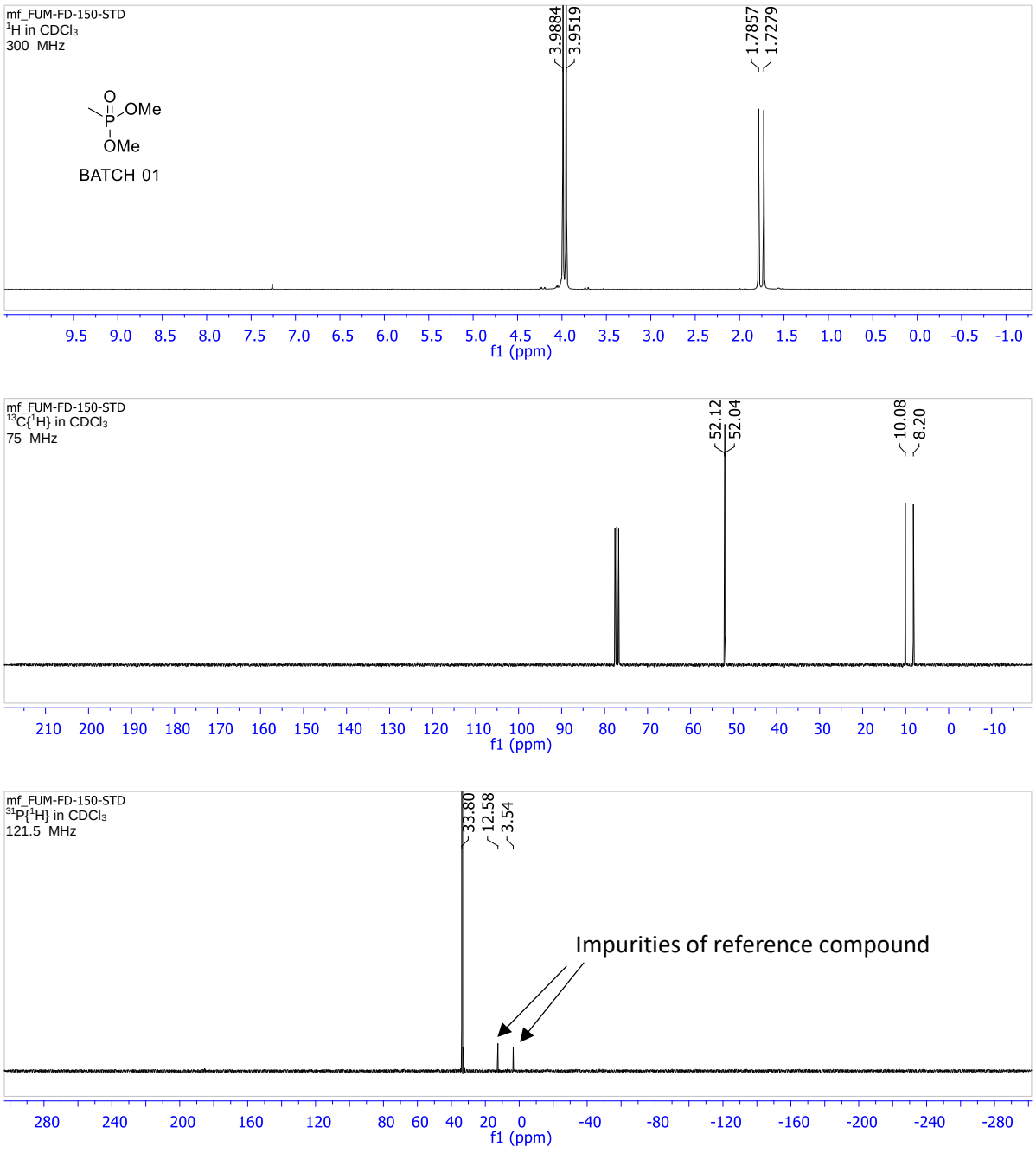

Fig SI01a. ^{1}H-, ^{13}C- and ^{31}P-NMR of dimethyl methylphosphonate (reference compound for ^{31}P-NMRs; BATCH 01).

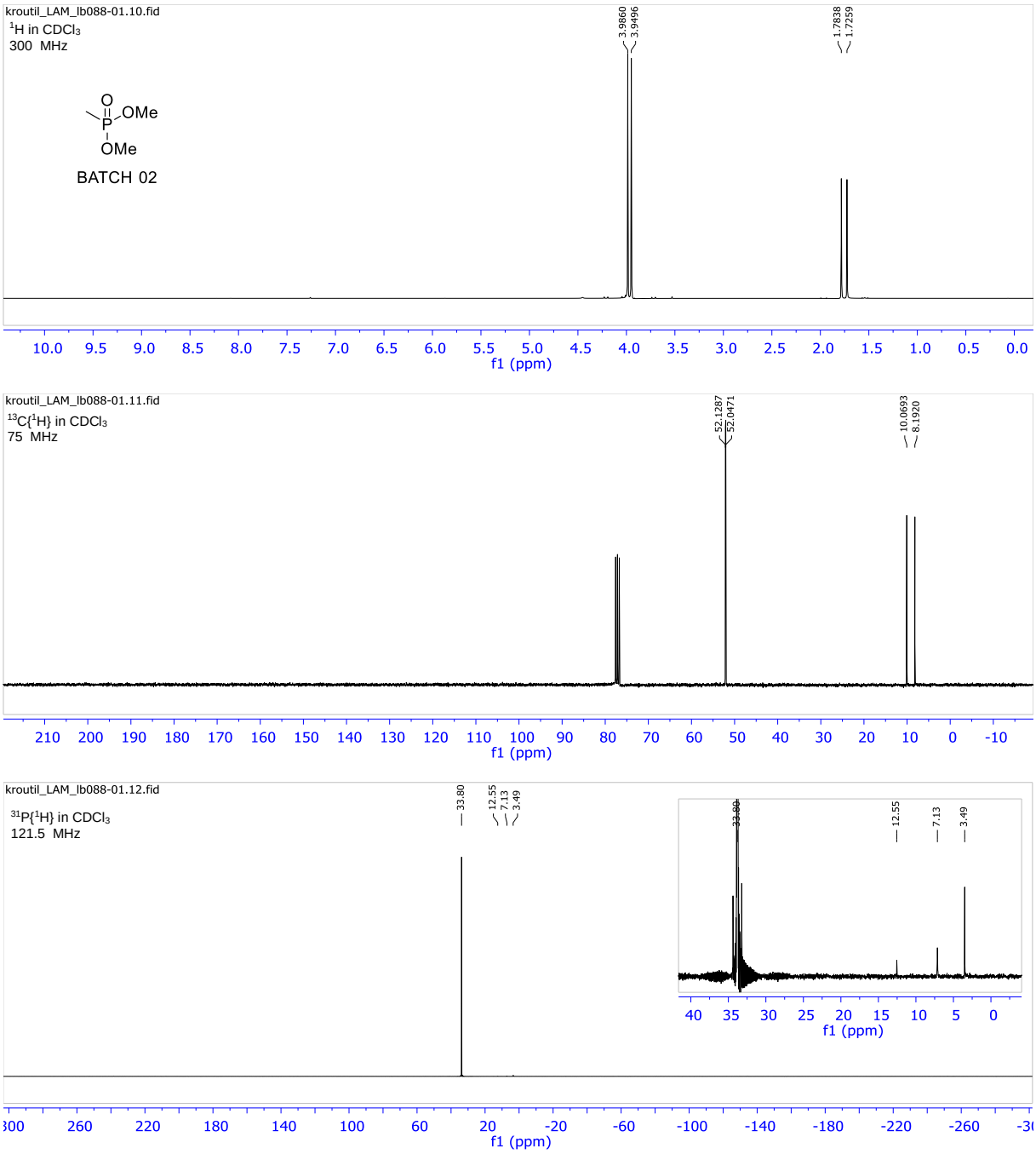

Fig SI01b. ^{1}H-, ^{13}C- and ^{31}P-NMR of dimethyl methylphosphonate (reference compound for ^{31}P-NMRs; BATCH 02).

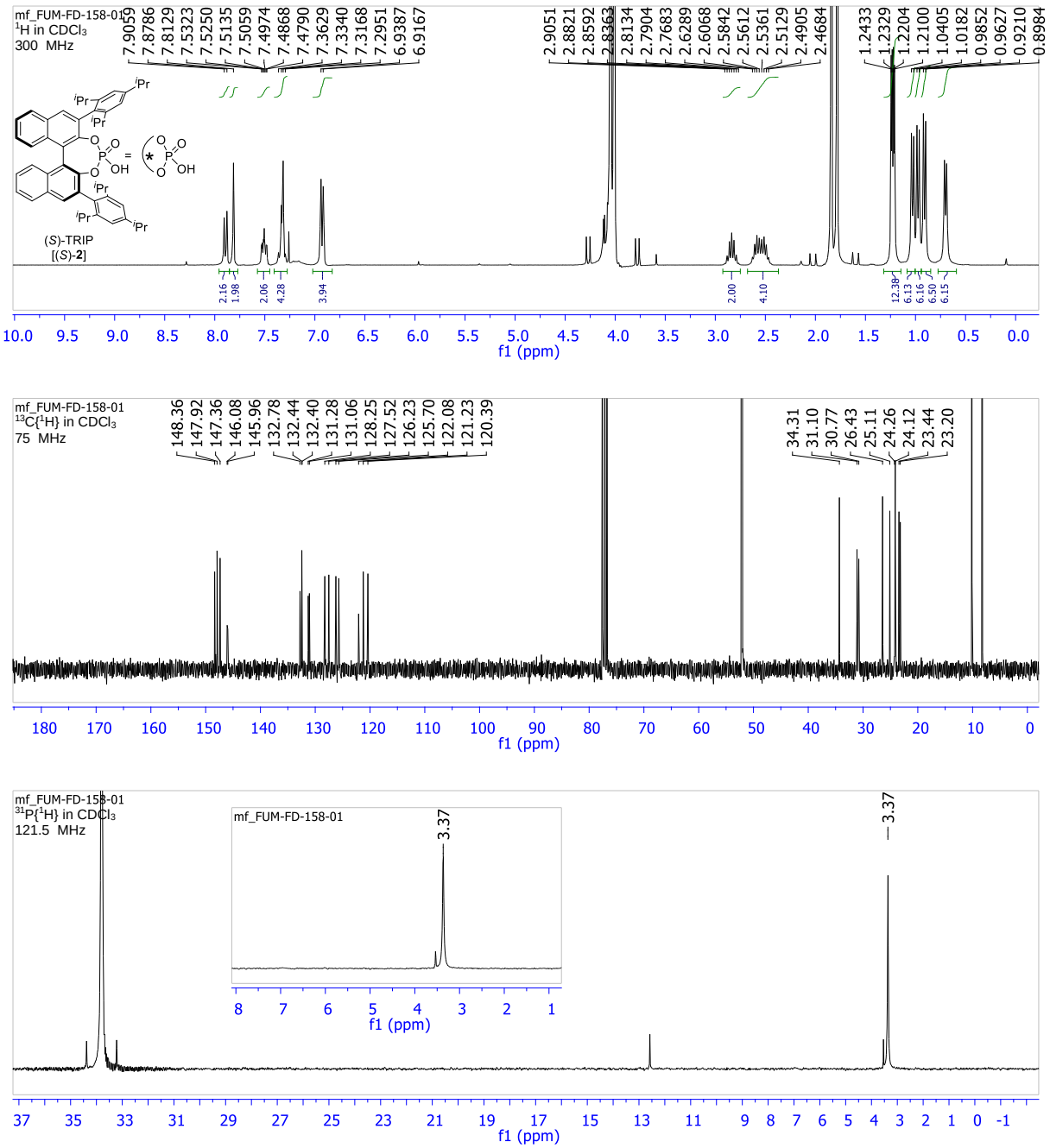

Fig SI02a. ^{1}H-, ^{13}C- and ^{31}P-NMR of TRIP [**2**, + reference compound (BATCH 01)].

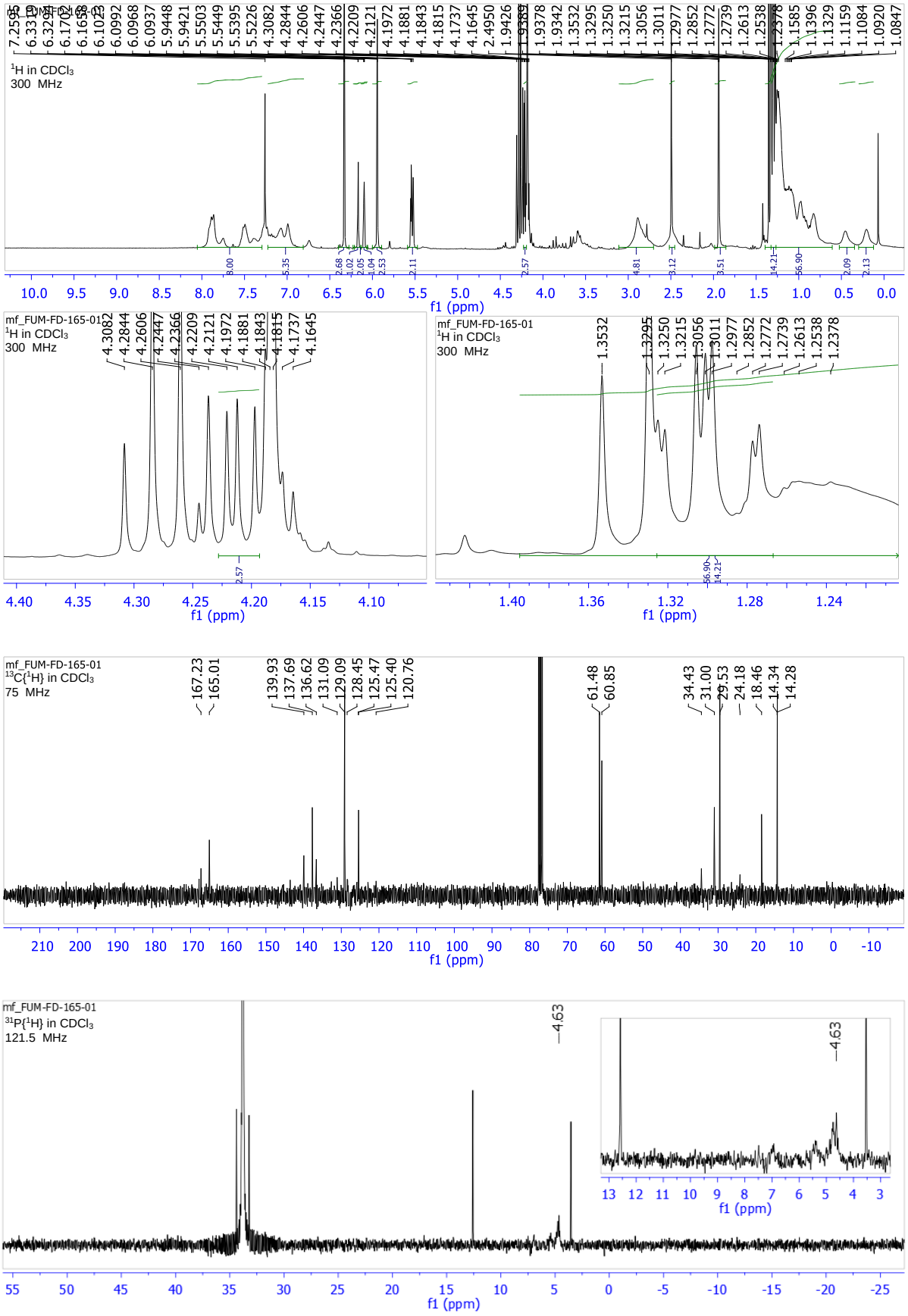

Fig SI02b. ^{1}H- (including expansion of O<u>*CH*$_2$</u> signal showing additional peaks, and OCH$_2$<u>*CH*$_3$</u> signal showing a second set of peaks as a dt), ^{13}C- and ^{31}P-NMR of (*S*)-TRIP (**2**) in the presence of zinc reagent

4 [assumend structure **8a** + reference compound (BATCH 01)]. Note: No NOEs between (*S*)-TRIP and the reagent were found in the NOESY experiment (data not shown).

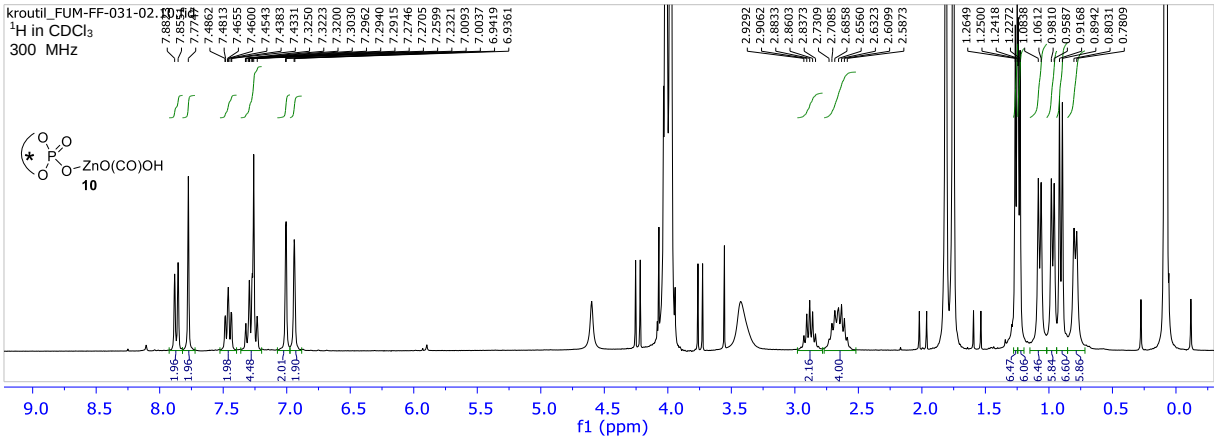

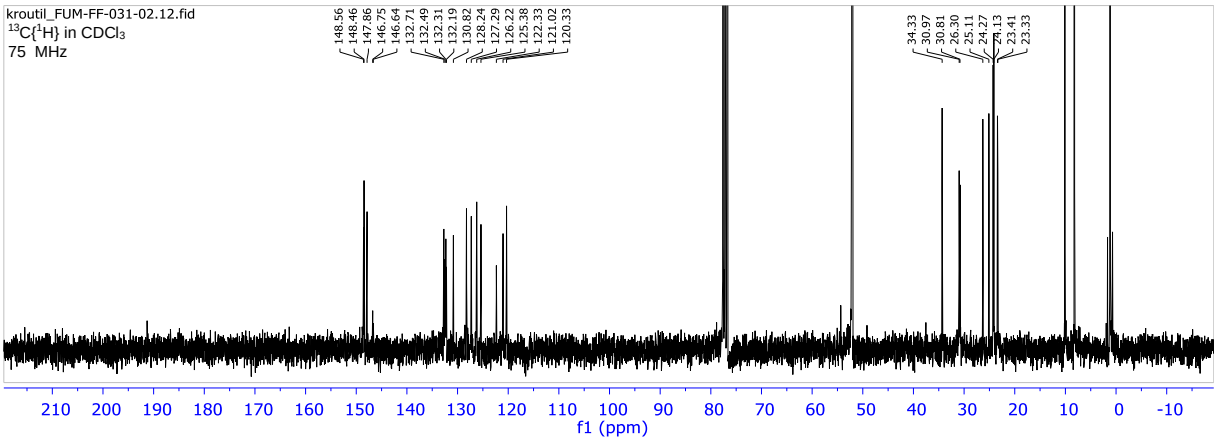

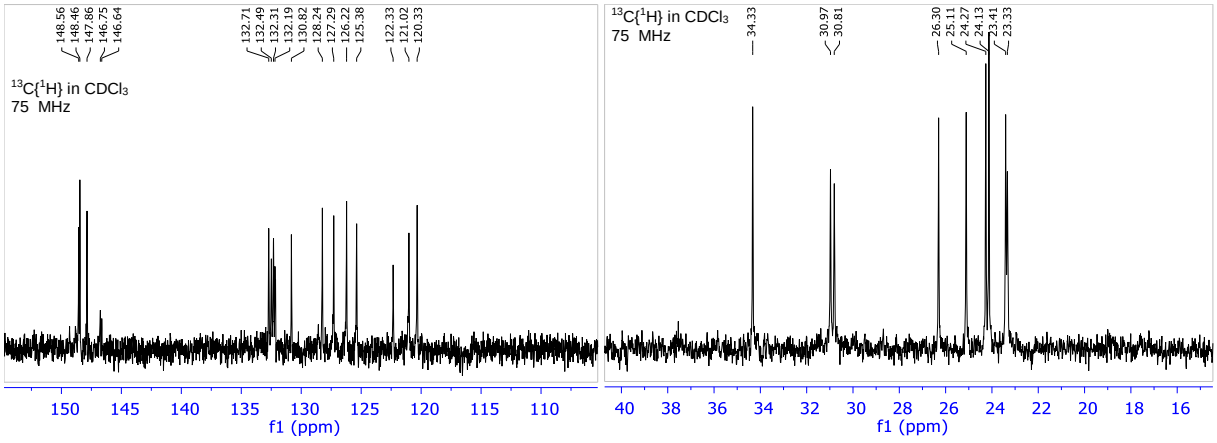

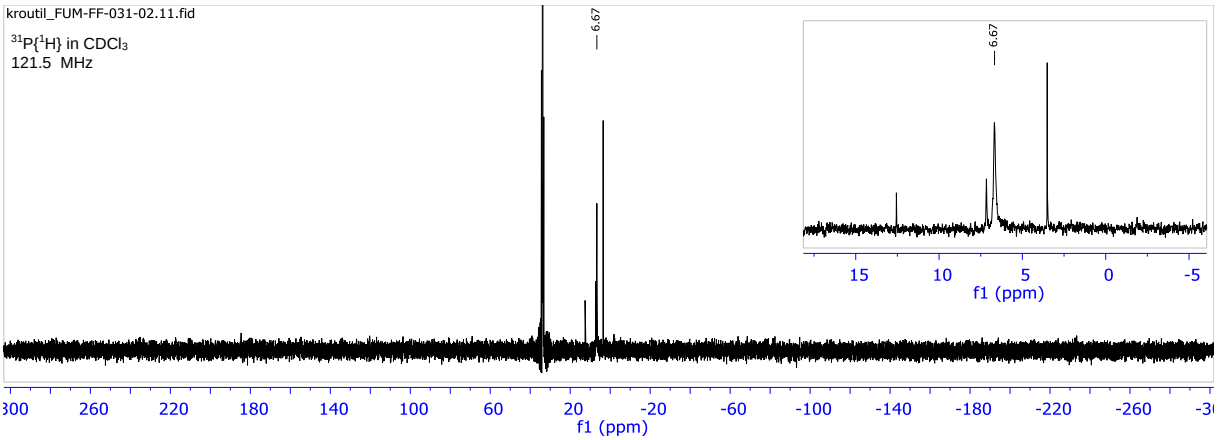

Figure SI02c. ^{1}H-, ^{13}C- and ^{31}P-NMR of zinc phosphate salt **10** [**10** + reference compound (BATCH 02)].

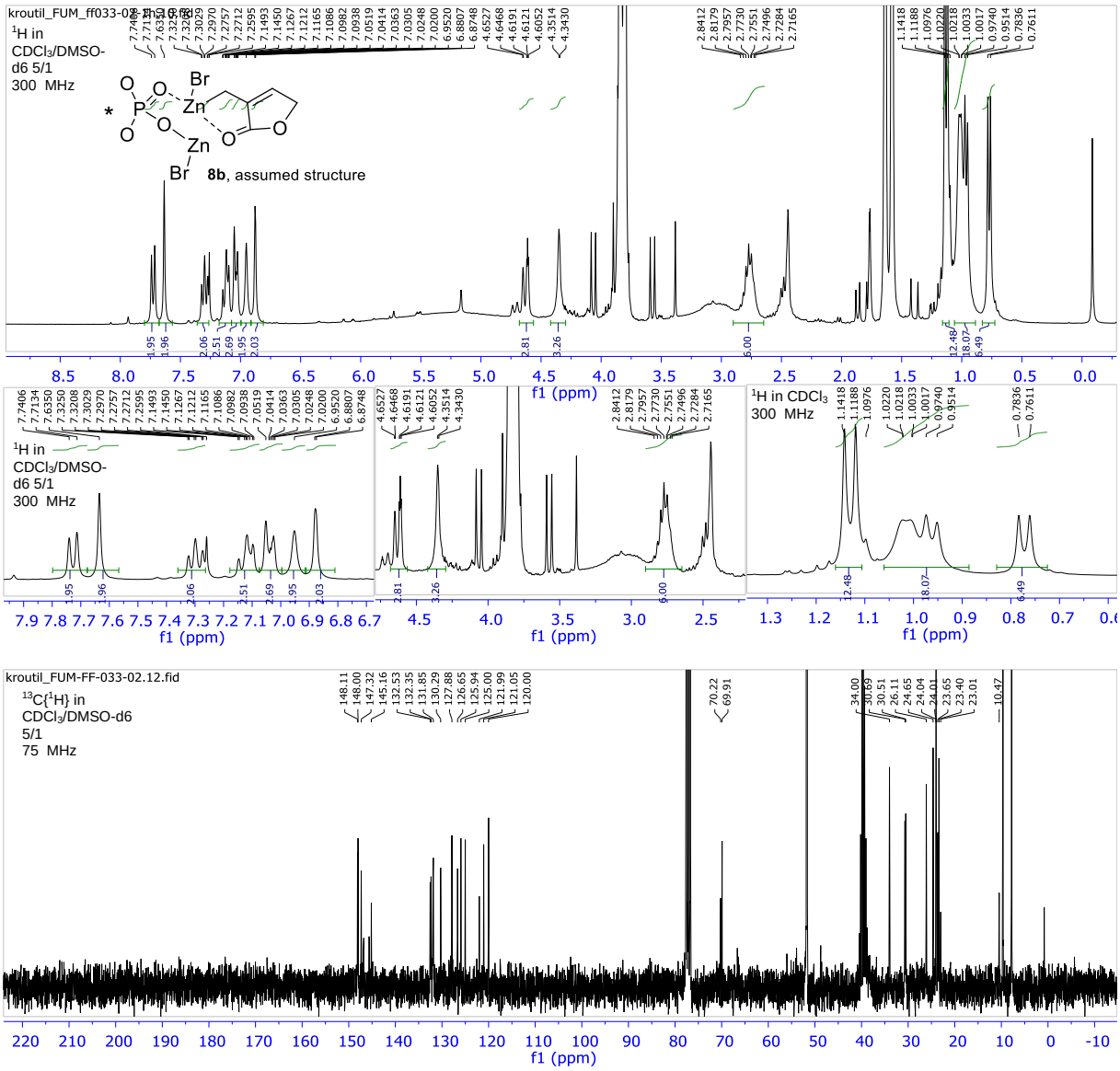

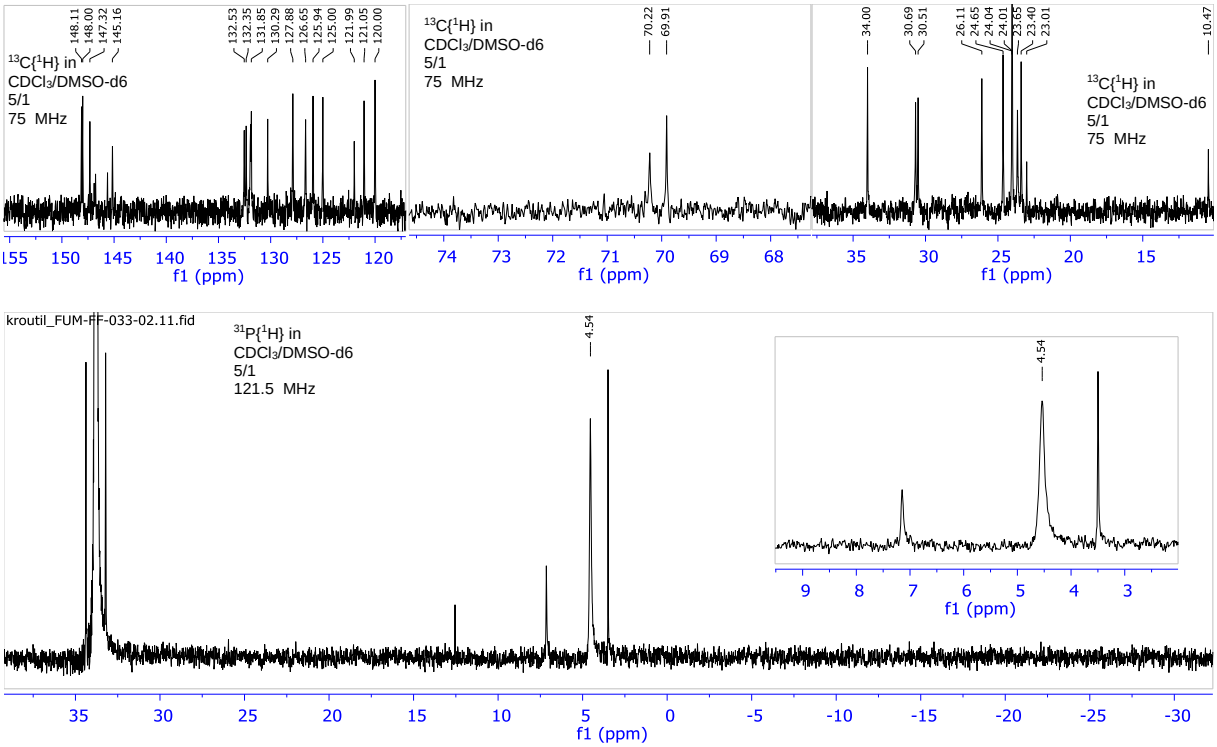

Figure SI02d. ^{1}H-, ^{13}C- and ^{31}P-NMR of the reaction mixture forming the zinc phosphate complex of assumed structure **8b** [includes the ^{31}P-reference compound (BATCH 02)].

2.3. Time study of the zinc insertion reaction forming reagent **9.**

Table SI01a. Conversion of **3** into reagent **9** over time

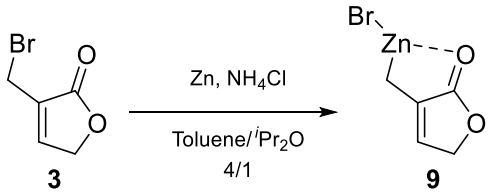

Entry	Reaction time [h]	Amount [%][a,b]		Peak area [ ][a]	
		3	**9**	**3**	**9**
1	0	100	0	-	-
2	0.5	84.0	16.0	1345.9	258.7
3	2	79.1	20.9	1094.8	353.1
4	4	72.2	27.8	1180.3	717.9
5	23	16.1	83.9	127.3	3102.8

[a] … determined via GC-FID analysis and peak area integration of the obtained chromatograms; [b] … mol-% of compound compared to overall concentration of lactone product (**9**) and starting material **3**.

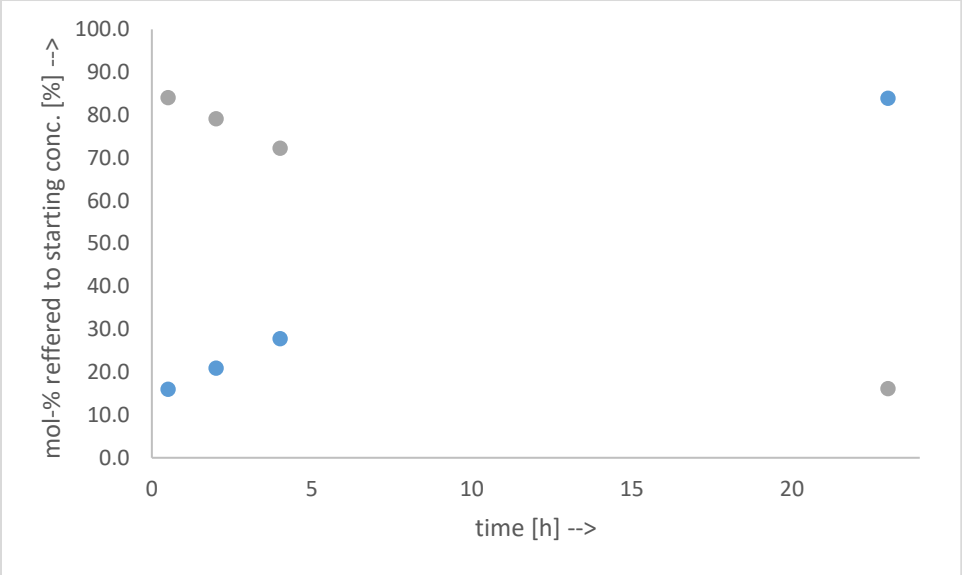

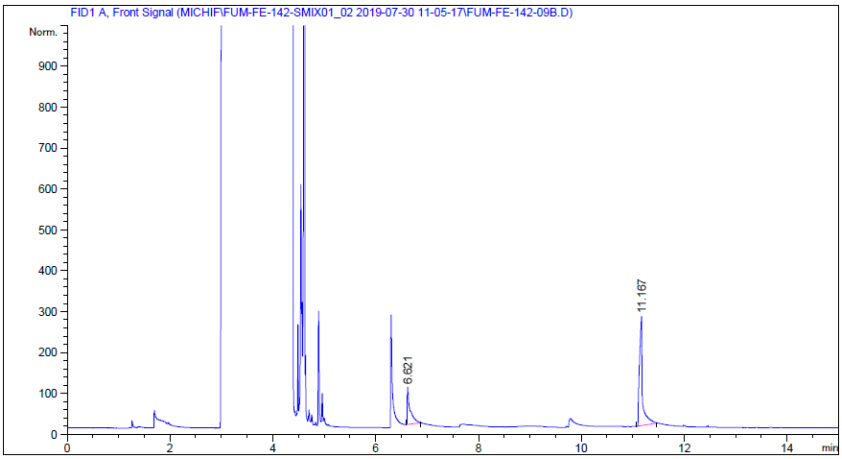

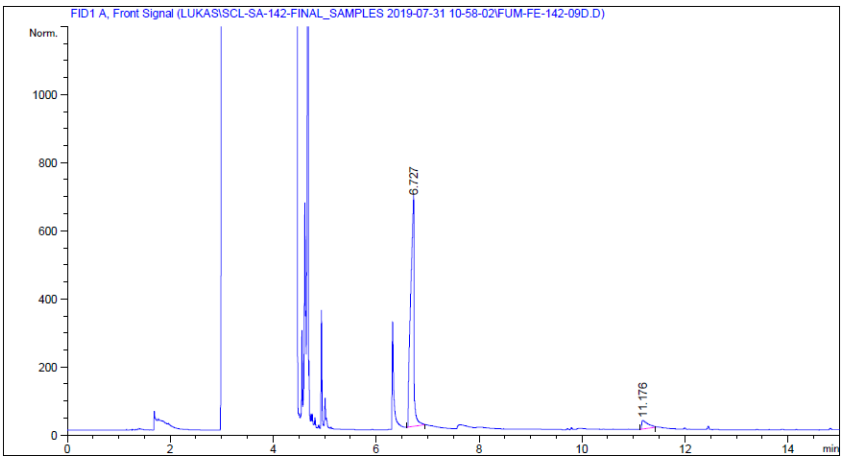

Fig. SI03. Top: Amounts of **3** (grey dots) and **9** (blue dots) over time; middle: example chromatogram after 2 h; bottom example chromatogram after 23 h.

2.4. Time study of the catalytic reaction with regard to the accumulation of **9** over time.

Table SI01b. Conversion of **3** into reagent **9** and product **SI01** over time

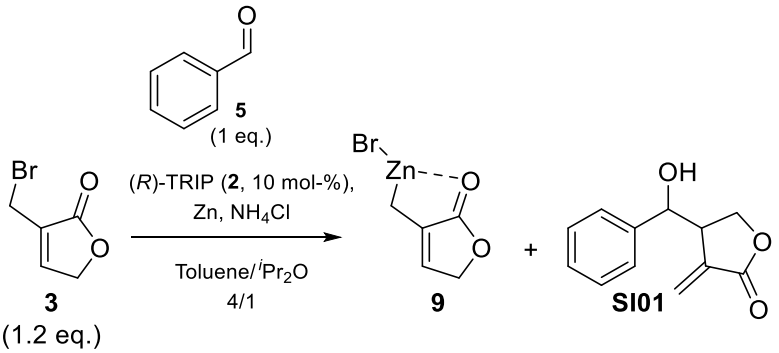

Entry	Reaction time [h]	Amount [%][a,b]			Peak area [ ][a]		
		3	**9**	**SI01**	**3**	**9**	**SI01**
1	0	100	0	0	-	-	-
2	0.5	44.9	5.9	49.2	1211.8	48	660.3
3	2	38.3	7.6	54.1	1198.5	231.4	856.7
4	4	23.3	7.4	69.3	849.7	336.2	1386.3
5	23	<1	15.9	84.1	<1	1670.2	2417.3

[a] … determined via GC-FID analysis and peak area integration of the obtained chromatograms; [b] … mol-% of compound compared to overall concentration of lactone products (**9** and **SI01**) and starting material **3**.

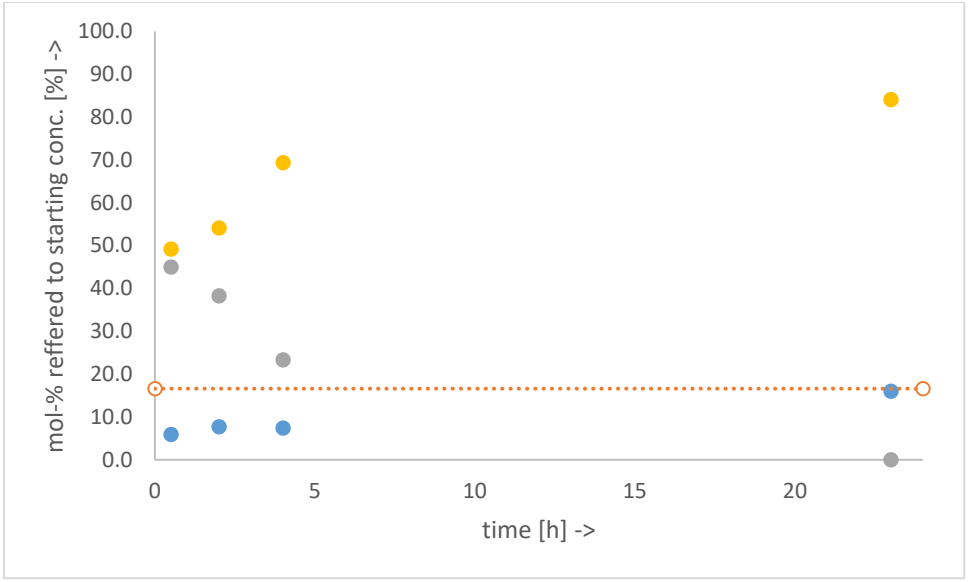

Fig. SI04. Top: Amounts of **3** (grey dots), **9** (blue dots) and **SI01** (orange dots) over time. The orange line indicates the maximum level of compound **9**, which is allowed in order to support the argument from the main text (see paragraph "*comparison to the uncatalyzed reaction*"). The level consists of 10% of quenched reagent by the acid proton of the catalyst and 10% of resting state **B1** or **ed1**$_a$, respectively. This sums up to 20%, but as 1.2 eq. of starting material **3** are used, this 20% need to be divided by that factor yielding 16.7%; middle: example chromatogram after 2 h; bottom: example chromatogram after 23 h.

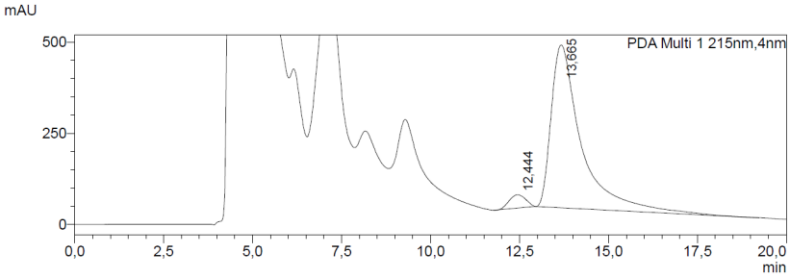

PDA Ch1 215nm

Peak#	Ret. Time	Name	Area	Height	Area%
1	12,444		1169674	36276	4,248
2	13,665		26366459	446493	95,752
Total			27536133	482769	100,000

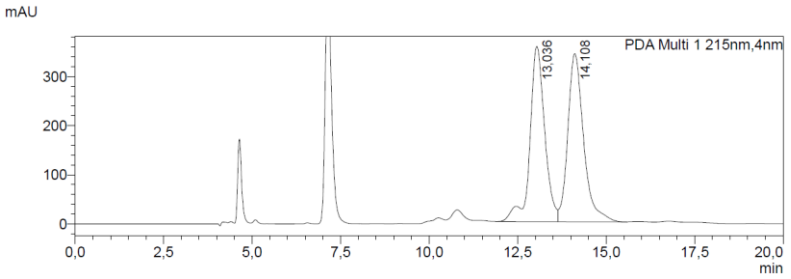

PDA Ch1 215nm

Peak#	Ret. Time	Name	Area	Height	Area%
1	13,036		10396701	356518	49,422
2	14,108		10639754	342099	50,578
Total			21036455	698617	100,000

Fig. SI05a. Top: HPLC chromatogram of crude **SI01** after 23 h reaction time on a chiral stationary phase; bottom: HPLC chromatogram of racemic reference of **SI01** on a chiral stationary phase.

The final ee of 92% demonstrates that >90% of the formed product underwent the catalytic process.

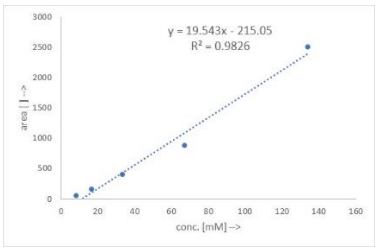

Calibration **3**

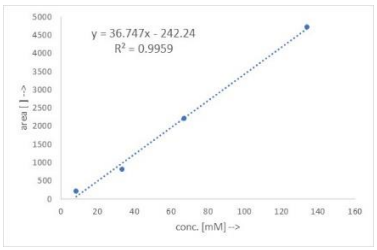

Calibration of quenched **9**

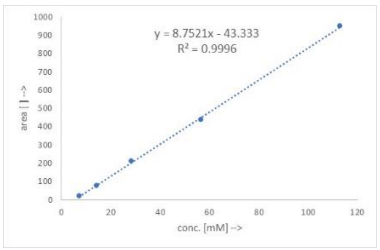

Calibration **SI02**

Fig. SI05b. Calibration Curves for **3**, quenched **9** and **SI01** (GC-FID analysis)

2.5. GC-MS headspace measurements for the indirect detection of the zinc phosphate salt of **2**

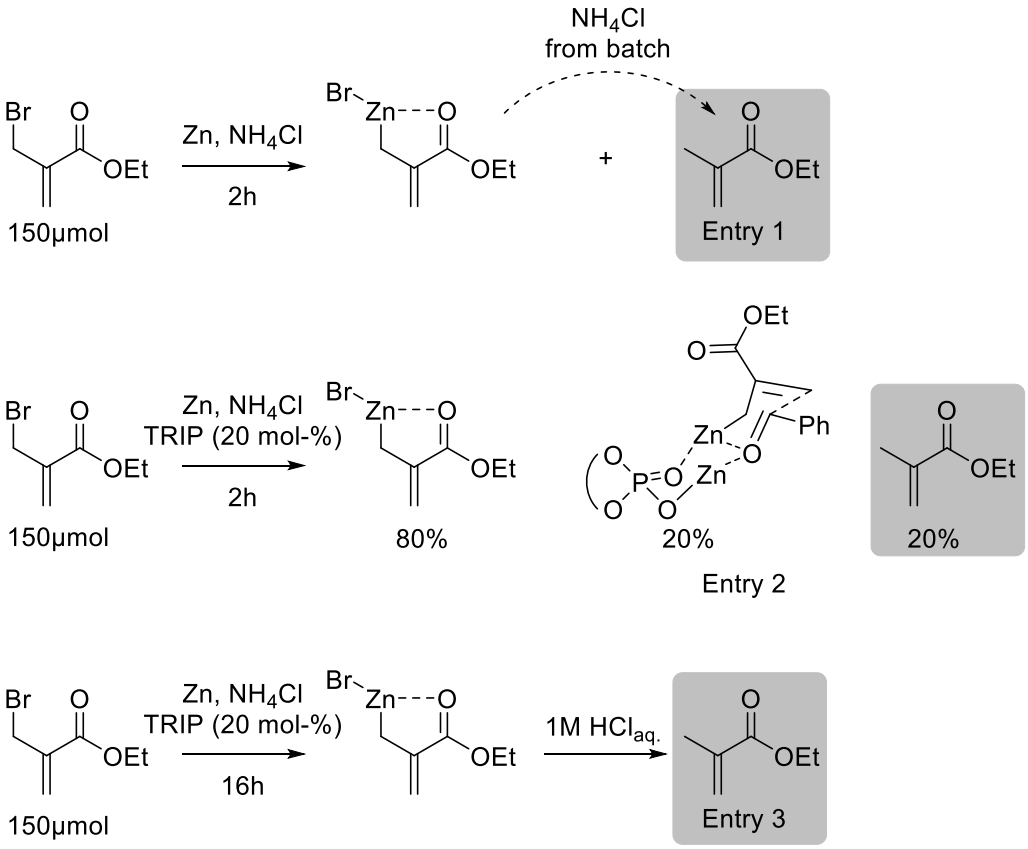

Figure SI06. Measured GC-MS headspace samples

Table SI02. GC-MS headspace results

Entry	Area [ ]	µmol/sample[a]	Mol-% referred to starting material
Control	n.d.	< detection limit	< detection limit
1	11406575	6	4%
2	91082096	46	31%
3	211492699	99	66%

n.d. … not detected; control: starting material in CH_2Cl_2. [a] determined via peak area integration and calibration curve.

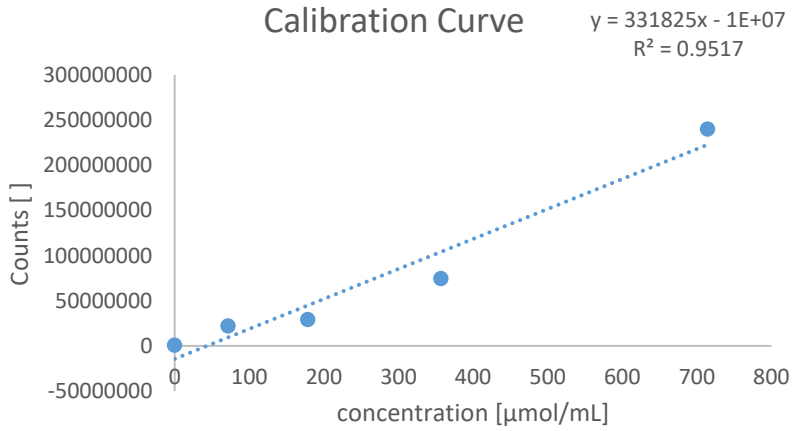

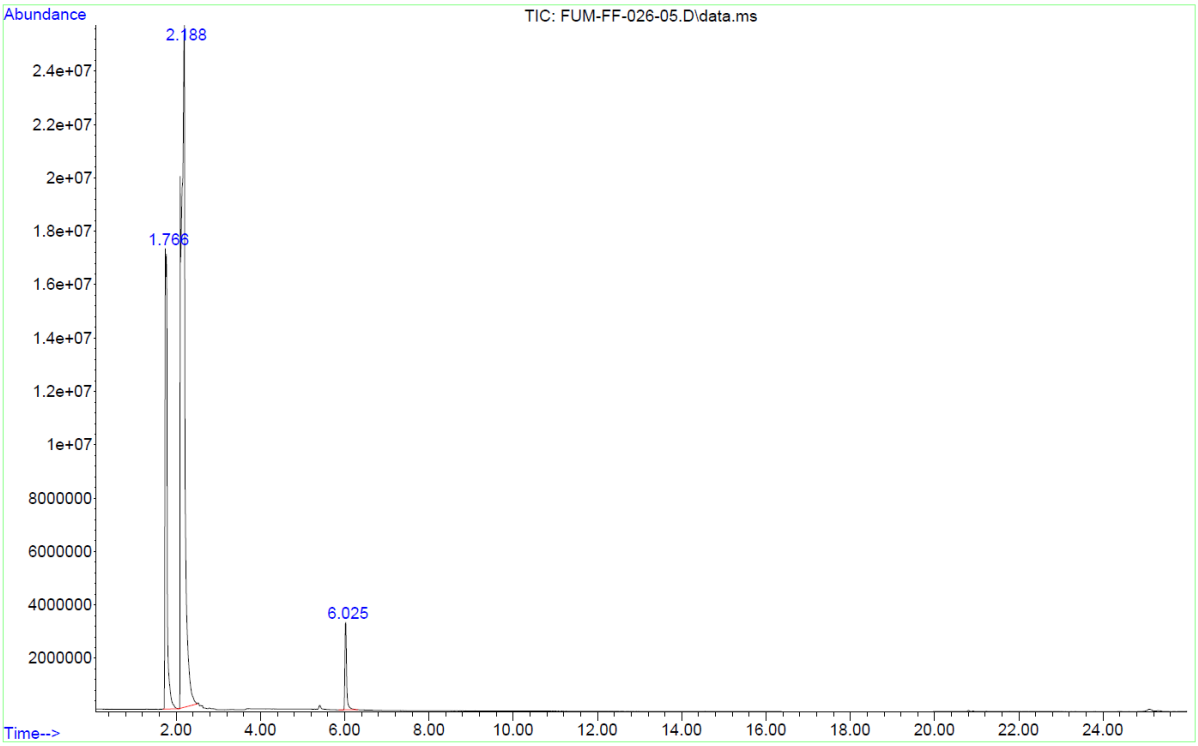

peak #	R.T. min	first scan	max scan	last scan	PK TY	peak height	corr. area	corr. % max.	% of total
1	1.766	177	186	217	BV	16981860	612635710	36.92%	25.930%
2	2.188	217	232	267	PV 3	25779513	1659323449	100.00%	70.232%
3	6.025	639	657	689	BB	3268238	90684416	5.47%	3.838%

Figure SI07. GC-MS headspace sampling referring to entry 2 in Table SI02

2.6. Catalytic potential of compounds **2**, **10** and complex **8b**

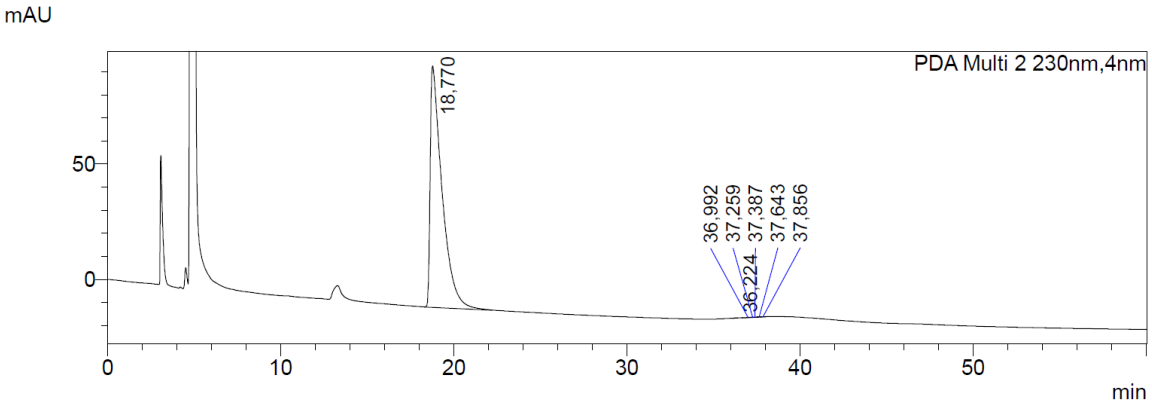

Benzaldehyde (**5**)

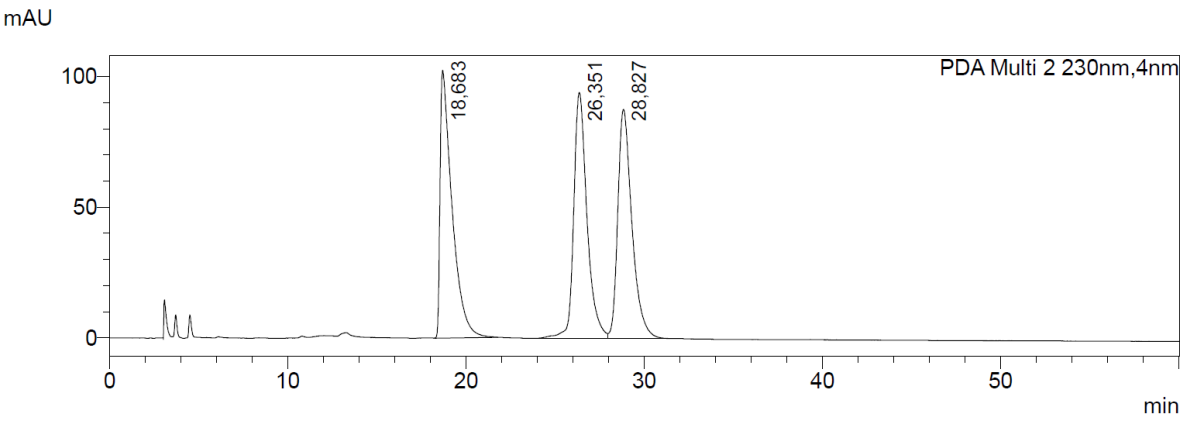

PDA Ch2 230nm

Peak#	Ret. Time	Name	Area	Height	Area%
1	18,683		4776408	102343	33,024
2	26,351		4869098	94003	33,664
3	28,827		4818149	87570	33,312
Total			14463656	283915	100,000

Racemate of **SI01**

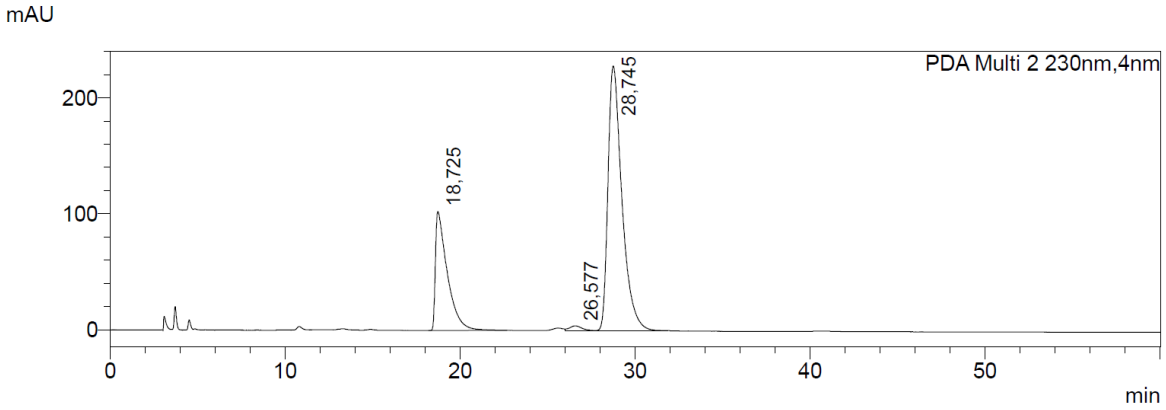

PDA Ch1 215nm

Peak#	Ret. Time	Name	Area	Height	Area%
1	18,724		8655122	181968	13,766
2	26,580		971567	18957	1,545
3	28,744		53244703	923154	84,688
Total			62871391	1124080	100,000

Reaction catalyzed by free acid **2**

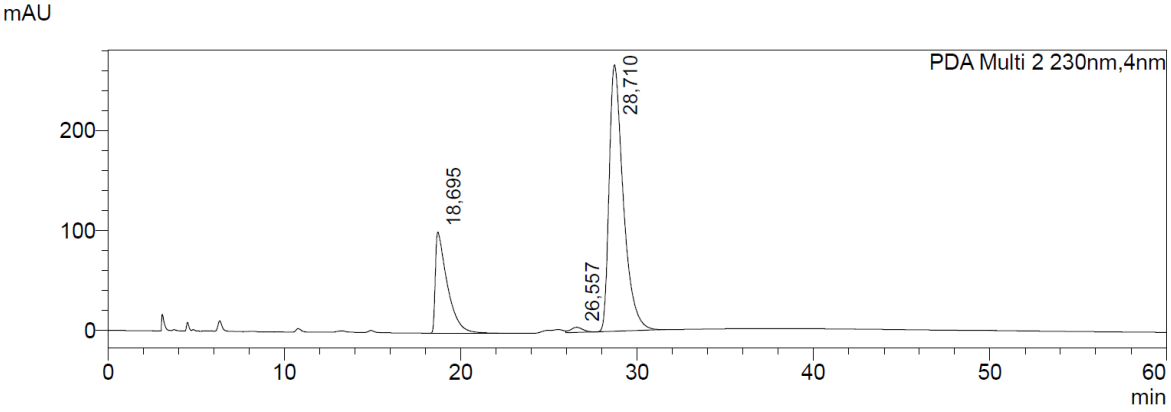

PDA Ch1 215nm

Peak#	Ret. Time	Name	Area	Height	Area%
1	18,694		8582905	179393	12,098
2	26,546		1361162	24814	1,919
3	28,709		60998167	1048884	85,983
Total			70942234	1253092	100,000

Reaction catalyzed by zinc phosphate **10**

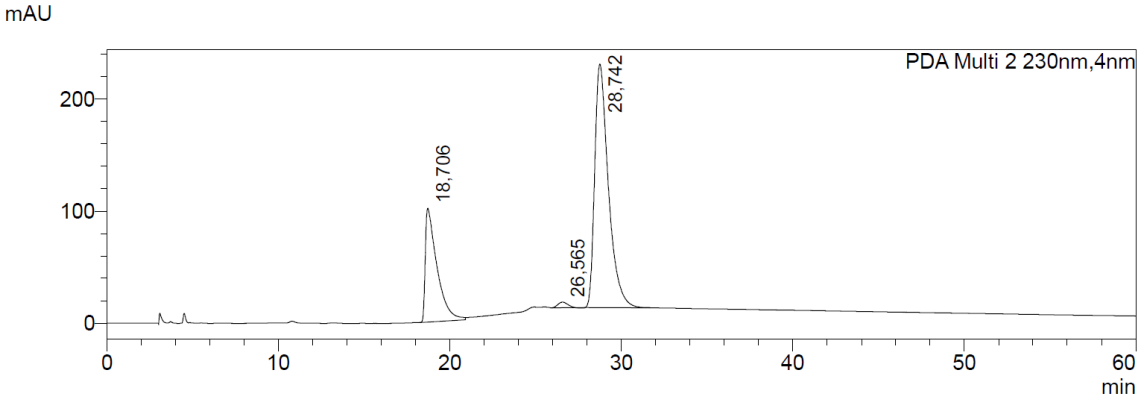

PDA Ch1 215nm

Peak#	Ret. Time	Name	Area	Height	Area%
1	18,705		8364549	179487	13,951
2	26,553		940172	22323	1,568
3	28,742		50651698	883840	84,481
Total			59956420	1085650	100,000

Reaction catalyzed by complex **8b**

2.7. NMR data of obtained products

3-Methylene-5-phenyldihydrofuran-2(3*H*)-one (**8b**).

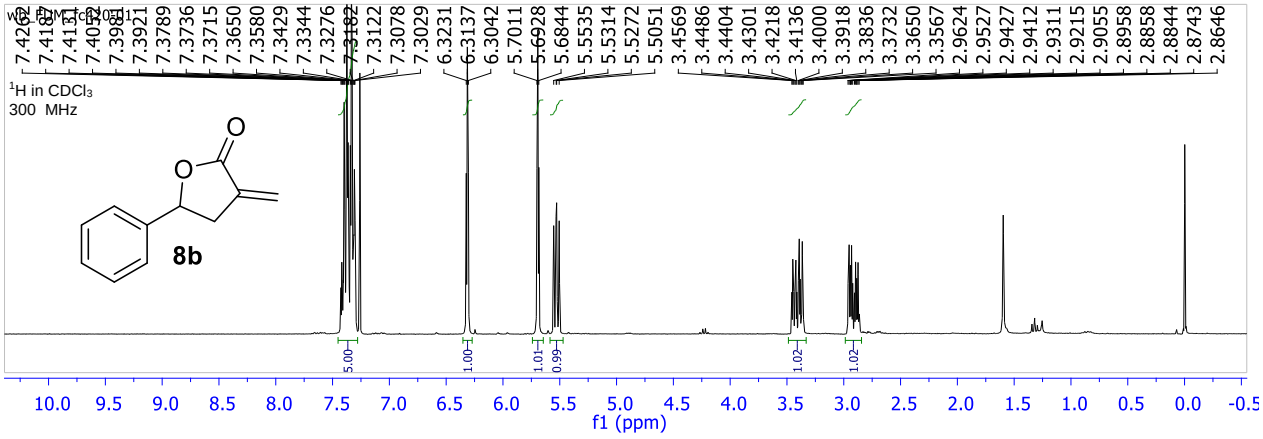

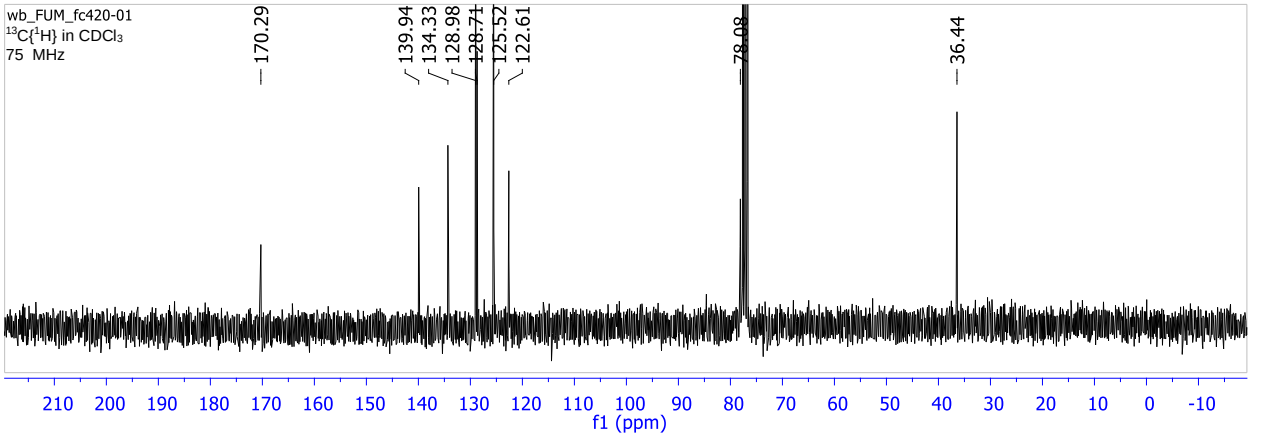

2.6. HPLC trace of product **7**

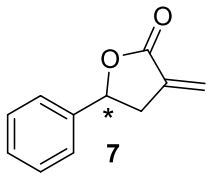

7

<Chromatogram>

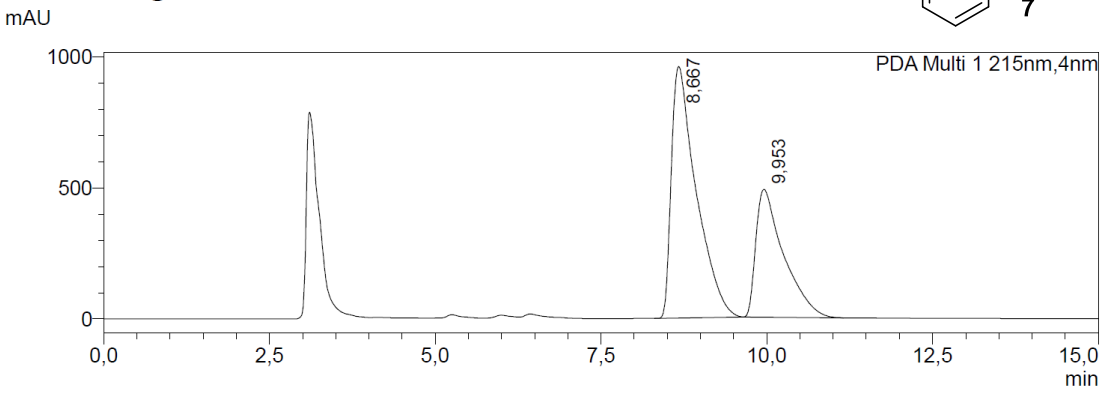

<Peak Table>

PDA Ch1 215nm

Peak#	Ret. Time	Name	Area	Height	Area%
1	8,667		25061090	960265	63,824
2	9,953		14205006	488202	36,176
Total			39266096	1448467	100,000

Product obtained under TRIP catalysis (compound **7**)

<Chromatogram>

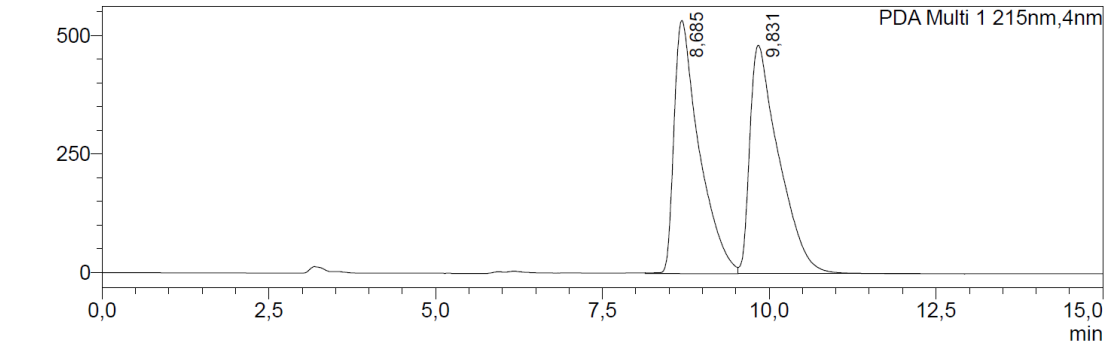

<Peak Table>

PDA Ch1 215nm

Peak#	Ret. Time	Name	Area	Height	Area%
1	8,685		14035097	533520	49,041
2	9,831		14583770	481837	50,959
Total			28618868	1015357	100,000

Racemic reference material

3. Computational Part

3.1. Remarks regarding the Labelling

The notation employed in this section is based on the mechanistic cycles depicted further below (section 3.4). The complexes mentioned in the main text of the paper are indicated in the corresponding sections. The suffixes “ma” and “mi” refer to either the major (experimentally favored) or minor (experimentally disfavored) enantiomer.

3.2. Abbreviations and Units used in the Tables

A short explanation for the abbreviations used in the following part of the SI is given taking Table SI03 as an example. For simplicity the same units as in the example are given for all data from here.

Table SI03. Explanation of the abbreviations used

complex	**ZPE**	**S**	**G**	**ΔZPE to ISR**	**ΔG to ISR**	**ΔZPE to 16_1**	**ΔG to 16_1**
xxxxxxxxx	xx.x	xx.x	xx.x	xx.x	xx.x	xx.x	xx.x

Given from the left to the right:

- Name of the complex
- Zero Point Energy (ZPE) of the complex in kJ/mol
- Entropy S of the complex in J/molK
- Gibbs free energy correction G for the complex in kJ/mol
- Difference (“Δ”) of the Zero Point Energy corrected energy of the complex referenced to the infinitely separated reactants (“ISR”)
- Difference (“Δ”) of the Gibbs free energy corrected energy of the complex referenced to the infinitely separated reactants (“ISR”)
- difference of the Zero Point Energy corrected energy of the complex in reference to - in this particular case - complex **16_1**
- difference of the Gibbs free energy of the complex in reference to - in this particular case - complex **16_1**

Additionally, “n.b.” is the abbreviation for “no barrier” when shown instead of the energy of a transition state. Approximate transition state energies obtained from the reaction pathway calculations employing the woelfling-program[1] (meaning that the corresponding transition state geometries are not fully optimized) are denoted by “woelfling”.

3.3. Summary of the Relabelling of the Complexes

- Zinc complexes:
  - The pathway starting from **14γ-int-ma** (major enantiomer) is referred to as pathway ***fav.*** in the main text.
  - The pathway starting from **14γ-sim.-mi** (minor enantiomer) is referred to as pathway ***dis.*** in the main article.
  - The four most stable educt complexes are relabelled as follows: **14j-ma** = **B2**, **14d-ma** = **B2h**, **14d-mi** = **A2h** and **14j-mi** = **A2**. The addition of “h” indicates the coordination pattern in Figure SI22.
  - Complexes **13** (stemming from removing the aldehyde from complexes **14**) are relabelled: **13j-ma** = **B1**, **13d-ma** = **B1h**, **13d-mi** = **A1h** and **13j-mi** = **A1**.

- Products **15d-2-ma** = **B3h$_1$**, **15n-ma** = **B3h$_2$**, **15d-ma** = **B3h$_3$**, **15q-ma** = **B3h$_4$**, **15d-mi** = **A3h$_1$**, **15r-mi** = **A3h$_2$**; the intermediates and transition states were renamed accordingly.

3.4. Introduction

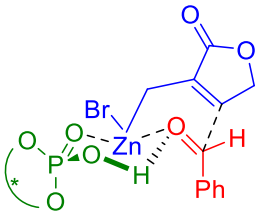

Figure SI08. Initially proposed mechanism[2]

For the Zn^{2+} mediated Barbier-type allylation, the originally proposed intermediates agree with experimental ee (the minor enantiomer being $S_{cat}S_{alcohol}R$ and the major enantiomer being $S_{cat}R_{acohol}S$).[2] However, after the first catalytic step, the catalyst would bind the zinc ion (see Figure SI08) and therefore from this point on would lack the required acidic proton. Herein, we discuss two alternative scenarios involving the zinc salt of the chiral phosphoric acid **2** (see Figure SI09).

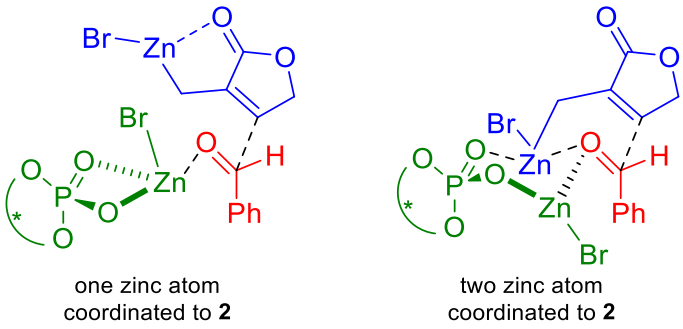

Figure SI09. Alternative proposals discussed below

Both alternatives have been investigated (see Figure SI24, Tables SI27 and SI30). The whole catalytic cycles of the investigated mechanisms are shown in the Figures below (see Figures SI10-SI1).

Depending on the order in which the educts bind to the catalytic site, different mechanistic cycles arise for the alternative initial proposal containing one zinc(II) ion. Two are depicted in Figure SI10, where the lactone moiety has been changed to an allyl group for reasons of clarity.

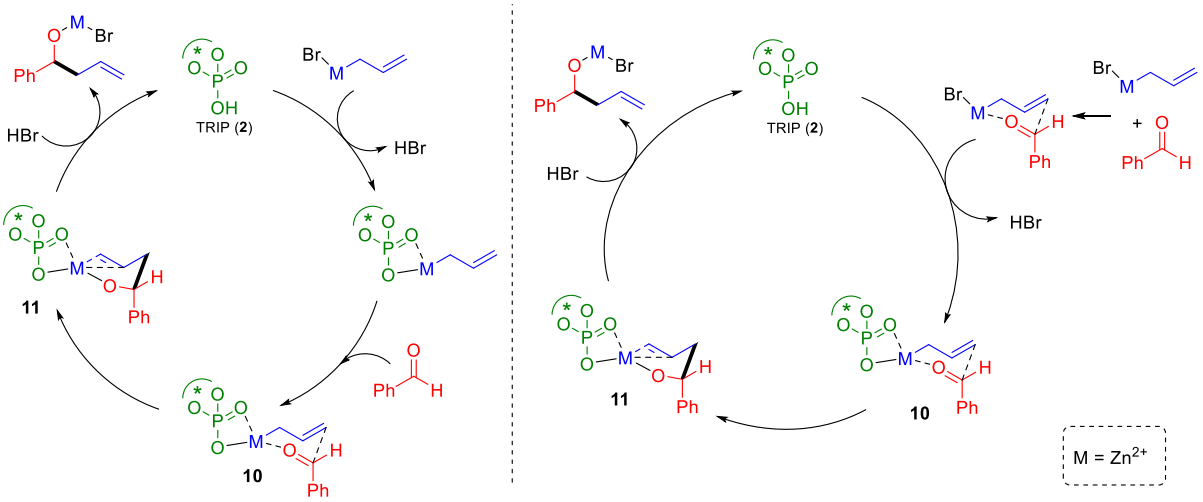

Figure SI10. Two possible mechanistic cycles with one coordinated zinc atom (note: the lactone moiety has been omitted for clarity)

Due to different orientations of the lactone moiety and the possible coordination patterns of the lactone carbonyl group to the zinc ion, several geometries for complexes **11** and **12** arise, which were labelled **a-f**. For an easier understanding, one of the two mechanistic cycles containing one zinc-ion depicted in Figure SI10 is shown again in Figure SI11.

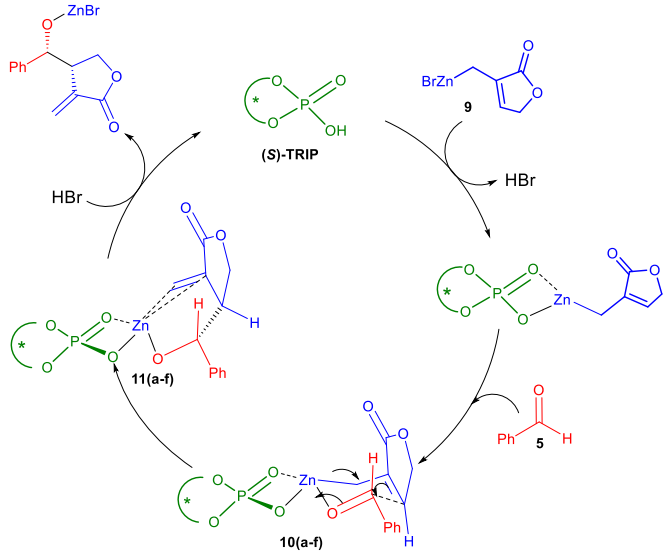

Figure SI11. Mechanistic cycle containing one zinc atom

For the mechanism containing two zinc-ions (compare Figure SI09) three different mechanistic cycles can be envisaged, again dependent on the order of substrate binding. Two are depicted in Figure SI12, where the lactone moiety has been changed to an allyl group again.

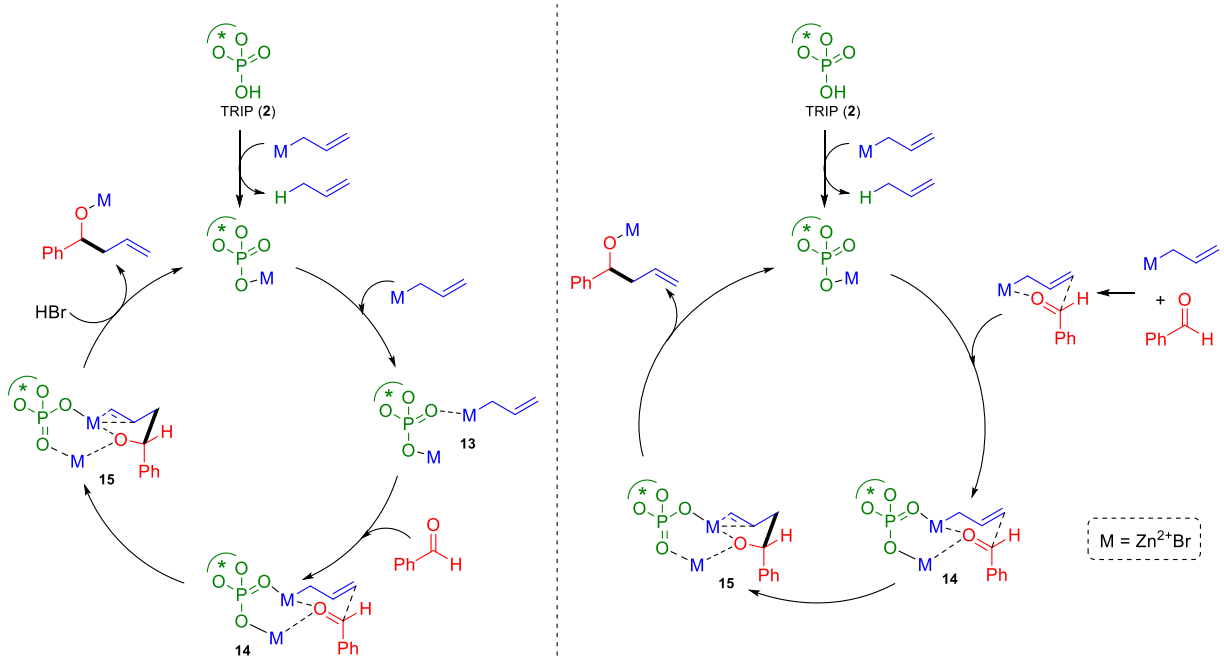

Figure SI12. Two mechanistic cycles containing two coordinated zinc atoms (note: the lactone moiety has been omitted for clarity)

Because of the possible coordination of the lactone carbonyl group to the second zinc ion (i.e. the zinc ion not originally bound to lactone **1**), each of the above mechanistic cycles for the mechanisms containing two Zn^{2+} ions can be realized in two ways. Figure SI13 depicts both alternatives for the left cycle shown in Figure SI12. We assigned letters **a-l** to the complexes screened for the mechanism with coordination of the lactone carbonyl moiety and **m-t** as well as **greek letters** to the complexes for the mechanism without coordination of the lactone carbonyl group.

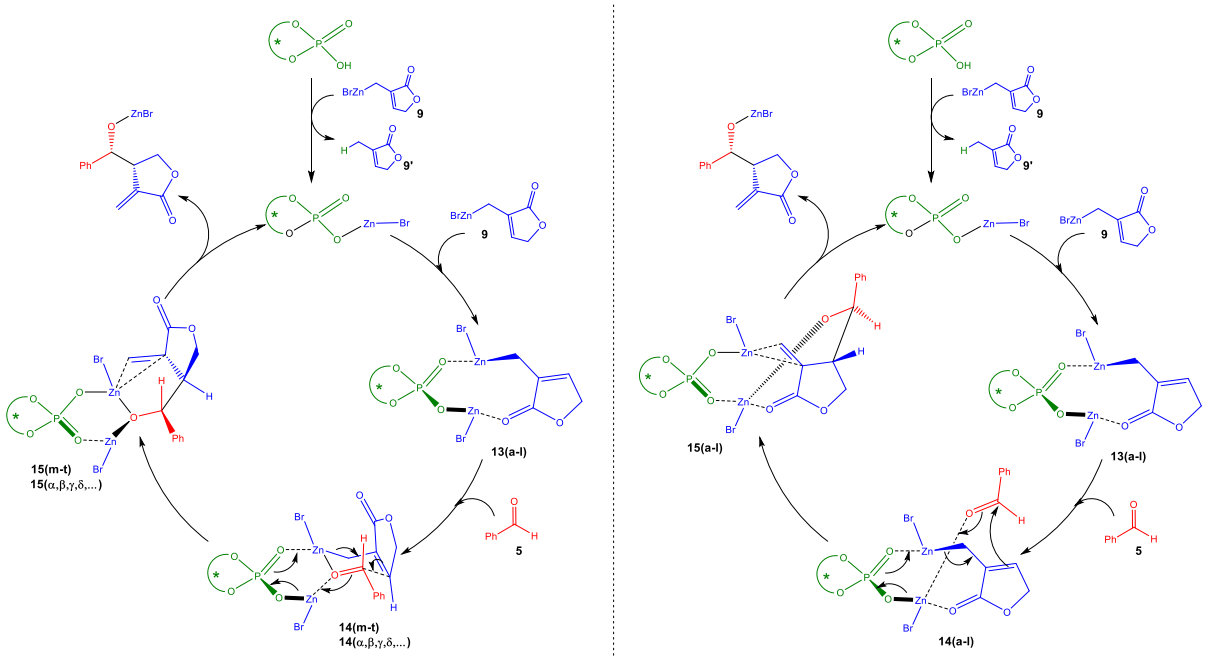

Figure SI13. Subdivision of the mechanistic cycles containing two Zn atoms: Without coordination of lactone carbonyl (left) and with coordination of lactone carbonyl (right)

3.5. Conformational analysis of the Catalyst systems

The lowest energy conformers of the catalyst (as the acid or the zinc salt) and the substrates were computed, and all further geometries were built from these. The computed, most stable conformers of the full catalyst were compared with previous computational work.[3-4] The analysis of the conformers of the phosphoric acid has been subject of the research of Houk and coworkers,[4] and they concluded that, depending on the relative orientation of the two *para*-located isopropyl groups, four conformers remain (see Figure SI14).

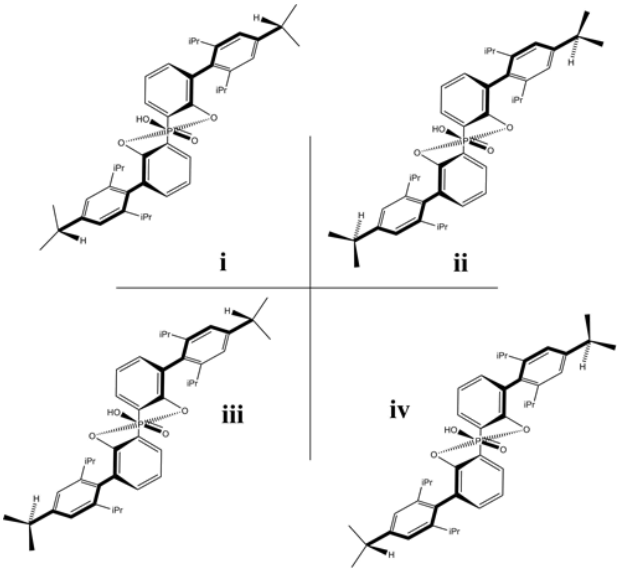

Figure SI14. The four remaining conformations according to Houk and coworkers (see the supporting information of reference 4).

Houk and coworkers conclude that the most stable conformer is conformer **iv** (see the supporting information of reference 4) and found the energy differences between these conformers to be small. Goodman and coworkers[3] used essentially the same conformer as Houk and coworkers,[4] but for one 2,4,6-triisopropylphenyl-substituent one of the *ortho*-isopropyl groups is facing the backbone with its methyl-groups. This is certainly sterically less favorable, as indicated by Houk and coworkers,[4] but the work of both research groups gives essentially consistent results concerning the mechanism.[3-4]

This means that the relative orientation of the isopropyl groups of the catalyst does not seem to interfere with the predictive value of the calculations. This is further indicated by the fact that the conformational analysis (performed with the COSMOconf program)[5] yielded many energetically similar conformers.

For (*S*)-TRIP the most stable conformer found by the conformational analysis is conformer **i** (Figure SI15). For the zinc salt of (*S*)-TRIP, conformational analysis also yields conformer $\mathbf{i}_{\mathbf{Zn\text{-}DZ}}$ as the most stable structure [Figure SI16, the Zn is coordinated to both available oxygen atoms of the phosphoric acid moiety ("**DZ**"-coordination pattern)].

If the possibility of an interaction of the Zn^{2+} to the aromatic system is considered ("**AR**"-coordination pattern), the most stable conformer is found to be conformer $\mathbf{i}_{\mathbf{Zn\text{-}AR}}$ (see Figure SI14), followed by conformer $\mathbf{iii}_{\mathbf{Zn\text{-}AR}}$ (see Figure SI14). The energy difference between $\mathbf{i}_{\mathbf{Zn\text{-}AR}}$ and $\mathbf{iii}_{\mathbf{Zn\text{-}AR}}$ amounts to only 1.11 kJ/mol at the RI-PBE-D3/def2-SVP level (ΔG+COSMO), 1.25 kJ/mol at the RI-PBE-D3/def2-TZVPPD level (ΔG+COSMO), 1.22 kJ/mol at the B3LYP-D3/def2-TZVPPD level (ΔG+COSMO) and 1.28 kJ/mol at the DLPNO-CCSD(T)/cc-pVTZ level and, thus, is well within the accuracy limits of the underlying methods (compare Figure SI16).

Relative to $\mathbf{i}_{\text{Zn-AR}}$, $\mathbf{i}_{\text{Zn-DZ}}$ lies +20.1 kJ/mol higher in energy at the RI-PBE-D3/def2-SVP level (ΔG+COSMO). This is diminished to +5.19 kJ/mol at the RI-PBE-D3/def2-TZVPPD level (ΔG+COSMO) and +13.25 kJ/mol at the B3LYP-D3/def2-TZVPPD level (ΔG+COSMO).

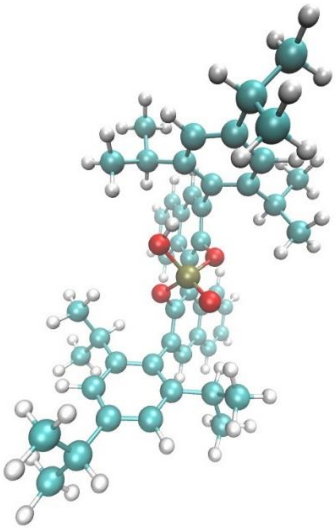

Figure SI15. Most stable conformer (**i**) of TRIP (free phosphoric acid)

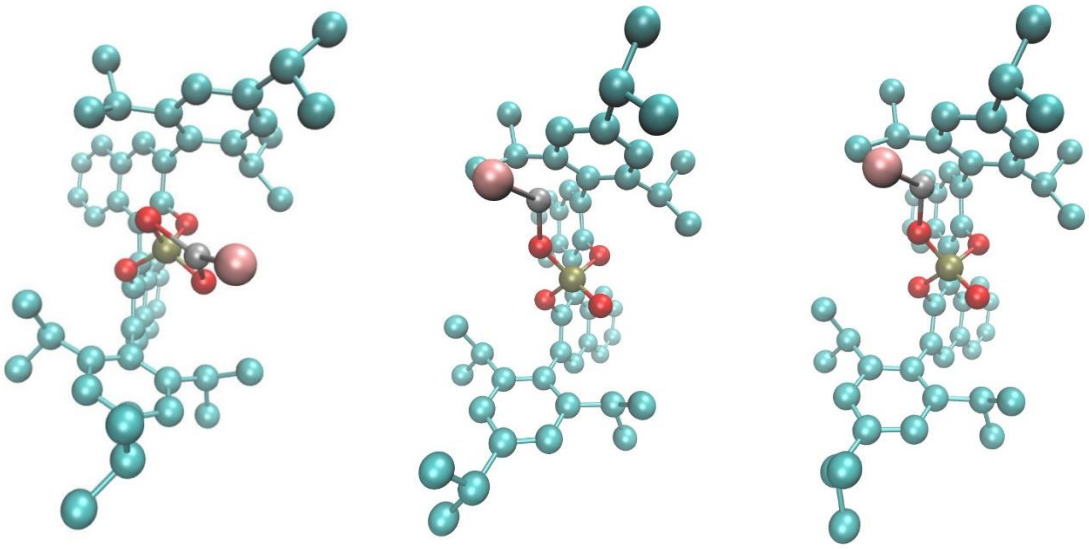

$\mathbf{i}_{\text{Zn-DZ}}$	$\mathbf{i}_{\text{Zn-AR}}$	$\mathbf{iii}_{\text{Zn-AR}}$
+13.25 kJ/mol	+0.00 kJ/mol	+1.22 kJ/mol

Figure SI16. Most stable conformers ($\mathbf{i}_{\text{Zn-DZ}}$) of the zinc salt's high-energy coordination pattern "**DZ**" (left) and the two most stable conformers of the low-energy coordination pattern "**AR**" [middle: most stable ($\mathbf{i}_{\text{Zn-AR}}$); right: second most stable ($\mathbf{iii}_{\text{Zn-AR}}$)]

Calculations on the Zn-model were performed using the most stable conformer $\mathbf{i}_{\text{Zn-AR}}$. The difference in conformation should not matter regarding the obtained results since both conformers $\mathbf{i}_{\text{Zn-AR}}$ and $\mathbf{iii}_{\text{Zn-AR}}$ should be readily accessible at room temperature due to the minute difference in their respective energies. Furthermore, one can expect conformer $\mathbf{i}_{\text{Zn-DZ}}$ (Figure SI16, left picture) to be accessible, too.

3.6. The uncatalyzed background reaction

A conformational search was performed for the complex consisting of the zinc organyl **9** (see Figure SI30) and benzaldehyde (**5**), labelling the Zimmermann-Traxler like adducts **16$_n$**, with index n rising in order of increasing energy. The results are listed in Table SI04 - the energy difference between the conformers were determined to be small.

Table SI04. ΔG+COSMO values [kJ/mol] for adducts **16$_n$**, given relative to the ISR

complex	RI-PBE-D3/def2-SVP	RI-PBE-D3/def2-TZVPPD	B3LYP-D3/DEF2-TZVPPD	DLPNO-CCSD(T)/cc-pVTZ
16$_1$	-15.5	7.4	2.9	0.6
16$_2$	-14.0	7.3	2.9	---
16$_3$	-9.2	11.8	4.0	---
16$_4$	-7.3	18.0	14.5	---
16$_5$	-9.5	7.7	0.9	---

Table SI05. ZPE [kJ/mol], entropy [J/molK] and chem. pot. values [kJ/mol] for adducts **16$_n$**, product **17$_1$** and **TS$_1$**

complex	ZPE	S	chem. pot.
16$_1$	530.7	0.5911	410.03
16$_2$	530.6	0.5925	409.52
16$_3$	531.2	0.5754	414.50
16$_4$	529.8	0.5908	409.24
16$_5$	531.3	0.5909	410.73
17$_1$	538.1	0.5493	425.78
TS$_1$	533.0	0.5471	420.73

Attempts were made to optimize the chair and boat conformation of the adducts, which lead to conformers **16$_1$** (chair) and **16$_3$** (boat), respectively. The corresponding product **17$_1$** was optimized, followed by reaction pathway calculations and TS-optimization of **TS$_1$**. The data for pathway **1** (**16$_1$** – **TS$_1$** – **17$_1$**) is summarized in Table SI06 and SI10:

Table SI06. ΔG+COSMO values [kJ/mol] for pathway **1** (**16$_1$** – **TS$_1$** – **17$_1$**) at the various levels of theory, given relative to the ISR

complex	educt	TS	product
RI-PBE-D3/def2-SVP	-15.5	31.3	11.7
RI-PBE-D3/def2-TZVPPD	7.4	49.9	26.9
B3LYP-D3/def2-TZVPPD	2.9	67.3	35.8
DLPNO-CCSD(T)/cc-pVTZ	0.6	76.1	20.2

Table SI07. ΔE+ZPE+COSMO values [kJ/mol] for pathway **1** (**16$_1$** – **TS$_1$** – **17$_1$**) at the various levels of theory, given relative to the ISR

complex	educt	TS	product
RI-PBE-D3/def2-SVP	-58.5	-20.2	-39.7
RI-PBE-D3/def2-TZVPPD	-35.6	-1.5	-24.5
B3LYP-D3/def2-TZVPPD	-40.1	15.8	-15.6
DLPNO-CCSD(T)/cc-pVTZ	-42.4	24.7	-31.1

3.7. Preactivation of the Catalyst

The catalyst is added to the reaction mixture as the free acid [for the calculations we chose the (*S*)-enantiomer]. Therefore, the pre-activation (formation of the zinc salt) was modeled. There are five possibilities for the formation of the zinc salt from the catalyst and the zinc species of the lactone (**9**, see Figure SI17). They are depicted in Figure SI17. Four involve a four-membered cyclic TS (and differ only in the coordination pattern of the zinc species of the lactone) – they are denoted **C**-**F**. The fifth possibility (**G**) involves a six-membered transition state.

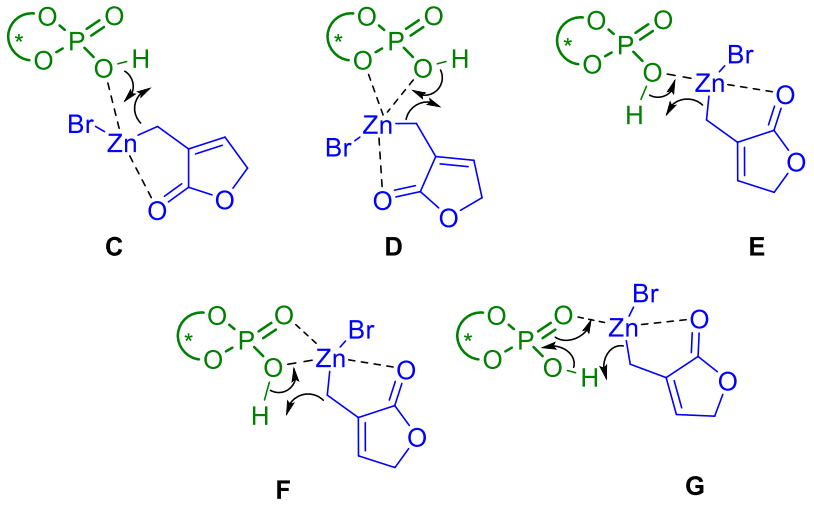

Figure SI17. Five possible TSs for the formation of the zinc salt

The electronic energies obtained by optimization of the five corresponding educts $\mathbf{C}_{ed.}$ to $\mathbf{G}_{ed.}$ are given in Table SI08. $\mathbf{C}_{ed}$ and $\mathbf{D}_{ed}$ yield the same structure. The educt complexes belonging to pathways **E** and **F** both convert to the coordination pattern of educt $\mathbf{G}_{ed}$, the latter being the starting point for the six-ring-mechanism (Figure SI17).

Thus, Table SI08 indicates a preference for the six-membered ring mechanism and in the following discussion pathways **E** to **F** are relabeled as **G1** to **G3** in order to stay consistent with the labelling of the pathways in Figure SI17.

Table SI08. Electronic energies [kJ/mol] of the five educts at the RI-PBE-D3/def2-SVP level

complex	Δ to ISR	Δ to $\mathbf{E3}_{ed}$
$\mathbf{C}_{ed}$	-105.5	83.9
$\mathbf{D}_{ed}$	-105.3	84.1
$\mathbf{E}_{ed} = \mathbf{G1}_{ed}$	-176.0	13.3
$\mathbf{F}_{ed} = \mathbf{G2}_{ed}$	-122.6	66.7
$\mathbf{G}_{ed} = \mathbf{G3}_{ed}$	-189.3	0.0

Subsequently, the product complexes were constructed from the optimized geometries of the remaining four educts ($\mathbf{D}_{ed}$ and $\mathbf{G1}_{ed}$ to $\mathbf{G3}_{ed}$) and optimized; they are labelled with a subscript “prod”, see Table SI09. The reaction pathways between each educt complex and the corresponding product complex were calculated, leading to intermediates $\mathbf{G1}_{int}$ and $\mathbf{G2}_{int}$, which are located after the reaction has taken place. Thus, new pathways were calculated, substituting $\mathbf{G1}_{prod}$ by $\mathbf{G1}_{int}$ and analogously for **G2**.

Table SI09. Electronic energies of the four products at the RI-PBE-D3/def2-SVP level

complex	Δ to ISR	Δ to $E3_{ed}$
D_{prod}	-231.4	-42.1
$G1_{prod}$	-248.8	-59.5
$G2_{prod}$	-226.2	-36.9
$G3_{prod}$	-231.4	-42.0
$G1_{int}$	-185.3	4.0
$G2_{int}$	-228.7	-39.3

Transition states were optimized for pathways **G1** and **G2** (Table SI10, they will be labelled with "TS"), but not for pathway **D** because of its high energy educt complex and not for pathway **G3** because of the high energy obtained for the approximate TS by the reaction pathway calculations, despite $G3_{ed}$ being the most stable educt complex.

Table SI10. Electronic energies of the four TS at the RI-PBE-D3/def2-SVP level

complex	woelfling/optimized	Δ to ISR	Δ to corresponding substrate complex
D_{ed}	woelfling	-71.3	34.0
$G1_{ed}$	optmized	-69.9	106.2
$G2_{ed}$	optimized	-121.1	1.7
$G3_{ed}$	woelfling	-41.1	148.3

Pathway **G2** proves promising, as it exhibits the lowest TS of the pathways and a low-energy product, even though the corresponding educt $G2_{ed}$ is relatively high in energy (see Tables SI08 and SI10). ΔG+COSMO values were calculated for pathways **G1** and **G2**. The RI-PBE-D3/def2-SVP data were verified with RI-PBE-D3/def2-TZVPPD single point calculations. The ΔG+COSMO values of the reference structure $G3_{ed}$ were obtained as -95.7 kJ/mol for RI-PBE-D3/def2-SVP and -41.3 kJ/mol for RI-PBE-D3/def2-TZVPPD, respectively. By these values and the data provided in Tables SI12 and SI13, a systematic shift in the Gibbs free energies relative to the ISR can be observed – for further details see section "Pathways from complexes **7** (educts) to **8** (products)" (section 3.9).

The relative differences (referenced to $G3_{ed}$) decrease in general upon increasing the basis set size, making especially $G2_{ed}$ energetically more favorable and leading to the conclusion that a six ring mechanism like pathway **G2** is indeed an energetically reasonable mechanistic pathway for the pre-activation of the catalyst.

Table SI11. ZPE [kJ/mol], entropy [J/molK] and chem. pot. [kJ/mol] for pathways **G1** and **G2** and for $G3_{ed}$

complex	ZPE	S	chem. pot.
$G1_{ed}$	2716	1.4053	2477.39
$G1_{TS}$	2704	1.3994	2466.66
$G1_{int}$	2717	1.4006	2481.68
$G2_{ed}$	2713	1.4284	2469.64
$G2_{TS}$	2707	1.4051	2468.34
$G2_{int}$	2718	1.4148	2478.62
$G3_{ed}$	2714	1.3989	2477.76

Table SI12. ΔG+COSMO data [kJ/mol] of pathway **G1** at the RI-PBE-D3/def2-SVP level relative to ISR

complex	educt	TS	product
RI-PBE-D3/def2-SVP	-80.3	11.3	-87.4
RI-PBE-D3/def2-TZVPPD	-34.9	53.2	-33.2

Table SI13. ΔG+COSMO data [kJ/mol] of pathway **G2** at the RI-PBE-D3/def2-TZVPPD level rel. to ISR

complex	educt	TS	product
RI-PBE-D3/def2-SVP	-40.3	-38.0	-134.4
RI-PBE-D3/def2-TZVPPD	-3.6	3.1	-85.3

Table SI14. ΔG+COSMO data [kJ/mol] of pathway **G1** level relative to **$G3_{ed}$**

complex	educt	TS	product
RI-PBE-D3/def2-SVP	15.4	107.0	8.3
RI-PBE-D3/def2-TZVPPD	6.4	94.5	8.1

Table SI15. ΔG+COSMO data [kJ/mol] of pathway **G2** at the RI-PBE-D3/def2-TZVPPD level rel. to **$G3_{ed}$**

complex	educt	TS	product
RI-PBE-D3/def2-SVP	55.4	57.7	-38.7
RI-PBE-D3/def2-TZVPPD	37.8	44.4	-44.0

3.8. Transition states of the mechanistic proposal in the main text

Note: For the detailed discussion of the pre-complexes **B1** and **B1h** in the main text please see chapters 3.9.2.3 and 3.9.2.4 in this supporting information.

After ruling out the mechanism involving only one zinc ion (compare Figures SI09, SI10 and SI11; see section 3.4) and thoroughly investigating the mechanistic pathways involving the two-zinc complexes **14a-t** (see section 3.9), we arrived at an alternative model explaining the experimentally observed enantiomeric excess.

The starting point to the calculations outlined in this chapter was the association of structures like **16** (the Zimmermann-Traxler projection of the uncatalyzed reaction) to the zinc salt of TRIP (see below and Figure SI12) with the goal to arrive at complexes **14d/j** (the importance of the latter is discussed in section 3.9). However, instead of complexes **14d/j**, we obtained new intermediates, which exhibited new coordination patterns. Compared to other double coordination complexes (see section 3.9) these educt complexes are in a reasonable energetic range (**14ξ-ma**, ΔE to **14j-ma** = +42.9 kJ/mol), and lead to a further investigations of potential transition states.

In order to get an overview and to reduce computational demand, in a first step we optimized several complexes (denoted by greek letters) for the major enantiomer, which were obtained by coordinating complexes **16** to the zinc salt of the TRIP catalyst. The data of the optimized educt complexes **14** are given in Table SI16, along with the data from the RI-PBE-D3/def2-TZVPPD single points. For several coordination patterns two possibilities were tested, constructed from the chair and the boat conformers of **16**; they are denoted by a suffix "2". **14ξ-ma** and **14π-ma** are the complexes obtained as intermediates from the reaction pathway calculations of the association of complexes **16** to the zinc salt of the TRIP catalyst.

Subsequently, in energetically reasonable cases (**14γ,ε,λ,ν,ξ-ma** and **14γ,ν-mi**), we performed optimizations of the corresponding educt complexes of the minor enantiomer and the corresponding products and of the transition states between the educts and their corresponding products for both the minor and the major enantiomer. The obtained electronic energies of the educt complexes **14-mi** are included in Table SI16, along with any intermediates appearing during the reaction pathway optimizations (denoted with "int"). Table SI17 displays the electronic energy data of the calculated structures.

Only the last transition states of the pathways, namely the ones in which the C-C bond formation takes place, were optimized, each. Complex **14γ-mi** is missing in Table SI16, as during the reaction pathway optimization of its major enantiomer analogue it became clear that an intermediate would necessarily have to be located between **14γ-mi** and the corresponding product **15γ-mi**. Therefore, when investigating the corresponding reaction pathways, we started directly from **14γ-int1-mi**, which was constructed from **14γ-int-ma**.

Table SI16. ΔE data [kJ/mol] of the optimized educt complexes and intermediates for RI-PBE-D3/def2-SVP and RI-PBE-D3/def2-TZVPPD; important coordination patterns are denoted in brackets

		RI-PBE-D3/def2-SVP		RI-PBE-D3/def2-TZVPPD	
	complex	**Δ to ISR**	**Δ to 14j-ma**	**Δ to ISR**	**Δ to 14j-ma**
major	**14α**	-189.4	122.9	-142.3	106.1
	14β	-275.8	36.5	-218.1	30.4
	14γ	-303.0	9.3	-247.9	0.6
	14γ-int (Γ)	-296.1	16.2	-236.9	11.5
	14γ-2	-193.3	119.0	-150.3	98.1
	14δ	-252.5	59.9	-193.3	55.1
	14ε	-266.8	45.5	-209.8	38.6
	14ζ	-169.3	143.1	-118.5	129.9
	14ζ-2	-210.6	101.7	-156.5	92.0
	14η	-255.0	57.4	-196.4	52.0
	14θ	-169.1	143.2	-118.4	130.0
	14ι	-251.8	60.5	-191.6	56.8
	14κ	-163.0	149.3	-107.5	140.9
	14λ	-274.2	38.2	-220.5	28.0
	14λ-int	-272.9	39.4	-216.8	31.6
	14μ	-189.9	122.4	-117.2	131.3
	14ν (N)	-305.4	7.0	-243.4	5.0
	14ν-2 (N2)	-259.5	52.8	-205.4	43.0
	14ξ	-269.4	42.9	-222.2	26.2
	14π	-204.7	107.6	-162.0	86.4
minor	**14γ-int1 (N)**	-322.6	-10.2	-258.7	-10.3
	14γ-int2 (N)	-318.2	-5.8	-248.9	-0.5
	14γ-sim. (Γ)	-310.5	1.8	-249.7	-1.3
	14ν-2 (N2)	-295.5	16.8	-237.5	10.9

Table SI17. ΔE data [kJ/mol] of the calculated pathways at the different levels of theory referenced to **14j-ma** (**B2**; see chapter 3.9.2.3 herein); important coordination patterns are denoted in brackets

		RI-PBE-D3/def2-SVP			RI-PBE-D3/def2-TZVPPD		
	from	**Ed**	**TS**	**prod**	**Ed**	**TS**	**prod**
major	**14γ-int (Γ)**	16.2	30.8	-2.1	11.5	30.5	1.1
	14ε	45.5	71.6	46.2	38.6	68.4	42.3
	14λ-int	39.4	61.3	41.4	31.6	56.5	35.4
	14ν (N)	7.0	46.2	26.2	5.0	45.1	22.0
	14ξ[a]	42.9	110.6	-28.6	---	---	---
minor	**14γ-int2 (N)**	-5.8	27.0	1.0	-0.5	34.0	8.6
	14γ-sim. (Γ)	1.8	50.6	8.1	-1.3	40.6	6.0
	14ν-2 (N2)	16.8	57.1	41.1	10.9	47.1	35.1

[a] woelfling data only

However, upon inspection of the resulting geometries (see Figure SI35) of the intermediates, it becomes clear that **14γ-int-ma** does not have the same coordination pattern **Γ** (double coordination

of aldehyde by two zinc atoms, bridged by one bromine, see Figure SI18, left structure) as its **14γ-int1-mi** and **14γ-int2-mi** congeners, which lead to the experimentally disfavored enantiomer [the **Γ** coordination pattern proved unstable for complex **14γ-int1-mi** during optimization]. Instead, **14γ-int1-mi** and **14γ-int2-mi** exhibit the same coordination pattern as **14ν-ma**, which is referred to as **N** coordination (see Figure SI18, middle structure) pattern from here on. This is also the reason for the exclusion of **14ν-mi** from Table SI16. Therefore, in order to obtain the minor enantiomer analogue of **14γ-int-ma**, which also exhibits the **Γ** coordination pattern, it was constructed explicitly and optimized, and is labelled **14γ-sim-mi.** Likewise, we will denote the coordination pattern of both **14ν-2-ma/mi** by **N2** (see Figure SI18, right structure).

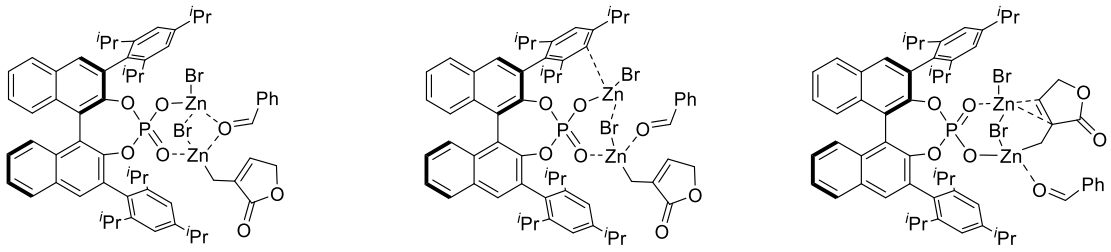

coordination pattern **Γ** coordination pattern **N** coordination pattern **N2**

Figure SI18: Explanation of the three coordination patterns "**Γ**","**N**" and "**N2**"

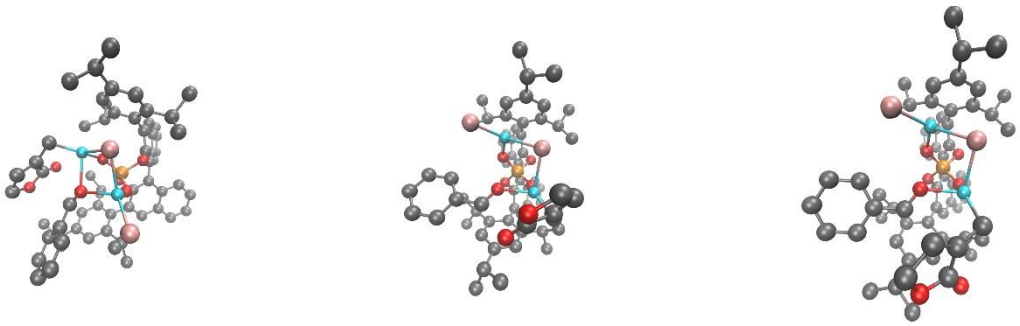

14γ-int-ma (Γ) **14γ-int1-mi (N)** **14γ-int2-mi (N)**

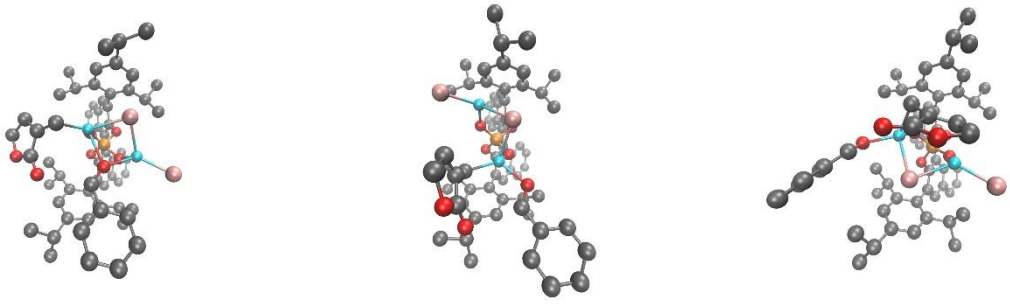

14γ-sim. (Γ) **14ν-ma (N)** **14ν-2-ma (N2)**

Figure SI19: Rendered structures of **14γ-int-ma**, **14γ-int1-mi**, **14γ-int2-mi**, **14ν-ma**, **14γ-sim.** and **14ν-2-ma**; coordination patterns are denoted in brackets

From Table SI17, the lowest energy pathways were selected based on both the energies of the educts and the height of the energetic barriers. Moreover, in order to be as accurate as possible, we decided to investigate all pathways included in Table SI17 which correspond to the minor enantiomer. Thus, the pathways starting from **14γ-int-ma**, **14ν-ma**, **14γ-int2-mi**, **14γ-sim.** and **14ν-2** were investigated in

more detail by employing the COSMO model and calculating single points at higher levels of theory; Tables SI21 to SI29 summarize the corresponding data.

As can be easily seen from Tables SI18 to SI26, the pathway starting from **14γ-int-ma** (**Γ** coordination pattern) remains the lowest energy pathway for all methods employed. Which of the pathways starting from **14γ-int2-mi**, **14γ-sim.-mi** and **14ν-2-mi** and leading to the the experimentally non-observed enantiomer exhibits the lowest energetic barrier varies depending on the method used. However, independent of the method, these barriers are in all cases considerably higher than the pathway leading to the experimentally observed enantiomer (starting from **14γ-int-ma**).
The data used to construct the energy diagram in Figure SI22 in the main text of the manuscript are marked in bold and colored in blue. The TS presented in this section lie lower in energy than the ones in the alternative pathways discussed below.

- The pathway starting from **14γ-int-ma** (major enantiomer) is referred to as pathway ***fav.*** (favored) in the main text.
- The pathway starting from **14γ-sim.-mi** (minor enantiomer) is referred to as pathway ***dis.*** (disfavoured) in the main text.

Table SI18: ΔG data for the selected lowest energy pathways at the different levels of theory referenced to the ISR; coordination patterns are denoted in brackets

		RI-PBE-D3/ def2-SVP			RI-PBE-D3/ def2-TZVPPD			B3LYP-D3/ def2-TZVPPD			DLPNO-CCSD(T)/ cc-pVTZ		
	from	**Ed**	**TS**	**prod**	**Ed**	**TS**	**prod**	**Ed**	**TS**	**prod**	**Ed**	**TS**	**prod**
major	**14γ-int (Γ)**	-172.7	-152.8	-180.9	-113.5	-89.2	-113.8	-139.8	-95.4	-126.8	-124.1	-83.5	---
	14ν (N)	-183.1	-142.6	-159.2	-121.2	-79.8	-99.6	-147.5	-83.7	-112.7	---	---	---
minor	**14γ-int2 (N)**	-189.6	-150.0	-174.0	-120.3	-79.1	-102.5	-149.8	-87.6	-122.6	-134.5	-77.5	---
	14γ-sim. (Γ)	-187.1	-139.3	-171.4	-126.3	-85.5	-109.6	-150.8	-91.5	-123.1	-133.4	-77.1	---
	14ν-2 (N2)	-182.0	-132.4	-139.6	-124.0	-78.5	-81.7	-141.3	-83.8	-112.3	---	---	---

Table SI19: ΔG+COSMO data for the selected lowest energy pathways at the different levels of theory referenced to the ISR; coordination patterns are denoted in brackets

		RI-PBE-D3/ def2-SVP			RI-PBE-D3/ def2-TZVPPD			B3LYP-D3/ def2-TZVPPD			DLPNO-CCSD(T)/ cc-pVTZ		
	from	**Ed**	**TS**	**prod**	**Ed**	**TS**	**prod**	**Ed**	**TS**	**prod**	**Ed**	**TS**	**prod**
major	**14γ-int (Γ)**	-139.0	-120.3	-151.3	-77.8	-55.0	-82.1	-104.1	-61.2	-95.1	**-88.3**	**-49.3**	**---**
	14ν (N)	-149.7	-111.1	-129.4	-86.0	-46.7	-68.3	-112.3	-50.6	-81.5	---	---	---
minor	**14γ-int2 (N)**	-154.9	-117.4	-145.3	-83.4	-44.6	-71.7	-112.9	-53.1	-91.8	-97.5	-43.0	---
	14γ-sim. (Γ)	-152.1	-108.8	-141.3	-89.0	-53.3	-77.8	-113.4	-59.3	-91.4	**-96.0**	**-45.0**	**---**
	14ν-2 (N2)	-151.1	-94.6	-109.3	-91.5	-38.3	-49.1	-108.7	-43.6	-79.7	---	---	---

Table SI20: ΔG data for the selected lowest energy pathways at the different levels of theory referenced to **14j-ma** (**B2**; see chapter 3.9.2.3 herein); coordination patterns are denoted in brackets

		RI-PBE-D3/ def2-SVP			RI-PBE-D3/ def2-TZVPPD			B3LYP-D3/ def2-TZVPPD			DLPNO-CCSD(T)/ cc-pVTZ		
	from	**Ed**	**TS**	**prod**	**Ed**	**TS**	**prod**	**Ed**	**TS**	**prod**	**Ed**	**TS**	**prod**
major	**14γ-int (Γ)**	19.5	39.5	11.3	14.8	39.2	14.5	31.5	75.9	44.5	28.0	68.6	---
	14v (N)	9.1	49.6	33.0	7.2	48.5	28.7	23.8	87.6	58.6	---	---	---
minor	**14γ-int2 (N)**	2.7	42.3	18.2	8.0	49.2	25.8	21.5	83.7	48.7	17.6	74.6	---
	14γ-sim. (Γ)	5.1	52.9	20.9	2.0	42.9	18.7	20.5	79.8	48.2	18.7	75.0	---
	14v-2 (N2)	10.2	59.8	52.6	4.3	49.8	46.6	30.0	87.5	59.0	---	---	---

Table SI21: ΔG+COSMO data for the selected lowest energy pathways at the different levels of theory referenced to **14j-ma** (**B2**; see chapter 3.9.2.3 herein); coordination patterns are denoted in brackets

		RI-PBE-D3/ def2-SVP			RI-PBE-D3/ def2-TZVPPD			B3LYP-D3/ def2-TZVPPD			DLPNO-CCSD(T)/ cc-pVTZ		
	from	**Ed**	**TS**	**prod**	**Ed**	**TS**	**prod**	**Ed**	**TS**	**prod**	**Ed**	**TS**	**prod**
major	**14γ-int (Γ)**	23.1	41.8	10.8	19.4	42.2	15.1	36.1	79.0	45.1	**32.6**	**71.7**	**---**
	14v (N)	12.4	51.0	32.7	11.2	50.5	28.9	27.9	89.6	58.7	---	---	---
minor	**14γ-int2 (N)**	7.2	44.7	16.8	13.8	52.6	25.5	27.3	87.1	48.4	23.5	78.0	---
	14γ-sim. (Γ)	10.0	53.3	20.8	8.2	43.9	19.4	26.8	80.9	48.8	**25.0**	**76.0**	**---**
	14v-2 (N2)	11.0	67.5	52.9	5.7	58.9	48.1	31.5	96.6	60.5	---	---	---

Table SI22: ΔE+ZPE for the selected lowest energy pathways at the different levels of theory referenced to the ISR; coordination patterns are denoted in brackets

		RI-PBE-D3/ def2-SVP			RI-PBE-D3/ def2-TZVPPD			B3LYP-D3/ def2-TZVPPD			DLPNO-CCSD(T)/ cc-pVTZ		
	from	**Ed**	**TS**	**prod**	**Ed**	**TS**	**prod**	**Ed**	**TS**	**prod**	**Ed**	**TS**	**prod**
major	**14γ-int (Γ)**	-286.7	-271.1	-297.0	-227.5	-207.5	-230.0	-253.8	-213.8	-243.0	-238.1	-201.8	---
	14v (N)	-293.9	-255.7	-270.7	-232.0	-192.9	-211.0	-258.3	-196.8	-224.2	---	---	---
minor	**14γ-int2 (N)**	-305.8	-272.9	-293.9	-236.5	-202.0	-222.4	-266.0	-210.6	-242.5	-250.7	-200.5	---
	14γ-sim. (Γ)	-299.1	-252.4	-287.8	-238.3	-198.5	-226.0	-262.8	-204.5	-239.6	-245.4	-190.2	---
	14v-2 (N2)	-286.1	-245.8	-253.8	-228.1	-191.9	-196.0	-245.3	-197.2	-226.5	---	---	---

Table SI23: ΔE+ZPE+COSMO for the selected lowest energy pathways at the different levels of theory referenced to the ISR; coordination patterns are denoted in brackets

		RI-PBE-D3/ def2-SVP			RI-PBE-D3/ def2-TZVPPD			B3LYP-D3/ def2-TZVPPD			DLPNO-CCSD(T)/ cc-pVTZ		
	from	Ed	TS	prod	Ed	TS	prod	Ed	TS	prod	Ed	TS	prod
major	14γ-int (Γ)	-253.0	-238.7	-267.4	-191.8	-173.4	-198.2	-218.0	-179.6	-211.2	-202.3	-167.7	---
major	14ν (N)	-260.6	-224.2	-240.9	-196.9	-159.8	-179.7	-223.2	-163.7	-192.9	---	---	---
minor	14γ-int2 (N)	-271.1	-240.3	-265.2	-199.6	-167.5	-191.6	-229.1	-176.1	-211.7	-213.7	-166.0	---
minor	14γ-sim. (Γ)	-264.1	-221.8	-257.8	-201.0	-166.3	-194.3	-225.4	-172.4	-207.9	-208.0	-158.0	---
	14ν-2 (N2)	-255.1	-208.0	-223.5	-195.5	-151.7	-163.4	-212.8	-157.0	-193.9	---	---	---

Table SI24: ΔE+ZPE for the selected lowest energy pathways at the different levels of theory referenced to **14j-ma** (**B2**; see chapter 3.9.2.3 herein); coordination patterns are denoted in brackets

		RI-PBE-D3/ def2-SVP			RI-PBE-D3/ def2-TZVPPD			B3LYP-D3/ def2-TZVPPD			DLPNO-CCSD(T)/ cc-pVTZ		
	from	Ed	TS	prod	Ed	TS	prod	Ed	TS	prod	Ed	TS	prod
major	14γ-int (Γ)	16.2	31.8	5.9	11.5	31.5	9.1	28.2	68.3	39.0	24.7	61.0	---
major	14ν (N)	9.0	47.2	32.2	7.0	46.1	28.0	23.7	85.2	57.8	---	---	---
minor	14γ-int2 (N)	-2.8	30.0	9.0	2.5	37.0	16.6	16.0	71.4	39.5	12.1	62.3	---
minor	14γ-sim. (Γ)	3.8	50.6	15.1	0.7	40.6	13.0	19.2	77.5	42.4	17.4	72.7	---
	14ν-2 (N2)	16.8	57.1	49.1	10.9	47.1	43.1	36.7	84.8	55.5	---	---	---

Table SI25: ΔE+ZPE+COSMO for the selected lowest energy pathways at the different levels of theory referenced to **14j-ma** (**B2**; see chapter 3.9.2.3 herein); coordination patterns are denoted in brackets

		RI-PBE-D3/ def2-SVP			RI-PBE-D3/ def2-TZVPPD			B3LYP-D3/ def2-TZVPPD			DLPNO-CCSD(T)/ cc-pVTZ		
	from	Ed	TS	prod	Ed	TS	prod	Ed	TS	prod	Ed	TS	prod
major	14γ-int (Γ)	19.8	41.1	5.4	16.1	34.5	9.7	32.9	71.3	39.7	29.4	64.0	---
major	14ν (N)	12.2	48.7	31.9	11.1	48.1	28.2	27.7	87.2	58.0	---	---	---
minor	14γ-int2 (N)	1.7	32.5	7.6	8.3	40.4	16.3	21.8	74.9	39.2	18.0	65.7	---
minor	14γ-sim. (Γ)	8.7	51.0	15.1	7.0	41.6	13.6	25.5	78.6	43.0	23.7	73.7	---
	14ν-2 (N2)	17.7	64.9	49.3	12.4	56.3	44.6	38.1	94.0	57.0	---	---	---

Table SI26. Thermochemical data ([kJ/mol] or [J/molK])

	from	Ed			TS			prod		
		ZPE	**S**	**G**	**ZPE**	**S**	**G**	**ZPE**	**S**	**G**
major	**14γ-int (Γ)**	2983	1.6259	2711.35	2984	1.5994	2716.75	2991	1.6058	2721.50
	14ν (N)	2985	1.6361	2710.24	2984	1.6188	2711.47	2989	1.6268	2714.84
minor	**14γ-int2 (N)**	2986	1.6137	2716.57	2986	1.5808	2723.30	2991	1.5934	2725.28
	14γ-sim. (Γ)	2985	1.6337	2711.36	2983	1.6201	2710.38	2990	1.6082	2720.82
	14ν-2 (N2)	2983	1.6637	2701.41	2983	1.6204	2710.74	2991	1.6166	2719.60

The rendered structures of **14γ-int-ma**, **14γ-int2-mi**, **14ν-ma** and **14γ-sim.-mi** are shown in Figure SI20. As discussed in the main text of the paper, the alignment of the two substrates is considerably worse in **14γ-sim.-mi** than in **14γ-int-ma**. All attempts to improve the alignment of the two substrates in **14γ-sim.-mi** reverted back to the "open" geometry depicted in Figure SI20, hinting that a geometry in which the two substrates are located closer to each other is disfavored.

Moreover, the initial geometry of **14γ-int1-mi** before geometry optimization was constructed (analogously to **14γ-int-ma**) in such a way that it exhibits the **Γ** coordination pattern (vide supra). However, upon geometry optimization, the coordination of the carbonyl group of the aldehyde to the second zinc ion (as in **14γ-int-ma**) opened and was replaced the coordination of the second zinc ion to one of the phenyl moieties of the catalyst, leading to the **N** coordination pattern (compare Figure SI18 above). This does not happen for **14γ-int-ma** as the coordination to the phenyl moiety is blocked by the isopropyl substituents. Subsequently, the reaction pathway was calculated between **14γ-int1-mi** and the corresponding product **15γ-mi**, leading to intermediate **14γ-int2-mi**, which geometrically is very similar to **14γ-int1-mi** (**N** coordination pattern, see Figure SI19). In the thereafter calculated reaction pathway between **14γ-int2-mi** and **15γ-mi**, structure **γ-transient-mi**, which exhibits excellent alignment between the two substrates as well as the **Γ** coordination patter, appears as a transient geometry but not as an intermediate. This provides further indication that for the minor enantiomer, contrary to the major enantiomer, it is not possible to have both – good alignment of the two substrates as well as the **Γ** coordination pattern – meaning that a perfect analogue to **14γ-int-ma** does not exist and constituting a further explanation of the observed enantiomeric excess.

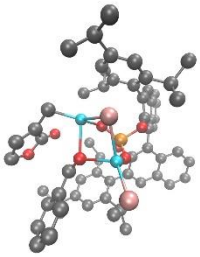

14γ-int-ma (Γ)

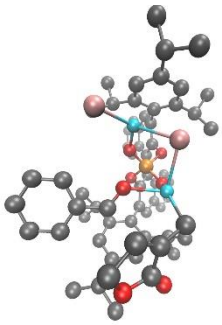

14γ-int2-mi (N)

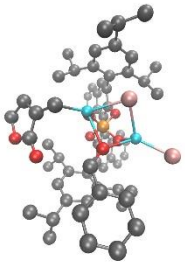

14γ-sim.-mi (Γ)

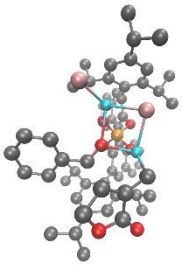

γ-mi-transient (Γ)

Figure SI20: Rendered structures of **14γ-int-ma**, **14γ-int2-mi**, **14γ-sim.-mi**, and **γ-mi-transient**

The complete proposed mechanistic cycle is depicted in Figure SI21, proceeding via initial formation of **B1** (as discussed in the main text of the paper and in the subsequent sections, and is also labelled **13j-ma**).

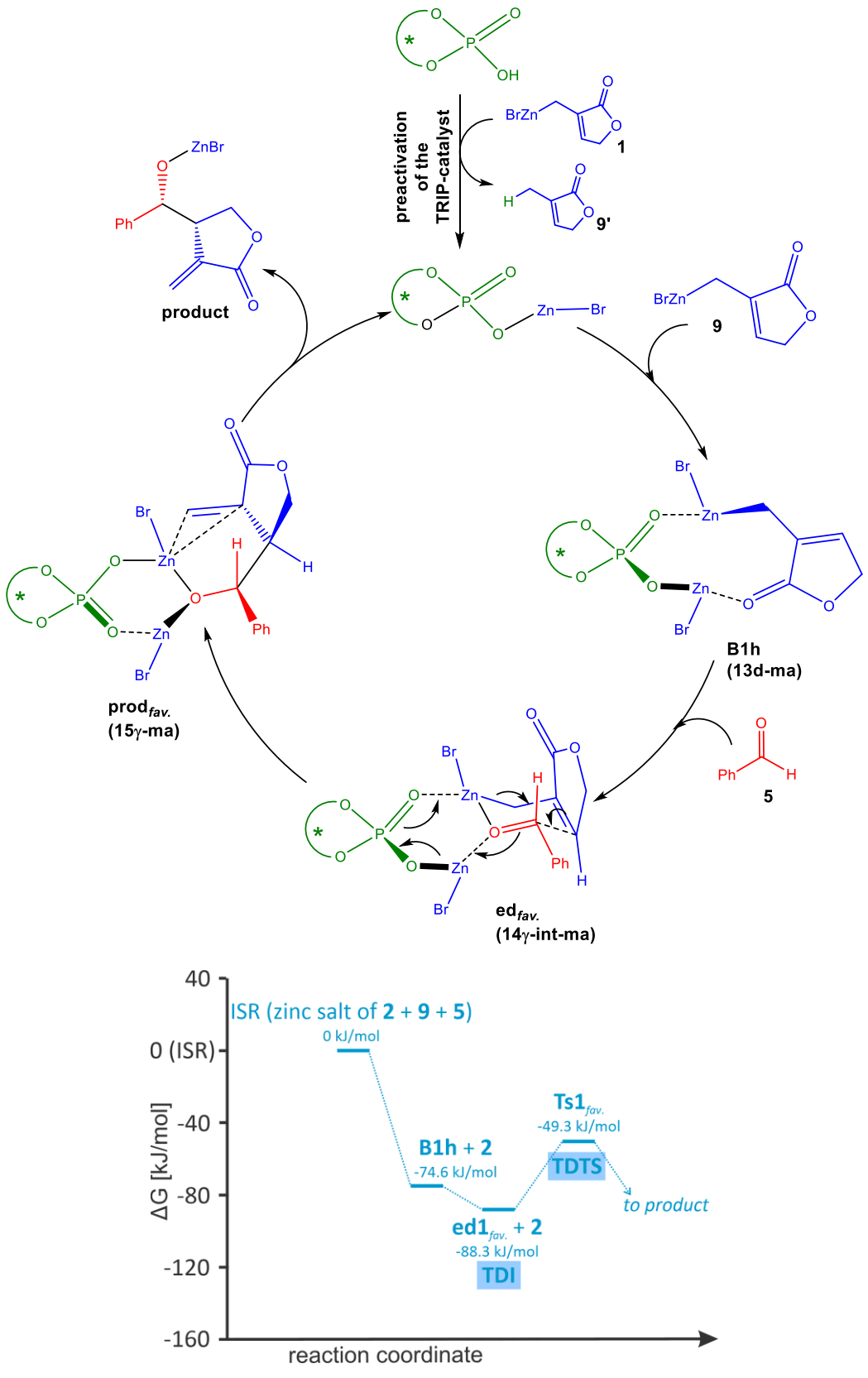

Figure SI21: Proposed mechanistic cycle for the TRIP-catalyzed reaction (top) and energetic representation of the full reaction profile starting from the zinc salt of **2** and the ISR and ending with the product formation (bottom); all presented data are given on the DLPNO-CCSD(T)/cc-pVTZ ΔG+COSMO level; the refence point (0 kJ/mol) represents the indefinitely separated reactants [the

zinc salt of TRIP, reagent **9** and benzaldehyde (**5**)]; TDI … TOF determining intermediate; TDTS … TOF determining transition state.[6]

3.9. Other Pathways from complexes **14** (educts) to **15** (products)

An alternative model explaining the experimentally observed enan-tiomeric excess, is described in this section. Subsection 3.9.1 provides an overview and the discussion of the matter and subsection 3.9.2 deals with a more detailed description of the performed calculations.

3.9.1. Overview and discussion

Formation of the educt complexes for the allylation process

The insertion of benzaldehyde (**5**) into **B1** gives rise to several possible geometries due to different coordination patterns (complexes **14a-t**, which were relabelled as described in the subsection 3.9.2). They can be attributed to either the experimentally observed enantiomer (path **B**, see Figure SI22) or the experimentally non-observed one (path **A**, see Figure SI22).

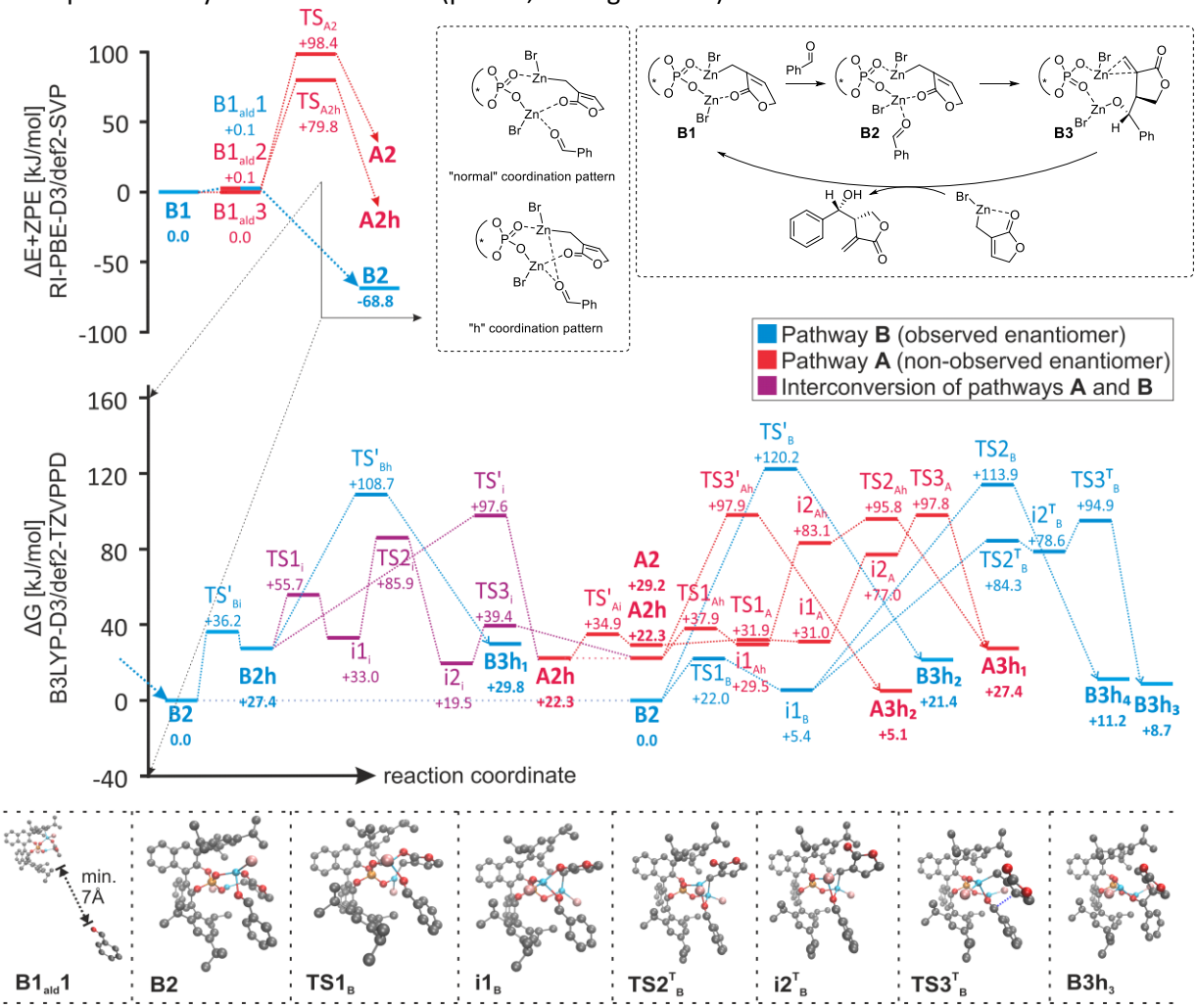

Figure SI22. Upper left corner: Energy diagram (RI-PBE-D3/def2-SVP+COSMO) for the association of the reagent to complex **B1** (energies given in ΔE+ZPE rel. to ISR, for the reasons discussed in the text); top in the middle: Definition of the "**h**" coordination pattern; upper right corner: Proposed mechanistic cycle; middle: Energy diagram (B3LYP-D3/def2-TZVPPD+COSMO) of the relevant pathways starting from **B2** [TS = transition state, I = intermediate, ■ blue refers to Pathway **B** (observed enantiomer), ■ red refers to Pathway **A** (non-observed enantiomer), ■ purple: interconversion between pathway **B** and **A**; a prime indicates a path without intermediates, a superscript "T" marks a pathway involving transmetalation between the two zinc atoms, the missing transition states are without any energetic barrier; different conformations of **A3h** and **B3h** are denoted **A3h**$_{1,2}$ and **B3h**$_{1,2,3,4}$]; bottom: Rendered structures of pathway **B** (hydrogen atoms were omitted for clarity).[7]

In order to evaluate as many conformers as possible, we proceeded treating the backbone of the catalyst as a simplified biphenol structure. However, in the resulting geometries the substrate molecules ended up exactly at positions where the phenyl groups of the catalyst would be located.

Hence, we had to go back to the large TRIP catalyst system. Using this approach, the most stable complexes identified for each enantiomer are **B2** (**14j-ma**) and **A2h**, and the second most stable complexes are **B2h** and **A2** [based on the ΔG values (see top of Figure SI22; **h** refers to the coordination pattern depicted in Figure SI22]. The investigated starting points are labelled **B1**, **A1**, **A1h** and **B1h** as their minima could be obtained by optimization of their respective **"2"** analogues after removing the aldehyde moiety, respectively.

Next, the association pathways of aldehyde **5** into complexes **B1**, **A1h** and **B1h** were calculated. The starting complex **A1** ($\Delta\Delta G_{B1}$ = 62.1 kJ/mol) was not considered due to its high energy. Complex **B1** (ΔG = -115.2 kJ/mol rel. to ISR) was taken as a reference for the energies of the association pathways, setting it to zero kJ/mol. Upon addition of the aldehyde to **B1** three very similar intermediates can be formed - **B1$_{ald}$1**, **B1$_{ald}$2** and **B1$_{ald}$3**. These intermediates lie at approximately the same energy (see Figure SI22) as **B1** when looking at the ΔE+ZPE values at 0 K, but +30.3 to +45.7 kJ/mol higher in energy than **B1** when considering the ΔG values. The ΔE+ZPE values of these adducts exhibit only a small standard deviation but obviously a rather large one for the ΔG values. Here, the hyperplane is very flat, and the investigated complexes are rather large (141 atoms). As a result, we were in some cases not able to remove all the imaginary modes necessary. For these reasons the $\Delta\Delta G^{TS}$ values need to be treated with caution here and we rather consider the ΔΔE+ZPE values being representative for the association barriers (see Figure SI22, top diagram).

For the $\Delta\Delta E_{B1}^{TS} + ZPE$ data, **B1$_{ald}$1** converts to complex **B2** without any barrier and is energetically highly favored (for ΔΔG values see ESI, Tables SI47 to SI54). The high preference for **B2** becomes apparent by inspecting the structures (Figure SI23) of complexes **A1/B1** and **A1h/B1h**: Structure **B1h** has a counterpart in **A1h**. Both require large geometrical changes to bind the approaching aldehyde. This leads to high energy transition states (regardless of using ΔE+ZPE or ΔG values). In contrast, complex **B1** requires only slight structural changes of the lactone to create space for the coordination of the aldehyde (Figure SI23). The coordination of the phenyl moiety of the catalyst to the zinc(II) ion – as in complex **B1** (interaction of the cation with the π-system of the aromat) – is energetically not feasible for the non-observed enantiomer complex **A1** for geometric reasons (for details see ESI, Table SI57). The zinc atom is coordinated to the P-O moiety further away from the aromatic ring and the coordination to the second, closer ring is blocked by the isopropyl groups and the orientation of the lactone. This results in a different geometry and significantly raises the energy for **A1**. Therefore, an easy association is found only for path **B**, which leads to **B2** as the predominantly formed complex and finally to the observed enantiomer product **B3.** The associations are all exothermic/exergonic (e.g. association of the aldehyde **5** to **B1** to give **B2** yields ΔG = -21.4 kJ/mol).

Interconversion between pathways B and A versus product formation of the observed enantiomer

The interconversion of pathway **B** to pathway **A** during the aldehyde insertion (**TS$_{A2}$** or **TS$_{A2h}$**, see Figure SI22, top energy diagram) involves high energy transition states ($\Delta\Delta E_{B1}^{TS} + ZPE$ = +79.8 kJ/mol and $\Delta\Delta E_{B1}^{TS} + ZPE$ = +98.4 kJ/mol). On the other hand, the energy difference between presumably formed **B2** and **A2h** is only 22.3 kJ/mol. Therefore, an interconversion at this later stage has to be considered

as an alternative option as well (Figure SI22, large energy diagram, purple lines). Complex **B2** (ΔG = -115.2 kJ/mol rel. to ISR) was taken as a reference for the energies of this interconversion and the reaction pathways, setting it to zero kJ/mol. The hyperplane appears very flat again, but in general the ΔG values are reliable here within the error of the method. The overall picture outlined remains the same also for the ΔE+ZPE data (Tables SI38-45 and SI60-61).

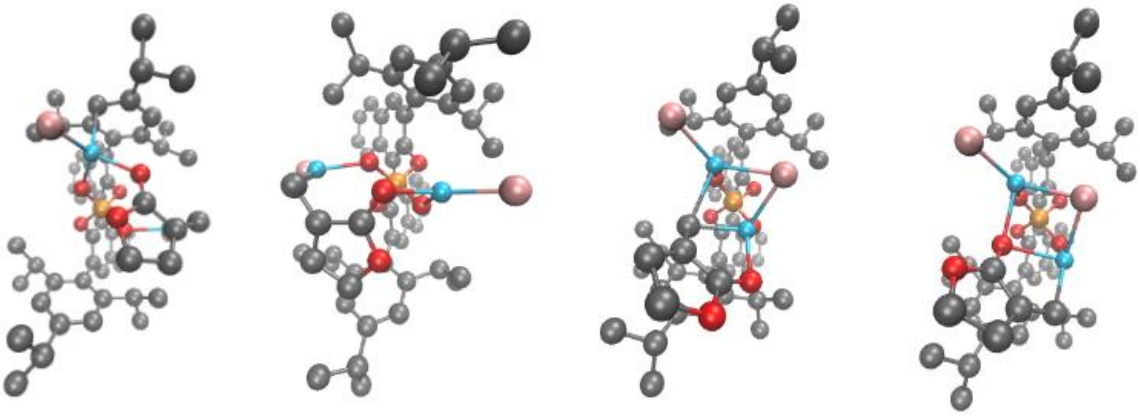

B1 **A1** **B1h** **A1h**

Figure SI23. Rendered structures of **B1, A1**, **B1h** and **A1h** (hydrogen atoms were omitted for clarity)[7]

Complexes belonging to the same enantiomer (**B2**/**B2h** and **A2**/**A2h**) readily interconvert in a single step (**TS'$_{Bi}$** and **TS'$_{Ai}$**, see Figure SI22). The interconversion from pathway **B** to **A** is more difficult: The two lowest routes proceed first to **B2h** and thereafter either via a high energy transition state (denoted **TS$_i$**$'$; $\Delta\Delta G_{B2}^{TS}$ = +97.6 kJ/mol) or via many intermediates with high energies [highest barrier: $\Delta\Delta G_{B2}^{TS}$ = +85.9 kJ/mol (**TS2$_i$**)]. DLPNO-CCSD(T)/cc-pVTZ single-point calculations – performed for the highest barriers – confirm these findings (see ESI, Tables SI60 and SI61).

Starting from the four complexes **B2**, **B2h**, **A2** and **A2h** we calculated the pathways to all possible product complexes (generated from all screened educt-complexes) and identified the pathways with the lowest barriers. The interconversion of pathways **A** and **B** lies 9.0 kJ/mol lower than the barrier for the conversion of **B2** to the favored and observed enantiomer **B3h$_4$** and **B3h$_3$** ($\Delta\Delta G_{B2}^{TS}$ = +113.9 kJ/mol and +94.9 kJ/mol). Both **A2** and **A2h** convert under similar energetic barriers to the disfavored enantiomer **A3h$_1$** [**TS3$_A$** ($\Delta\Delta G_{B2}^{TS}$ = +97.8 kJ/mol) and **TS2$_{Ah}$** ($\Delta\Delta G_{B2}^{TS}$ = +95.8 kJ/mol), respectively].

Nevertheless, **B2** represents the thermodynamic sink in all calculation results and according to the energetic barriers converts into intermediate **i1$_B$** predominantly. From the latter there are two possible pathways: the backward reaction to **B2** which demonstrates the equilibrium between these two intermediates (**B2** and **i1$_B$**; ΔG = +5.4 kJ/mol, $\Delta\Delta G_{B2}^{TS}$ = +22.0 kJ/mol) and the irreversible forward reaction (due to subsequent NH_4Cl quench, see main article), forming the C-C bond. The transition states of this pathway are in the same range as the interconversion pathways [highest barrier is ΔΔG = +94.9 kJ/mol (**TS3^T_B**); compare to +85.9 kJ/mol for the interconversion (**TS'$_i$**)] regarding the absolute energies. However, for all alternative scenarios **B2h** needs to be formed first. In comparison with **i1$_B$**, the formation of **B2h** is thermodynamically disfavored by 22.0 kJ/mol (see Figure SI22) and the route to product **A3** requires severe geometric changes, represented by a high number of intermediates. Therefore, most starting material will be present as **B2** and **i1$_B$** and all material is channeled into the observed enantiomer pathway **B** and interconversion from pathway **B** to **A** is not observed.

Therefore, the observed enantioselectivity of the catalytic process would be based on the formation of the energetically highly favored intermediates **B2** and **i1$_B$** in this case, whereas the subsequent C-C bond formation is very similar regarding the energetic barriers for the two pathways **A** and **B** [e.g.: compare **TS3^T_B** ($\Delta\Delta G_{B2}^{TS}$ = +94.9 kJ/mol) to **TS2$_A$** ($\Delta\Delta G_{B2}^{TS}$ = +95.8 kJ/mol)].

Obviously, with intermediates **B2** and **i1$_B$** being favored over the formed product **B3h$_3$** (ΔG = +8.7 kJ/mol), the reaction should not take place, but stop at the intermediates. Therefore, an additional driving force is required (as described for all other allylation processes in this manuscript) to pull the reaction to the product side, namely an NH_4Cl quench. Initially, we observed that NH_4Cl is required for both the uncatalyzed background reaction and for the catalytic reaction. We hypothesized that either the activation of the zinc may be performed by the ammonium salt or the quench of the product species. The high energy of the formed product species hints us to the latter hypothesis and directs the role of NH_4Cl to be the final pull on the equilibrium.

Mechanistic conclusion of alternative mechanistic scenarios – zinc based reagents

We conclude from our mechanistic computational studies that the stereo-determining step in this case would be found already in the coordination of the aldehyde to the preformed complex **B1** forming intermediate **B2**. The rate-determining step is the subsequent allylation process. The latter requires the highest energy input (see Figure SI22), which is reasoned by significant structural rearrangements. The catalytic activity is based on the double activation of the aldehyde by both zinc atoms [Zn-(O=C) distances of **TS3^T_B** = 2.0 Å and 2.3 Å] occurring in the "**h**" coordination pattern (see Figure SI22). This is further corroborated by the lowest pathway for the formation of product **B3** via complex **B2** (for all complexes calculated within this chapter), which proceeds via intermediate **i1$_B$**, establishing the double activation before the C-C bond formation. All relevant product complexes exhibit double coordination of the former aldehyde oxygen. Dissociation of product **10** and the quench by the NH_4Cl proton followed by addition of another equivalent of **9** yields the starting point **B1** again and closes the catalytic cycle. For the reaction to proceed, a final pull on the equilibrium is required, as the formed intermediate products (e.g. **B3h$_3$**) lie higher in energy than the proceeding intermediates **B2** and **i1$_B$**. This explains the role of the employed NH_4Cl, which – by protonation of the zinc alcoholate **B3h$_3$** – yields the required driving force.

Comparison to the uncatalyzed reaction

In order to verify the catalytic activity, the energy barrier of the uncatalyzed background reaction was assessed. Structures for the Zimmermann-Traxler like chair (ΔG = +2.9 kJ/mol rel. to ISR) and boat adducts (ΔG = +4.0 kJ/mol rel. to ISR) of the reactants were calculated and their subsequent conversion to the products was probed (see Tables SI04 to SI7). The transition state for the chair conformer was found with a ΔG = +67.3 kJ/mol rel. to ISR. By that result, the uncatalyzed reaction is predicted to be faster than the catalyzed and the racemate should be obtained. However, the catalysis is preceeded by the *in-situ* formation of the allylzinc reagent. Taking into account that this reaction is a heterogeneous transformation, it may lead to low levels of the zinc reagent **9**. Indeed, we could determine max. 8% of reagent **9** during the reaction, which is below the catalyst loading (10 mol-%, for details see supporting information, chapter 2.4.2). As simple coordination of **9** to the TRIP salt is highly favored (ΔG = -115.2 kJ/mol rel. to ISR), all formed amounts of **9** are coordinated by the catalyst preventing the formation of the educt complex for the uncatalyzed reaction. This fact renders the TSs described in this chapter still a possibility for the reaction. Nevertheless, the TSs assessed in chapter 3.6.3. and the main article are of lower energies.

3.9.2. Detailed description of alternative pathways

From the mechanistic cycles in Figures SI12 and SI13, there exist many possibilities of different coordination patterns in complex **14** [a reminder of the used labelling: The educt complexes are labelled **10-(a-f)-ma/mi** (mechanism involving one zinc atom), **14(a-l)-ma/mi** (mechanism involving two-zinc atoms with the coordination of the lactone carbonyl group) and **14(m-t)-ma/mi** (mechanism involving two-zinc atoms without the coordination of the lactone carbonyl group); "ma" and "mi" refer to complexes corresponding to the experimentally favored (major) and disfavored (minor) enantiomer]. The coordination patterns corresponding to the letters are given in Figure SI24.

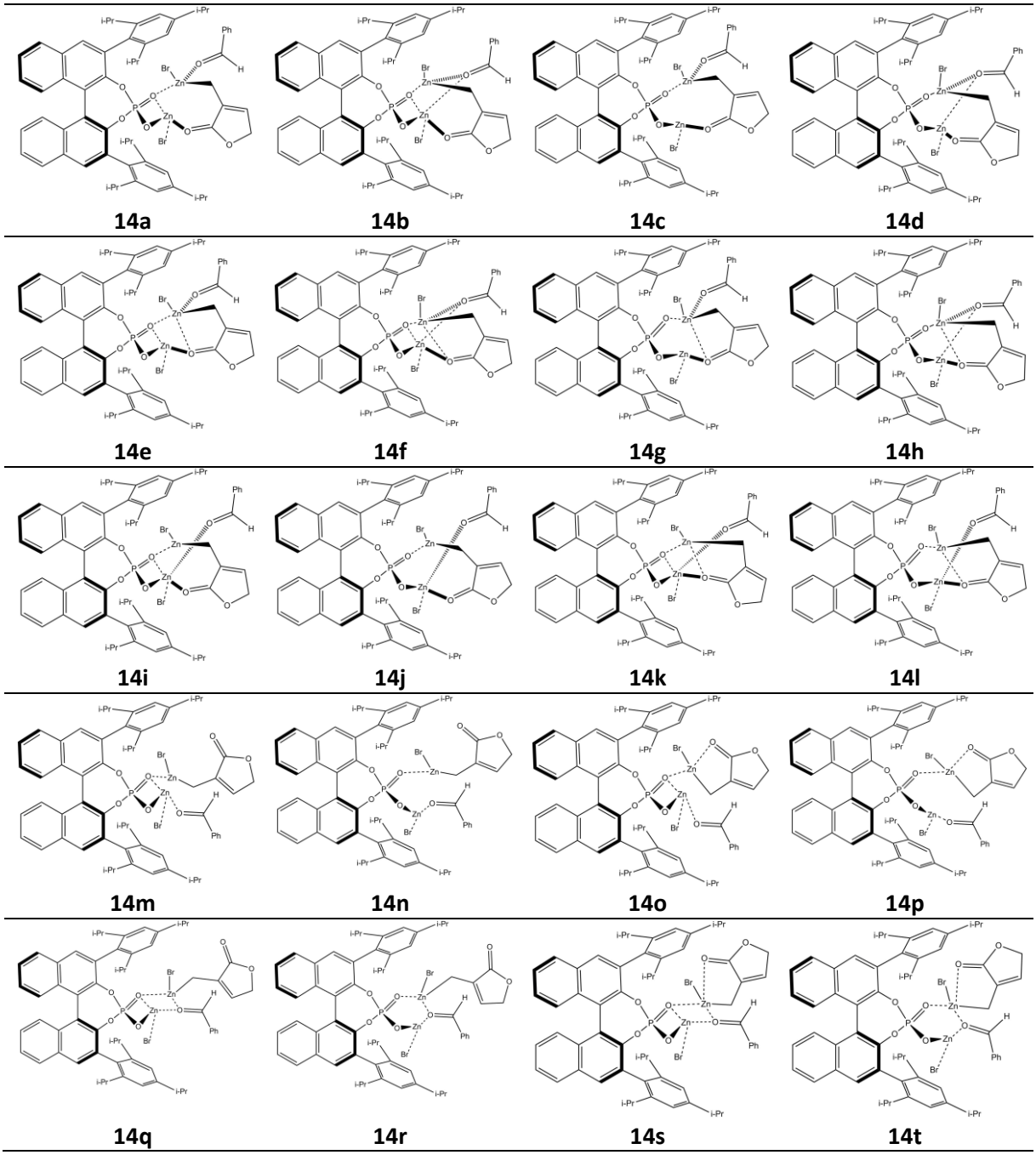

Figure SI24a. Possible coordination patterns of complex **7** (depicted for one enantiomer only)

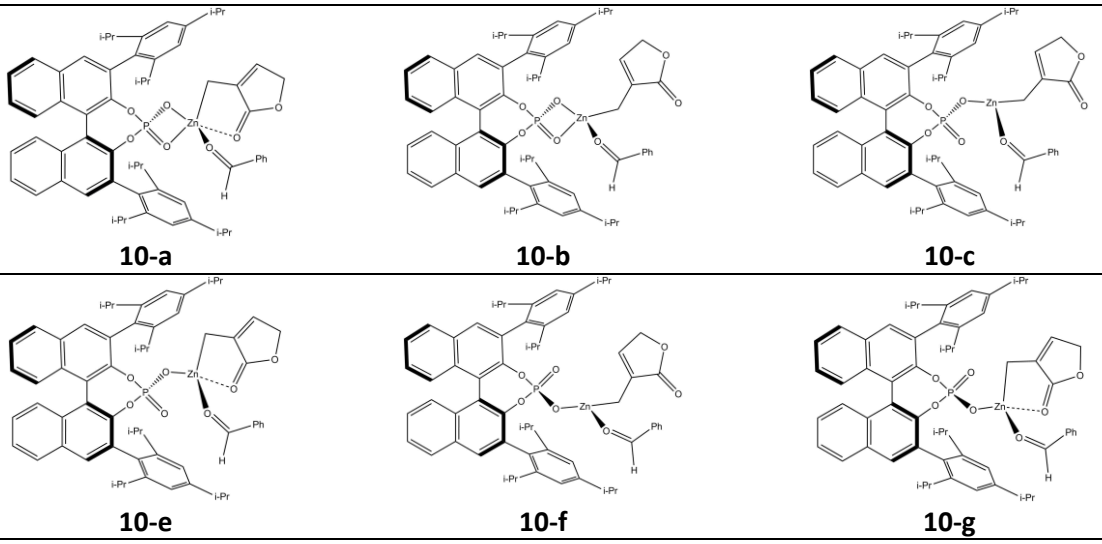

Figure SI24b. Possible coordination patterns of complex **10** (depicted for one enantiomer only)

All complex geometries were optimized in order to determine which coordination patterns have a local energy minimum associated. The coordination patterns which were retained after geometry optimizations are listed in Tables SI27 and SI28.

Table SI27. Electronic energies [kJ/mol] for complexes **10**

complex	Δ to ISR	Δ to 14j-ma
minor		
10-a	-113.2	216.6
10-b	-115.7	214.0
10-c	-123.9	205.9
10-d	-114.6	215.2
10-f	-111.9	217.9
major		
10-a	-108.8	221.0
10-b	-110.6	219.2
10-f	-109.1	220.7

Table SI28. Electronic energies [kJ/mol] for complexes **14**

complex	Δ to ISR	Δ to 14j-ma
minor		
14a	-274.6	37.7
14c	-283.7	28.7
14d	-286.3	26.0
14j	-293.7	18.6
14l	-270.3	42.1
14o	-209.5	102.9
14q	-232.1	80.2
14r	-254.1	58.2
14s	-224.4	88.0
major		
14b	-267.0	45.3
14c	-271.2	41.1
14d	-294.5	17.8
14j	-312.3	0.0
14l	-273.5	38.8
14n	-262.2	50.1
14o	-227.4	85.0
14p	-212.5	99.9
14q	-232.9	79.4
14r	-247.8	64.5

Table SI29. Electronic energies [kJ/mol] for complexes **15**

complex	Δ to ISR	Δ to 14j-ma
minor		
15a	-277.9	34.4
15c	-334.2	-21.9
15d	-338.2	-25.9
15j	-247.3	65.0
15l	-295.3	17.0
15o	-233.8	78.6
15q	-309.5	2.8
15r	-336.0	-23.7
15s	-330.2	-17.8
major		
15b	-266.2	46.2
15c	-281.9	30.5
15d	-345.4	-33.0
15d-2	-328.9	-16.6
15j	-315.3	-2.9
15l	-256.7	55.7
15n	-334.2	-21.9
15o	-292.1	20.3
15p	-274.6	37.8
15q	-327.3	-15.0
15r	-354.2	-41.8
15r-2	-316.3	-3.9

Table SI30. Electronic energies [kJ/mol] for complexes **11**

complex	Δ to ISR	Δ to 14j-ma
minor		
11a	-91.4	238.4
11b	-66.1	263.7
11c	-98.7	231.1
11d	-91.8	238.0
11f	-62.2	267.6
major		
11a	-92.5	237.3
11b	-116.1	213.7
11f	-126.8	203.0

Precomplexes of the kind of **10** lie around 100-200 kJ/mol higher in energy than complexes of the coordination pattern of **14**. Concerning complexes **14**, the structures exhibiting coordination of the lactone carbonyl group [**14(a-l)**] do lie approximately 50-100 kJ/mol lower in energy than the ones without [**14(m-t)**], indicating the expected extra stabilization of this dative bond. Hereafter, from every remaining complex (i.e. the ones exhibiting a coordination corresponding to a local minimum) the product structures were constructed and optimized. The resulting electronic energies of these product structures are given in Tables SI29 and SI30. It is important to point out that the labelling of the product complexes **15** and **11** does *not* imply any coordination pattern, in contrast to educt complexes **14** and **10**. It is *purely* an indication which educt complex is the origin of the geometry.

3.9.2.1. ΔG+COSMO values for the complexes of Tables SI28 and SI29

Table SI31. ΔG+COSMO values [kJ/mol] for complexes **14**

complex	Δ to ISR	Δ to 14j-ma
minor		
14a	-125.9	36.2
14c	-131.9	30.2
14d	-141.4	20.8
14j	-139.2	23.0
14l	-131.1	31.0
14o	-73.8	88.3
14q	-84.7	77.5
14r	-108.8	53.3
14s	-74.7	87.5
major		
14b	-126.3	35.8
14c	-128.4	33.8
14d	-141.4	20.8
14j	**-162.1**	**0.0**
14l	-121.2	40.9
14n	-107.7	54.5
14o	-85.7	76.4
14p	-65.7	96.4
14q	-83.8	78.3
14r	-108.8	53.3

Table SI32. ΔG+COSMO values [kJ/mol] for complexes **15**

complex	Δ to ISR	Δ to 14j-ma
minor		
15a	-108.1	54.1
15c	-150.8	11.4
15d	-164.3	-2.2
15j	-88.1	74.0
15l	-130.7	31.5
15o	-75.2	86.9
15q	-142.8	19.3
15r	-167.4	-5.3
15s	-157.9	4.2
major		
15b	-109.3	52.9
15c	-116.3	45.9
15d	-173.1	-11.0
15d-2	-155.5	6.6
15j	-162.4	-0.3
15l	-79.8	82.3
15n	-160.7	1.4
15o	-124.9	37.3
15p	-106.0	56.1
15q	-167.2	-5.1
15r	-178.8	-16.7
15r-2	-136.9	25.2

3.9.2.2. ΔE+ZPE+COSMO values for complexes from Tables SI28 and SI29

Table SI33. ΔE+ZPE+COSMO values [kJ/mol] for complexes **14**

complex	Δ to ISR	Δ to 14j-ma
minor		
14a	-234.8	38.0
14c	-246.9	25.9
14d	-248.5	24.3
14j	-257.9	14.9
14l	-235.7	37.1
14o	-177.6	95.3
14q	-192.3	80.5
14r	-215.9	56.9
14s	-184.6	88.2
major		
14b	-228.5	44.3
14c	-234.7	38.2
14d	-255.6	17.2
14j	**-272.8**	**0.0**
14l	-236.8	36.0
14n	-222.7	50.1
14o	-196.4	76.5
14p	-178.9	93.9
14q	-192.3	80.5
14r	-214.5	58.3

Table SI34. ΔE+ZPE+COSMO values [kJ/mol] for complexes **15**

complex	Δ to ISR	Δ to 15j-ma
minor		
15a	-225.7	47.2
15c	-277.0	-4.2
15d	-284.2	-11.4
15j	-203.9	68.9
15l	-243.9	29.0
15o	-187.6	85.2
15q	-256.8	16.0
15r	-283.3	-10.4
15s	-278.4	-5.6
major		
15b	-219.9	52.9
15c	-230.9	42.0
15d	-291.3	-18.5
15d-2	-277.0	-4.1
15j	-278.3	-5.4
15l	-204.0	68.8
15n	-285.1	-12.2
15o	-242.2	30.6
15p	-224.6	48.3
15q	-278.2	-5.4
15r	-299.1	-26.3
15r-2	-259.8	13.1

Two products could be obtained for complexes **15d-ma** and **15r-ma**. Again, the structures corresponding to the mechanism, which involves one zinc ion only, are energetically disfavored by 100-200 kJ/mol. Therefore, we concluded that the mechanism with one zinc atom can be ruled out, as it is thermodynamically highly disfavored compared to the mechanism, which involves two zinc ions. For complexes **14** and **15** the ΔG+COSMO values were calculated (see Tables SI31 and SI32). Tables SI35 and SI36 contain the corresponding thermochemical data - the "G" values are the computed corrections added to the electronic energies to obtain the absolute values of the Gibbs free enthalpy.

The four most stable complexes are relabeled in section 3.9.1: **14j-ma** = **B2**, **14d-ma** = **B2h**, **14d-mi** = **A2h** and **14j-mi** = **A2**. The addition of "h" indicates the coordination pattern in Figure SI22 of the supporting information.

Starting from the two most stable structures which lead to the two product enantiomers (**14j** and **14d**) the reaction pathways were calculated to every generated product of the same enantiomer. Intermediates were optimized if present and new pathways to them were calculated, followed by the optimization of the transition state. We report that the optimization of the TSs which lie between intermediates that differ only in conformation turned out difficult as the hyperplane appears to be very flat in these cases.

Table SI35. ZPE [kJ/mol], S [J/molK] and G [kJ/mol] values for complexes **14**

complex	ZPE	S	G
minor			
14a	2983	1.6444	2706.30
14c	2984	1.6199	2713.44
14d	2982	1.6548	2703.50
14j	2983	1.6020	2716.10
14l	2984	1.6589	2702.93
14o	2979	1.6701	2697.17
14q	2982	1.6515	2704.00
14r	2983	1.6497	2704.49
14s	2981	1.6445	2705.29
major			
14b	2982	1.6713	2698.62
14c	2982	1.6574	2702.69
14d	2984	1.6243	2712.65
14j	2983	1.6388	2708.08
14l	2984	1.6198	2713.92
14n	2983	1.6230	2712.41
14o	2980	1.6350	2705.06
14p	2980	1.6249	2707.59
14q	2982	1.6472	2704.86
14r	2981	1.6585	2701.05

Table SI36. ZPE [kJ/mol], S [J/molK] and G [kJ/mol] values for complexes **15**

complex	ZPE	S	G
minor			
15a	2992	1.5997	2723.96
15c	2994	1.5669	2734.60
15d	2993	1.5901	2727.33
15j	2988	1.6126	2718.16
15l	2991	1.6167	2718.59
15o	2990	1.6225	2716.75
15q	2992	1.6143	2720.35
15r	2993	1.6076	2723.22
15s	2991	1.5861	2725.83
major			
15b	2990	1.6294	2715.05
15c	2990	1.6132	2718.98
15d	2994	1.5986	2726.62
15d-2	2991	1.5786	2726.80
15j	2990	1.6022	2720.21
15l	2990	1.5711	2728.62
15n	2992	1.5708	2730.70
15o	2991	1.6045	2722.73
15p	2991	1.5924	2723.95
15q	2991	1.6284	2716.33
15r	2995	1.5879	2729.64
15r-2	2995	1.5755	2732.25

Tables SI37 to SI40 show the data obtained for the calculated pathways given relative to the most stable educt complex **14j-ma**. In the leftmost column the name of the product to which the pathway leads is noted [the enantiomer of the product is implied by the title of the table, for educts corresponding to the minor enantiomer lead to products corresponding to the minor enantiomer (indicated by "mi" for the disfavored (minor) enantiomer and "ma" for favored (major) enantiomer)]. The tables are divided in two sections: The left part contains the obtained gas-phase data while the right part contains the data obtained for the COSMO model. For both, the gas-phase and the COSMO model the electronic energies ("el."), ZPE-corrected energies ("ZPE") and Gibbs free enthalpies ("G") are given. We give a comparison of all these data here to show that the general picture is not dependent on the values chosen. Each of the subdivisions ("el", "ZPE" and "G") is made up of two columns: The energy of the transition states in the left column ("TS") and the energies of the intermediate/product which lies behind this TS in the right column ("I/P"). The tables are to be read in a zig-zag way within the box in the order of the occuring reaction. This means starting with the first transition state of a pathway in the upper left corner of a pathway (= one box) which is followed by the intermediate that lies after this transition state in the upper right corner. The second transition state is the left entry in the line below, followed again by the subsequent intermediate to its right. The last entry of a box (lower right corner) is the energy of the product of the described pathway. Empty cells indicate that the transition state was not calculated for reasons indicated in the footnotes of the tables. The last transition state of each pathway is the transition state in which the C-C bond formation takes place. An entry "nb." stands for "no barrier".

We give here an example for Table SI37 for the pathway leading from **14d-mi** to **15d-mi**: The Gibbs free enthalpy of the first transition state (the one following the educt complex **14d-mi**) obtained for the COSMO model is 29.5 kJ/mol. This TS leads to an intermediate of 21.0 kJ/mol. In the second line the pathway continues: The intermediate is followed by another TS (51.8 kJ/mol) leading to the next intermediate (47.1 kJ/mol). The next TS (57.3 kJ/mol) is the last TS of the reaction, leading to the product (**15d-mi**; -2.2 kJ/mol) via C-C bond formation.

Table SI37. Obtained data [kJ/mol] for the pathways starting from **14d-mi** referenced to **14j-ma**

	GAS						COSMO					
	el.		ZPE		G		el.		ZPE		G	
prod.	TS	I/P	TS	I/P	TS	I/P	TS	I/P	TS	I/P	TS	I/P
15d	30.8	24.7	29.8	25.7	31.9	21.9	28.3	23.7	27.3	24.7	29.5	21.0
	41.6	37.6	41.6	38.6	49.6	44.0	43.8	40.7	43.8	41.7	51.8	47.1
	39.9	-25.9	41.9	-15.9	52.6	-6.6	44.6	-21.4	46.6	-11.4	57.3	-2.2
15r	39.9	-23.7	41.9	-13.7	52.8	-8.6	44.5	-13.6	46.5	-10.4	57.5	-5.3
15c[a]		-21.9		-10.9		4.6						
15s[d]	106.5	-17.8	103.5	-9.8	115.5	0.1						
15q[a]		2.8		11.8		15.1						
15l[b,i]	93.1	17.0	90.1	25.0	95.9	27.5	95.1	21.0	92.1	29.0	97.9	31.5
15a[e]	81.2	51.3	79.2	51.3	88.0	46.3	79.6	52.4	77.6	52.4	86.4	47.3
	66.1	34.4	72.1	43.3	83.4	50.3	69.1	38.2	75.1	47.2	86.4	54.1
15j	92.3	65.0	92.3	70.0	93.0	75.1	89.8	63.9	89.8	68.9	90.5	74.0
15o[c]		78.5										

Comment marks are always written in the line they refer to.

[a] no TS given because we were unable to construct a chemically meaningful pathway

[b] lower convergence criteria had to be used to be able to converge the TS geometry

[c] no TS data because the product lies above the lowest pathway and need not be considered therefore

[d] woelfling data only because the woelfling-energy is very high compared to the lowest pathway; optimization did not make sense therefore

[e] woelfling data only because the second (converged) TS lies far above the lowest pathway

[i] More than one imaginary frequency remained from the transition state optimization

Table SI38. Obtained data [kJ/mol] for the pathways starting from **14j-mi** referenced to **14j-ma**

	GAS						COSMO					
	el.		ZPE		el.		ZPE		el.		ZPE	
prod.	TS	I/P	TS	I/P	TS	I/P	TS	I/P	TS	I/P	TS	I/P
15d	31.9	21.0	30.9	22.0	32.3	22.9	29.2	21.4	28.2	22.4	29.7	23.3
	42.1	37.6	42.1	38.6	nb.	51.4	44.1	40.5	44.1	41.5	nb.	54.4
	39.8	-25.9	41.8	-15.9	nb.	-6.6	44.5	-21.4	46.5	-11.4	55.3	-2.2
15r	33.4	24.8	32.4	24.8	33.5	22.7	30.9	24.7	29.9	24.7	31.0	22.6
	41.4	37.4	42.4	39.4	52.3	47.0	44.3	40.3	45.3	42.3	55.2	49.8
	39.7	-30.9	41.7	-18.9	52.9	-7.3	44.5	-24.8	46.5	-12.8	57.7	-1.2
[a]		-23.7		-13.7		-8.6		-20.4		-10.4		-5.3
15c[b]		26.9		27.9		31.1						
[d]		-1.9		-10.9		4.6						
15s[c]	70.1	-17.8	71.1	-9.8	75.1	-0.1	72.8	-13.6	73.8	-5.6	77.7	4.2
15q	104.8	2.8	102.8	11.8	105.5	15.1	15.5	7.0	103.5	16.0	106.1	19.3
15l[b]		6.2		7.2		9.4						
[b]		17.0		25.0		27.5						
15a[e]	95.5	48.7	91.5	49.7	102.1	48.3		51.6		52.6		51.2
[c]	65.0	34.4	67.0	43.4	72.6	50.3	79.2	38.2	81.2	47.2	86.8	54.1
15j	91.5	65.0	91.5	70.0	98.6	75.1	89.4	63.9	89.4	68.9	96.4	74.0
15o[d]	119.5	92.9										
[d]	145.4	78.5										

Comment marks are always written in the line they refer to.

nb. = no barrier

[a] no TS given for the last step because the third intermediate is located after the C-C bond formation takes place

[b] no TS given because we were unable to construct a chemically meaningful pathway

[c] lower convergence criteria had to be used to be able to converge the TS geometry

[d] woelfling data only because the product lies above the lowest pathway and it need not be considered therefore

[e] woelfling data only because the second (converged) TS lies far above the lowest pathway

Table SI39. Obtained data [kJ/mol] for the pathways starting from **14j-ma** referenced to **14j-ma**

	GAS						COSMO					
	el.		ZPE		G		el.		ZPE		G	
prod.	TS	I/P	TS	I/P	TS	I/P	TS	I/P	TS	I/P	TS	I/P
15r [T,f]	33.0	19.0	33.0	21.0	33.9	22.1	31.0	17.9	31.0	19.9	31.8	21.0
	79.2	49.8	78.2	52.8	85.9	56.3	78.9	47.7	77.9	50.7	85.6	54.1
	nb.	-41.8	nb.	-29.8	nb.	-20.3	nb.	-38.3	nb.	-26.3	nb.	-16.7
15r	33.0	19.0	33.0	21.0	33.9	22.1	31.0	17.9	31.0	19.9	31.8	21.0
	65.9	-41.8	68.9	-29.8	77.5	-20.3	68.9	-38.3	71.9	-26.3	80.5	-16.7
15r-2	33.0	19.0	33.0	21.0	33.9	22.1	31.0	17.9	31.0	19.9	31.8	21.0
	74.5	-3.9	77.5	8.1	90.5	20.2	79.0	1.1	81.0	13.1	89.3	25.2
15d	31.5	9.5	30.5	9.5	24.9	3.7	29.3	9.1	28.3	9.1	22.7	3.3
[T]	66.0	63.3	65.0	61.3	67.7	57.5	62.9	60.4	61.9	58.4	64.5	54.6
[T]	79.2	64.6	77.2	64.6	78.0	60.3	78.5	59.6	76.5	59.6	77.4	55.4
	65.4	-33.0	66.4	-22.0	72.3	-14.5	62.8	-29.5	63.8	-18.5	69.7	-11.0
15d	31.5	9.5	30.5	9.5	24.9	3.7	29.3	9.1	28.3	9.1	22.7	3.3
	64.1	-33.0	66.1	-22.0	76.0	-14.5	65.5	-29.5	67.5	-18.5	77.3	-11.0
15d-2	31.5	9.5	30.5	9.5	24.9	3.7	29.3	9.1	28.3	9.1	22.7	3.3
	64.4	-16.6	66.4	-8.6	74.7	2.1	65.5	-12.1	67.5	-4.1	75.8	6.6
15n	70.6	-21.9	72.6	-12.9	84.5	0.7	74.4	-21.2	76.4	-12.2	88.3	1.4
15q *[T],* [c]	31.5	9.0	30.5	9.0	24.9	4.0	29.3	8.4	28.3	8.4	22.7	3.4
[T], [d]	66.0	63.3	65.0	61.3	67.7	57.5	62.9	60.4	61.9	58.4	64.5	54.6
[a]	82.3	-15.0	80.3	-7.0	76.3	-6.7	81.2	-13.4	79.2	-5.4	75.2	-5.1
15j	105.1	-2.9	104.1	4.1	103.2	9.2	109.3	-12.4	108.3	-5.4	107.3	-0.3
15o	111.8	20.3	111.8	28.3	115.4	34.9	112.7	22.6	112.7	30.6	116.4	37.3
15c [e]	90.4	43.3	87.4	45.3	111.0	48.6		43.6		45.6		48.9
	64.4	30.5	66.4	37.5	76.6	41.4	66.0	35.0	68.0	42.0	78.2	45.9
15p [b]	130.8	80.9		77.9		72.2		80.2		77.2		71.5
[b]	126.6	37.8		45.8		53.6		40.3		48.3		56.1
15b [e]	99.2	44.9	97.2	44.9	106.8	37.5		45.1		45.1		37.7
	71.6	46.2	73.6	53.2	74.4	53.2	72.1	45.9	74.1	52.9	74.9	52.9
15l [e]	96.2	38.9	95.2	38.9	112.5	41.4		35.0		35.0		37.4
[f]	141.5	55.7	140.5	62.7	149.4	76.2	146.3	61.8	145.3	68.8	154.2	82.3

Comment marks are always written in the line they refer to.

nb. = no barrier

[T]: transmetallation step involved

[a] lower convergence criteria had to be used to be able to converge the TS geometry

[b] woelfling data only because the intermediate(s) lie(s) far above the lowest pathway for the minor enantiomer and this pathway need not be considered therefore

[c] same geometries as the first step of all pathways to 8d(2)

[d] same geometries as the second step of the transmetallation pathway to 8d, energy copied

[e] woelfling data only because the intermediate and/or the product and/or the optimized TS of the C-C bond formation lies above the lowest pathway for the minor enantiomer; path need not be considered therefore

[f] More than one imaginary frequency remained from the transition state optimization

Table SI40. Obtained data [kJ/mol] for the pathways starting from **14d-ma** referenced to **14j-ma**

	GAS						COSMO					
	el.		ZPE		G		el.		ZPE		G	
prod.	TS	I/P	TS	I/P	TS	I/P	TS	I/P	TS	I/P	TS	I/P
15r *[T]*	79.0	71.8	78.0	70.8	79.6	70.6	78.6	69.9	77.6	68.9	79.3	68.7
	77.5	-41.8	76.5	-29.8	81.3	-20.3	76.5	-38.3	75.5	-26.3	80.3	-16.7
15r-2	76.1	-3.9	79.1	8.1	88.0	20.2	81.6	1.1	84.6	13.1	93.5	25.2
15d[*T*,h]	80.2	63.3	77.2	61.3	94.5	57.5		60.4		58.4		54.6
[*T*,b]	79.2	64.6	77.2	64.6	78.0	60.3	78.5	59.6	76.5	59.6	77.4	55.4
[b]	65.4	-33.0	66.4	-22.0	72.3	-14.5	62.8	-29.5	63.8	-18.5	69.7	-11.0
15d-2	65.1	-16.6	65.1	-8.6	71.4	2.1	66.4	-12.1	66.4	-4.1	72.7	6.6
15n	63.8	-21.9	64.8	-12.9	73.7	0.7	65.2	-21.2	66.2	-12.2	75.2	1.4
15q *[T]*,[c]		63.3		61.3		57.5		60.4		58.4		54.6
[b]	82.3	-15.0	80.3	-7.0	76.3	-6.7	81.2	-13.4	79.2	-5.4	75.2	-5.1
15j	63.7	-2.9	64.7	4.1	72.4	9.2	65.1	-12.4	66.1	-5.4	73.8	-0.3
15o[d,i]	38.3	-0.2	38.3	0.8	37.4	1.9	32.9	-0.3	32.9	0.7	32.1	1.8
	111.7	20.3	112.7	28.3	117.9	34.9	112.6	22.6	113.6	30.6	118.8	37.3
15c[g]	78.9	54.3	75.9	52.3	95.7	43.8		38.9		36.9		28.5
	64.3	30.5	66.3	37.5	76.0	41.4	66.0	35.0	68.0	42.0	77.6	45.9
15p[e]	76.0	10.4	74.0	10.4	97.8	8.6		-0.1		-0.1		-1.9
[e]	81.5	66.6	80.5	64.6	89.5	62.0		64.2		62.2		59.6
[e]	123.5	80.9	119.5	77.9	132.3	73.4		80.3		77.3		72.7
[i]	115.0	37.8	113.0	45.8	119.1	53.6	115.3	40.3	113.3	48.3	119.3	56.1
15b[g]	93.0	44.9	88.0	44.9	107.1	35.2		45.1		45.1		35.4
	71.6	46.2	73.6	53.2	74.6	53.2	72.1	45.9	67.1	52.9	86.3	52.9
15l[f]	152.7	55.7	151.7	62.7	165.6	76.2						

Comment marks are always written in the line they refer to.
[T] : transmetallation step involved
[a] woelfling data only because the intermediates (and the TS) lie above the lowest pathway of the minor enantiomer
[b] first intermediate is the same as the second intermediate for the pathway from 7j-ma to 8d-ma which is the same as the second intermediate for the pathway from 7j-ma to 8q-ma; from there on copied - the pathway has to be the same
[c] no TS data because the subsequent TS lies above the lowest pathway
[d] the intermediate that appears is 7j-ma - therefore this is an interconversion TS
[e] woelfling data only because the intermediates and the last TS (converged) lie far above the lowest pathway
[f] woelfling data only because the approximate TS and the product are high in energy or lie above the lowest pathway for the minor enantiomer, respectively
[g] woelfling data only because the second (converged) TS lies above the lowest pathway
[h] woelfling data calculated only
[i] More than one imaginary frequency remained from the transition state optimization

From Tables SI37-SI40 it is easily deduced that a lot of the calculated pathways can be ruled out. We omitted from here on:

- **d-mi**: c,s,q,o
- **j-mi**: c,l,o
- **j-ma**: c,p,b,l
- **d-ma**: p,l

Concerning the relabelling in section 3.9.1: Products **15d-2-ma** = **B3h$_1$**, **15n-ma** = **B3h$_2$**, **15d-ma** = **B3h$_3$**, **15q-ma** = **B3h$_4$**, **15d-mi** = **A3h$_1$**, **15r-mi** = **A3h$_2$**; the intermediates and transition states were renamed accordingly.

The thermochemical data in the Tables SI41-SI44 is given in the same order as above: The left columns containing the data of the TS and the right columns the data of the intermediates/products, and are

read like the tables above (see Table SI37 and the text above). The "G" values are the computed additions to the electronic energies to obtain the absolute values of the Gibbs free enthalpy.

Table SI41. Thermochemical data ([kJ/mol] or [J/molK]) for the pathways starting from **14d-mi**

prod	TS			I/P		
	ZPE	S	G	ZPE	S	G
15d	2982	1.6267	2709.21	2984	1.6503	2705.36
	2983	1.6007	2716.09	2984	1.6159	2714.43
	2985	1.5866	2720.81	2993	1.5901	2727.33
15r	2985	1.5854	2721.07	2993	1.6076	2723.22
15c[a]	---	---	---	2994	1.5669	2734.60
15s[d]	2980	1.5671	2717.08	2991	1.5861	2725.83
15q[a]	---	---	---	2992	1.6143	2720.35
15l[b,f]	2980	1.5963	2710.84	2991	1.6167	2718.59
15a[e]	2981	1.5868	2714.92	2983	1.6576	2703.02
	2989	1.5759	2725.40	2992	1.5997	2723.96
15j	2983	1.6243	2708.78	2988	1.6126	2718.16

Comment marks are always written in the line they refer to.
[a] no TS given because we were unable to construct a chemically meaningful pathway
[b] lower convergence criteria had to be used to be able to converge the TS geometry
[c] no TS data because the product lies above the lowest pathway and need not be considered therefore
[d] woelfling data only because the woelfling-energy is very high compared to the lowest pathway; optimization did not make sense therefore
[e] woelfling data only because the second (converged) TS lies far above the lowest pathway
[f] More than one imaginary frequency remained from the transition state optimization

Table SI42. Thermochemical data ([kJ/mol] or [J/molK]) for the pathways starting from **14j-mi**

prod	TS			I/P		
	ZPE	S	G	ZPE	S	G
15d	2982	1.6281	2708.55	2984	1.6353	2709.99
	2983	1.6022	2715.84	2984	1.5805	2721.93
	2985	1.5938	2718.84	2993	1.5901	2727.33
15r	2982	1.6300	2708.17	2983	1.6404	2705.96
	2984	1.5924	2718.98	2985	1.6064	2717.61
	2985	1.5852	2721.28	2995	1.5790	2731.72
[a]	---	---	---	2993	1.6076	2723.22
15c[b]	---	---	---	2984	1.6257	2712.27
[d]	---	---	---	2994	1.5669	2734.60
15s[c]	2984	1.6113	2713.03	2991	1.5861	2725.83
15q	2981	1.6192	2708.74	2992	1.6143	2720.35
15l[b]	---	---	---	2984	1.6285	2711.29
[b]	---	---	---	2991	1.6167	2718.59
15a[e]	2979	1.5693	2714.67	2984	1.6409	2707.71
[c]	2985	1.6055	2715.73	2992	1.5997	2723.96
15j	2983	1.6024	2715.16	2988	1.6126	2718.16

Comment marks are always written in the line they refer to.
nb. = no barrier
[a] no TS given for the last step because the third intermediate is located after the C-C bond formation takes place
[b] no TS given because we were unable to construct a chemically meaningful pathway
[c] lower convergence criteria had to be used to be able to converge the TS geometry
[d] woelfling data only because the product lies above the lowest pathway and it need not be considered therefore
[e] woelfling data only because the second (converged) TS lies far above the lowest pathway

Table SI43. Thermochemical data ([kJ/mol] or [J/molK]) for the pathways starting from **14j-ma**

prod	TS			I/P		
	ZPE	S	G	ZPE	S	G
15r	2983	1.6274	2708.92	2985	1.6310	2711.20
[T,f]	2982	1.5938	2714.80	2986	1.6190	2714.56
	nb.	nb.	nb.	2995	1.5879	2729.64
15r	2983	1.6274	2708.92	2985	1.6310	2711.20
	2986	1.5914	2719.71	2995	1.5879	2729.64
15r-2	2983	1.6274	2708.92	2985	1.6310	2711.20
	2986	1.5750	2724.01	2995	1.5755	2732.25
15d	2982	1.6543	2701.51	2983	1.6616	2702.25
[T]	2982	1.6236	2709.73	2981	1.6261	2707.70
[T]	2981	1.6304	2706.92	2983	1.6549	2703.80
	2984	1.6079	2715.04	2994	1.5986	2726.62
15d	2982	1.6543	2701.51	2983	1.6616	2702.25
	2985	1.5887	2719.95	2994	1.5986	2726.62
15d-2	2982	1.6543	2701.51	2983	1.6616	2702.25
	2985	1.5936	2718.42	2991	1.5786	2726.80
15n	2985	1.5818	2721.96	2992	1.5708	2730.70
15q*[T],* [c]	2982	1.6543	2701.51	2983	1.6577	2703.13
[T], [d]	2982	1.6236	2709.73	2981	1.6546	2702.25
[a]	2981	1.6454	2702.11	2991	1.6284	2716.33
15j	2982	1.6348	2706.09	2990	1.6022	2720.21
15o	2983	1.6142	2711.71	2991	1.6045	2722.73
15c[e]	2980	1.5125	2728.67	2985	1.6218	2713.34
	2985	1.5863	2720.22	2990	1.6132	2718.98
15p[b]	---	---	---	2980	1.6614	2699.42
[b]	---	---	---	2991	1.5924	2723.95
15b[e]	2981	1.5769	2715.74	2983	1.6660	2700.68
	2985	1.6234	2710.85	2990	1.6294	2715.05
15l[e]	2982	1.5400	2724.40	2983	1.6296	2710.50
[f]	2982	1.5885	2715.96	2990	1.5711	2728.62

Comment marks are always written in the line they refer to.

nb. = no barrier

[T]: transmetallation step involved

[a] lower convergence criteria had to be used to be able to converge the TS geometry

[b] woelfling data only because the intermediate(s) lie(s) far above the lowest pathway for the minor enantiomer and this pathway need not be considered therefore

[c] same geometries as the first step of all pathways to 8d(2)

[d] same geometries as the second step of the transmetallation pathway to 8d, energy copied

[e] woelfling data only because the intermediate and/or the product and/or the optimized TS of the C-C bond formation lies above the lowest pathway for the minor enantiomer; path need not be considered therefore

[f] More than one imaginary frequency remained from the transition state optimization

Table SI44. Thermochemical data ([kJ/mol] or [J/molK]) for the pathways starting from **14d-ma**

prod	TS			I/P		
	ZPE	S	G	ZPE	S	G
15r *[T]*	2982	1.6233	2708.71	2982	1.6364	2706.92
	2982	1.6131	2711.86	2995	1.5879	2729.64
15r-2	2986	1.5895	2719.99	2995	1.5755	2732.25
15d[T,h]	2980	1.5414	2722.30	2981	1.6261	2707.70
[T,b]	2981	1.6304	2706.92	2983	1.6549	2703.80
[b]	2984	1.6079	2715.04	2994	1.5986	2726.62
15d-2	2983	1.6051	2714.30	2991	1.5786	2726.80
15n	2984	1.5942	2718.05	2992	1.5708	2730.70
15q *[T]*,[c]	---	---	---	2981	1.6261	2707.70
[b]	2981	1.6304	2706.92	2983	1.6549	2703.80
15j	2985	1.5776	2721.28	2991	1.6284	2716.33
15o[d,i]	2984	1.5983	2716.85	2990	1.6022	2720.21
	2983	1.6291	2707.23	2984	1.6324	2710.15
15c[g]	2984	1.6061	2714.24	2991	1.6045	2722.73
	2980	1.5268	2724.88	2981	1.6732	2697.60
15p[e]	2985	1.5876	2719.77	2990	1.6132	2718.98
[e]	2981	1.5045	2729.85	2983	1.6386	2706.28
[e]	2982	1.5836	2716.09	2981	1.6490	2703.46
[i]	2979	1.5593	2716.82	2980	1.6574	2700.53
15b[g]	2981	1.6017	2712.11	2991	1.5924	2723.95
	2978	1.5254	2722.21	2983	1.6741	2698.38
15l[f]	2985	1.6226	2711.10	2990	1.6294	2715.05
15r *[T]*	2982	1.5588	2720.98	2990	1.5711	2728.62

Comment marks are always written in the line they refer to.
[T] : transmetallation step involved
[a] woelfling data only because the intermediates (and the TS) lie above the lowest pathway of the minor enantiomer
[b] first intermediate is the same as the second intermediate for the pathway from 7j-ma to 8d-ma which is the same as the second intermediate for the pathway from 7j-ma to 8q-ma; from there on copied - the pathway has to be the same
[c] no TS data because the subsequent TS lies above the lowest pathway
[d] the intermediate that appears is 7j-ma - therefore this is an interconversion TS
[e] woelfling data only because the intermediates and the last TS (converged) lie far above the lowest pathway
[f] woelfling data only because the approximate TS and the product are high in energy or lie above the lowest pathway for the minor enantiomer, respectively
[g] woelfling data only because the second (converged) TS lies above the lowest pathway
[h] woelfling data calculated only
[i] More than one imaginary frequency remained from the transition state optimization

The data obtained from the calculation of single-points at higher levels of theory is summarized in Tables SI45 to SI56, for simplicity, only the ΔG+COSMO and ΔE+ZPE+COSMO values are shown.

By the data provided in Tables SI45 and SI47, systematic shifts in the energies relative to the ISR can be observed. Taking the DLPNO-CCSD(T)/cc-pVTZ data as a reference, RI-PBE-D3/def2-SVP gives in general too low energies compared to the ISR. This is a general trend in all the calculations (see e.g. Table SI12 and SI13). The magnitude of error is much lower for RI-PBE-D3/def2-TZVPPD and B3LYP-D3/def2-TZVPPD. Larger deviations are encountered for the complexes including TRIP, while the deviations for the background reaction (Tables SI06 and SI07) are smaller, likely due to the smaller system size. Concerning the qualitative results in case of the zinc mechanism this has no effect, as the complexes and transition states involved in the catalyzed reaction exhibit energies well below the uncatalyzed reaction for all the methods employed (*vide infra*).

Table SI45. ΔG+COSMO values [kJ/mol] for complexes **14** at different levels of theory relative to the ISR

complex	RI-PBE-D3/ def2-SVP	RI-PBE-D3/ def2-TZVPPD	B3LYP-D3/ def2-TZVPPD	DLPNO-CCSD(T)/ cc-pVTZ
minor				
14a	-125.9	-63.5	---	---
14c	-131.9	-54.2	---	---
14d	-141.4	-80.4	-117.9	-96.5
14j	-139.2	-71.1	-111.0	-93.5
14l	-131.1	-70.5	---	---
14o	-73.8	-20.6	---	---
14q	-84.7	-29.8	---	---
14r	-108.8	-43.0	---	---
14s	-74.7	-15.9	---	---
major				
14b	-126.3	-67.4	---	---
14c	-128.4	-67.8	---	---
14d	-141.4	-76.5	-112.8	-94.2
14j	**-162.1**	**-97.2**	**-140.2**	**-121.0**
14l	-121.2	-54.1	---	---
14n	-107.7	-43.1	---	---
14o	-85.7	-34.2	---	---
14p	-65.7	-7.6	---	---
14q	-83.8	-26.0	---	---
14r	-108.8	-48.6	---	---

Table SI46. ΔG+COSMO values [kJ/mol] for complexes **15** at different levels of theory relative to the ISR

complex	RI-PBE-D3/ def2-SVP	RI-PBE-D3/ def2-TZVPPD	B3LYP-D3/ def2-TZVPPD
minor			
15a	-108.1	-45.3	---
15c	-150.8	-56.2	---
15d	-164.3	-73.9	-112.8
15j	-88.1	-12.6	---
15l	-130.7	-60.9	---
15o	-75.2	-12.2	---
15q	-142.8	-75.5	---
15r	-167.4	-92.6	-135.1
15s	-157.9	-83.0	---
major			
15b	-109.3	-47.0	---
15c	-116.3	-49.4	---
15d	-173.1	-94.1	-129.0
15d-2	-155.5	-70.3	-110.4
15j	-162.4	-77.1	-115.2
15l	-79.8	-8.2	---
15n	-160.7	-82.1	-118.8
15o	-124.9	-61.8	---
15p	-106.0	-42.1	---
15q	-167.2	-102.0	-131.5
15r	-178.8	-96.7	---
15r-2	-136.9	-48.5	---

Table SI47. ΔE+ZPE+COSMO values [kJ/mol] for complexes **14** at different levels of theory rel. to the ISR

complex	RI-PBE-D3/ def2-SVP	RI-PBE-D3/ def2-TZVPPD	B3LYP-D3/ def2-TZVPPD	DLPNO-CCSD(T)/ cc-pVTZ
minor				
14a	-234.8	-172.4	---	---
14c	-246.9	-169.2	---	---
14d	-248.5	-187.5	-225.0	-203.6
14j	-257.9	-189.8	-229.8	-212.2
14l	-235.7	-175.1	---	---
14o	-177.6	-124.4	---	---
14q	-192.3	-137.4	---	---
14r	-215.9	-150.1	---	---
14s	-184.6	-125.9	---	---
major				
14b	-228.5	-169.6	---	---
14c	-234.7	-174.1	---	---
14d	-255.6	-190.8	-227.0	-208.5
14j	**-272.8**	**-207.9**	**-250.9**	**-231.7**
14l	-236.8	-169.7	---	---
14n	-222.7	-158.1	---	---
14o	-196.4	-144.9	---	---
14p	-178.9	-120.9	---	---
14q	-192.3	-134.4	---	---
14r	-214.5	-154.3	---	---

Table SI48. ΔE+ZPE+COSMO values [kJ/mol] for complexes **15** at different levels of theory rel. to the ISR

complex	RI-PBE-D3/ def2-SVP	RI-PBE-D3/ def2-TZVPPD	B3LYP-D3/ def2-TZVPPD
minor			
15a	-225.7	-162.9	---
15c	-277.0	-182.5	---
15d	-284.2	-193.9	-232.8
15j	-203.9	-128.4	---
15l	-243.9	-174.1	---
15o	-187.6	-124.5	---
15q	-256.8	-189.5	---
15r	-283.3	-208.4	-250.9
15s	-278.4	-203.4	---
major			
15b	-219.9	-157.7	---
15c	-230.9	-164.0	---
15d	-291.3	-212.3	-247.2
15d-2	-277.0	-191.7	-231.8
15j	-278.3	-192.9	-231.1
15l	-204.0	-132.5	---
15n	-285.1	-206.4	-243.1
15o	-242.2	-179.2	---
15p	-224.6	-160.7	---
15q	-278.2	-212.9	-242.4
15r	-299.1	-217.0	---
15r-2	-259.8	-171.4	---

Table SI49. ΔG+COSMO values [kJ/mol] for the pathways starting from **14d-mi** at the different levels of theory, referenced to **14j-ma**

	RI-PBE-D3/ def2-SVP		RI-PBE-D3/ def2-TZVPPD		B3LYP-D3/ def2-TZVPPD		DLPNO- CCSD(T)/ cc-pVTZ	
prod.	TS	I/P	TS	I/P	TS	I/P	TS	I/P
15d	29.5	21.0	25.5	24.7	31.9	31.0	---	---
	51.8	47.1	61.2	60.1	nb.	77.0	---	---
	57.3	-2.2	73.8	23.3	97.8	27.4	105.4	---
15r	57.5	-5.3	74.1	4.6	97.9	5.1	---	---
15l[a,c]	97.9	31.5	91.3	36.3	---	---	---	---
15a[b]	86.4	47.3	---	45.9	---	---	---	---
	86.4	54.1	99.4	51.9	---	---	---	---
15j	90.5	74.0	100.3	84.6	---	---	---	---

Comment marks are always written in the line they refer to.

[a] lower convergence criteria had to be used to be able to converge the TS geometry

[b] woelfling data only because the second (converged) TS lies far above the lowest pathway

[c] More than one imaginary frequency remained from the transition state optimization

Table SI50. ΔG+COSMO values [kJ/mol] for the pathways starting from **14j-mi** at the different levels of theory, referenced to **14j-ma**

	RI-PBE-D3/ def2-SVP		RI-PBE-D3/ def2-TZVPPD		B3LYP-D3/ def2-TZVPPD		DLPNO- CCSD(T)/ cc-pVTZ	
prod.	**TS**	**I/P**	**TS**	**I/P**	**TS**	**I/P**	**TS**	**I/P**
15d	29.7	23.3	29.0	22.4	37.9	29.5	---	---
	nb.	54.4	nb.	66.2	nb.	83.1	---	---
	55.3	-2.2	71.9	23.3	95.8	27.4	103.4	---
15r	31.0	22.6	28.0	24.6	36.9	31.1	---	---
	55.2	49.8	64.9	61.7	nb.	78.5	---	---
	57.7	-1.2	74.3	24.1	98.2	30.3	---	---
[a]		-5.3		4.6		5.1		---
15s[b]	77.7	4.2	83.1	14.3	---	---	---	---
15q	106.1	19.3	100.2	21.7	---	---	---	---
15a[c]		51.2		49.5		---		---
[b]	86.8	54.1	91.0	51.9	---	---	---	---
15j	96.4	74.0	106.3	84.6	---	---	---	---

Comment marks are always written in the line they refer to.
nb. = no barrier
[a] no TS given for the last step because the third intermediate is located after the C-C bond formation takes place
[b] lower convergence criteria had to be used to be able to converge the TS geometry
[c] no TS data because the second (converged) TS lies far above the lowest pathway

Table SI51. ΔG+COSMO values [kJ/mol] for the pathways starting from **14j-ma** at the different levels of theory, referenced to **14j-ma**

	RI-PBE-D3/ def2-SVP		RI-PBE-D3/ def2-TZVPPD		B3LYP-D3/ def2-TZVPPD		DLPNO- CCSD(T)/ cc-pVTZ	
prod.	**TS**	**I/P**	**TS**	**I/P**	**TS**	**I/P**	**TS**	**I/P**
15r	31.8	21.0	nb.	25.2	34.1	31.4	---	---
[*T*,i]	85.6	54.1	93.2	58.7	---	---	---	---
	nb.	-16.7	nb.	0.5	---	9.1	---	---
15r	31.8	21.0	23.9	25.2	34.1	31.4	---	---
	80.5	-16.7	91.5	0.5	119.7	9.1	---	---
15r-2	31.8	21.0	23.9	25.2	34.1	31.4	---	---
	89.3	25.2	103.3	48.7	---	---	---	---
15d	22.7	3.3	10.1	-3.7	22.0	5.4	---	---
[T]	64.5	54.6	62.3	49.7	84.3	78.6	---	---
[T]	77.4	55.4	75.5	53.8	94.1	69.1	95.1	---
	69.7	-11.0	73.3	3.1	99.2	11.2	106.7	---
15d	22.7	3.3	10.1	-3.7	22.0	5.4	---	---
	77.3	-11.0	84.7	3.1	113.9	11.2	---	---
15d-2	22.7	3.3	10.1	-3.7	22.0	5.4	---	---
	75.8	6.6	83.2	27.0	112.1	29.8	105.2	---
15n	88.3	1.4	97.7	15.1	120.2	21.4	136.9	---
15q[*T*,b]	22.7	3.3	10.1	-2.	22.0	5.4	---	---
[*T*,c]	64.5	54.6	62.3	49.7	84.3	78.6	---	---
[a]	75.2	-5.1	65.2	-4.8	94.9	8.7	107.9	---
15j	107.3	-0.3	108.1	20.1	---	---	---	---
15o	116.4	37.3	116.0	35.4	---	---	---	---

Comment marks are always written in the line they refer to.
nb. = no barrier
[T]: transmetallation step involved
[a] lower convergence criteria had to be used to be able to converge the TS geometry
[b] same geometries as the first step of all pathways to 8d(2), energy copied
[c] same geometries as the second step of the transmetallation pathway to 8d, energy copied

[i] More than one imaginary frequency remained from the transition state optimization

Table SI52. ΔG+COSMO values [kJ/mol] for the pathways starting from **14d-ma** at the different levels of theory, referenced to **14j-ma**

	RI-PBE-D3/ def2-SVP		RI-PBE-D3/ def2-TZVPPD		B3LYP-D3/ def2-TZVPPD		DLPNO- CCSD(T)/ cc-pVTZ	
prod.	**TS**	**I/P**	**TS**	**I/P**	**TS**	**I/P**	**TS**	**I/P**
15r[*T*]	79.3	68.7	86.9	70.0	---	---	---	---
	80.3	-16.7	82.1	0.5	---	9.1	---	---
15r-2	93.5	25.2	109.1	48.7	---	---	---	---
15d[*T*,e]		54.6		49.7		78.6		---
[*T*,a]	77.4	55.4	75.5	53.8	94.1	69.1	95.1	---
[a]	69.7	-11.0	73.3	3.1	99.2	11.2	106.7	---
15d-2	72.7	6.6	79.2	27.0	108.7	29.8	102.0	---
15n	75.2	1.4	82.7	15.1	---	21.4	---	---
15q[*T*],[b]		54.6		49.7		78.6		---
[a]	75.2	-5.1	65.2	-4.8	94.9	8.7	---	---
15j	73.8	-0.3	81.4	20.1	110.8	25.0	---	---
15o[c,f]	32.1	1.8	23.3	1.9	36.2	---	---	---
	118.8	37.3	118.3	35.4	---	---	---	---
15c[d]		28.5		24.1		---		---
	77.6	45.9	82.1	47.9	---	---	---	---
15b[d]		35.4		29.9		---		---
	86.3	52.9	84.4	50.2	---	---	---	---

Comment marks are always written in the line they refer to.
[T] transmetallation step involved
[a] first intermediate is the same as the second intermediate for the pathway from 7j-ma to 8d-ma which is the same as the second intermediate for the pathway from 7j-ma to 8q-ma; from there on copied - the pathway has to be the same
[b] no TS data because the subsequent TS lies above the lowest pathway
[c] the intermediate that appears is 7j-ma - therefore this is an interconversion TS
[d] no TS data because the second (converged) TS lies above the lowest pathway
[e] no TS data calculated
[f] More than one imaginary frequency remained from the transition state optimization

Table SI53. ΔE+ZPE+COSMO values [kJ/mol] for the pathways starting from **14d-mi** at the different levels of theory, referenced to **14j-ma**

	RI-PBE-D3/ def2-SVP		RI-PBE-D3/ def2-TZVPPD		B3LYP-D3/ def2-TZVPPD		DLPNO- CCSD(T)/ cc-pVTZ	
prod.	**TS**	**I/P**	**TS**	**I/P**	**TS**	**I/P**	**TS**	**I/P**
15d	27.3	24.7	23.3	28.4	29.8	34.7	---	---
	43.8	41.7	53.2	54.8	64.5	71.6	---	---
	46.6	-11.4	63.1	14.1	87.1	18.1	94.7	---
15r	46.5	-10.4	63.1	-0.5	87.0	0.0	---	---
15l[a,c]	92.1	29.0	85.5	33.8	---	---	---	---
15a[b]	77.6	52.4	---	51.0	---	---	---	---
	75.1	47.2	88.0	45.1	---	---	---	---
15j	89.8	68.9	99.6	79.5	---	---	---	---

Comment marks are always written in the line they refer to.
[a] lower convergence criteria had to be used to be able to converge the TS geometry
[b] woelfling data only because the second (converged) TS lies far above the lowest pathway
[c] More than one imaginary frequency remained from the transition state optimization

Table SI54. ΔE+ZPE+COSMO values [kJ/mol] for the pathways starting from **14j-mi** at the different levels of theory, referenced to **14j-ma**

	RI-PBE-D3/ def2-SVP		RI-PBE-D3/ def2-TZVPPD		B3LYP-D3/ def2-TZVPPD		DLPNO- CCSD(T)/ cc-pVTZ	
prod.	**TS**	**I/P**	**TS**	**I/P**	**TS**	**I/P**	**TS**	**I/P**
15d	28.2	22.4	27.6	21.5	36.4	28.6	---	---
	44.1	41.5	53.6	53.4	64.3	70.2	---	---
	46.5	-11.4	63.2	14.1	87.0	18.1	94.6	---
15r	29.9	24.7	26.9	26.7	35.8	33.2	---	---
	45.3	42.3	55.0	54.2	nb.	71.0	---	---
	46.5	-12.8	63.1	12.5	87.0	18.7	---	---
[a]		-10.4		-0.5		0.0		---
15s[b]	73.8	-5.6	79.1	4.5	---	---	---	---
15q	103.5	16.0	97.6	18.5	---	---	---	---
15a[c]		52.6		50.8		---	---	---
[b]	81.2	47.2	85.3	45.1	---	---	---	---
15j	89.4	68.9	99.2	79.5	---	---	---	---

Comment marks are always written in the line they refer to.
nb. = no barrier
[a] no TS given for the last step because the third intermediate is located after the C-C bond formation takes place
[b] lower convergence criteria had to be used to be able to converge the TS geometry
[c] no TS data because the second (converged) TS lies far above the lowest pathway

Table SI55. ΔE+ZPE+COSMO values [kJ/mol] for the pathways starting from **14j-ma** at the different levels of theory, referenced to **14j-ma**

	RI-PBE-D3/ def2-SVP		RI-PBE-D3/ def2-TZVPPD		B3LYP-D3/ def2-TZVPPD		DLPNO- CCSD(T)/ cc-pVTZ	
prod.	**TS**	**I/P**	**TS**	**I/P**	**TS**	**I/P**	**TS**	**I/P**
15r [T,d]	31.0	19.9	nb.	24.1	33.2	30.2	---	---
	77.9	50.7	85.5	55.2	---	---	---	---
	no bar	-26.3	nb.	-9.1	---	-0.4	---	---
15r	31.0	19.9	23.1	24.1	33.2	30.2	---	---
	71.9	-26.3	82.9	-9.1	111.1	-0.4	---	---
15r-2	31.0	19.9	23.1	24.1	33.2	30.2	---	---
	81.0	13.1	95.0	46.5	---	---	---	---
15d	28.3	9.1	15.7	2.1	27.5	11.3	---	---
[T]	61.9	58.4	59.6	53.5	81.6	77.0	---	---
[T]	76.5	59.6	74.4	58.0	93.3	73.4	94.2	---
	63.8	-18.5	67.4	-4.4	93.2	3.7	100.8	---
15d	28.3	9.1	15.7	2.1	27.5	11.3	---	---
	67.5	-18.5	74.9	-4.4	104.0	3.7	---	---
15d-2	28.3	9.1	15.7	2.1	27.5	11.3	---	---
	67.5	-4.1	74.9	16.2	103.7	19.1	96.9	---
15n	76.4	-12.2	85.9	1.5	108.3	7.8	125.0	---
15q[T,b]	28.3	8.4	15.7	2.1	27.5	11.3	---	---
[T,c]	61.9	58.4	59.6	53.5	81.6	77.0	---	---
[a]	79.2	-5.4	69.2	-5.0	96.7	8.5	109.7	---
15j	108.3	-5.4	109.1	15.0	---	---	---	---
15o	112.7	30.6	112.4	28.4	---	---	---	---

Comment marks are always written in the line they refer to.
nb. = no barrier
[T]: transmetallation step involved
[a] lower convergence criteria had to be used to be able to converge the TS geometry
[b] same geometries as the first step of all pathways to 8d(2), energy copied
[c] same geometries as the second step of the transmetallation pathway to 8d, energy copied
[d] More than one imaginary frequency remained from the transition state optimization

Table SI56. ΔE+ZPE+COSMO values [kJ/mol] for the pathways starting from **14d-ma** at the different levels of theory, referenced to **14j-ma**

	RI-PBE-D3/ def2-SVP		RI-PBE-D3/ def2-TZVPPD		B3LYP-D3/ def2-TZVPPD		DLPNO- CCSD(T)/ cc-pVTZ	
prod.	**TS**	**I/P**	**TS**	**I/P**	**TS**	**I/P**	**TS**	**I/P**
15r[T]	77.6	68.9	85.3	70.2	---	---	---	---
	75.5	-26.3	77.3	-9.1	---	-0.4	---	---
15r-2	84.6	13.1	100.1	36.5	---	---	---	---
15d[T,e]		58.4		53.5		77.0		---
[T,a]	76.5	59.6	74.4	58.0	93.3	73.4	94.2	---
[a]	63.8	-18.5	67.4	-4.4	93.2	3.7	100.8	---
15d-2	66.4	-4.1	73.0	16.2	102.5	19.1	95.8	---
15n	66.2	-12.2	73.7	1.5	---	7.8	---	---
15q[T,b]		58.4		53.5		77.0		---
[a]	79.2	-5.4	69.2	-5.0	96.7	8.5	---	---
15j	66.1	-5.4	73.7	15.0	103.1	19.8	---	---
15o[c,f]	32.9	0.7	24.1	0.8	37.1	---	---	---
	113.6	30.6	113.2	28.8	---	---	---	---
15c[d]		36.9		32.6		---		---
	68.0	42.0	72.4	44.0	---	---	---	---
15b[d]		45.1		39.6		---		---
	67.1	52.9	65.3	50.3	---	---	---	---

Comment marks are always written in the line they refer to.
[T] transmetallation step involved
[a] first intermediate is the same as the second intermediate for the pathway from 7j-ma to 8d-ma which is the same as the second intermediate for the pathway from 7j-ma to 8q-ma; from there on copied - the pathway has to be the same
[b] no TS data because the subsequent TS lies above the lowest pathway
[c] the intermediate that appears is 7j-ma - therefore this is an interconversion TS
[d] no TS data because the second (converged) TS lies above the lowest pathway
[e] no TS data calculated
[f] More than one imaginary frequency remained from the transition state optimization

Upon comparison of the energies relative to the ISR of the pathways to the ones for the background reaction, it can be seen that the catalyzed reaction is energetically preferred at all levels of theory.

The pathways favor the minor enantiomer over the major for RI-PBE-D3/def2-SVP. Upon increasing the basis set size, the difference in the energy barriers between major and minor enantiomer becomes far smaller than for RI-PBE-D3/def2-SVP, even switching to being in favor to the major enantiomer for the RI-PBE-D3/def2-TZVPPD and B3LYP-D3/def2-TZPPD ΔG+COSMO values (though by a relatively small ΔΔG). Interestingly, at higher levels of theory the pathway to **15q-ma**, which involves a transmetallation step of the organometallic carbon to the second zinc ion, becomes the reaction coordinate with the lowest energy when considering the ΔG+COSMO values.

3.9.2.3. Association of the substrates

From the proposed mechanistic cycles depicted in Figures SI12, SI13and SI21 three possibilities arise for the order of the association of the starting materials to the catalyst: The zinc species of the lactone reactant binding first, followed by the aldehyde, or vice versa, and as a third alternative an association of a Zimmermann-Traxler-like complex preformed from the starting materials to the catalyst. Only the first two possibilities are treated in this section, for the third one, see the main text and section 3.8.

Our approach for the first two possibilities was to optimize the structures in which either the zinc species of the lactone or the benzaldehyde is missing from complexes **14j/d-ma/mi** = **A**/**B2(h)**. This leads to four catalyst-lactone-complexes [**13j/d-ma/mi** = **A1(h)**/**B1(h)**] and four catalyst-aldehyde complexes [**12-j/d-ma/mi**], where the labelling corresponds to the corresponding complex **14** from which the structure was obtained from.

Complexes **13** are thus relabeled in Figure SI22: **13j-ma** = **B1**, **13d-ma** = **B1h**, **13d-mi** = **A1h** and **13j-mi** = **A1**.

The structural features of complexes **13** are discussed in section 3.9.1, where it is noted that **13d-ma/mi** (**B1h**/**A1h**) exhibit the same coordination pattern whereas the two structures **13j-ma** and **13j-mi** (**B1** and **A1**) do not have the same pattern. To make sure that **13j-mi (A1)** does not play a role in the association and that we are not misled by judging that the preference for **14j-ma (B2)** stems from the different geometries of these two complexes we tried to enforce the coordination pattern (the Zn-atom interacting with a phenyl ring of the catalyst) of **13j-ma** onto **13j-mi** by distorting the geometry of the latter and subsequent optimization. This results in a geometry of even higher energy (**13j-mod-mi**), thus the strain introduced is quite substantial (see Table SI57). Only three complexes **12** were obtained, as **12-j-ma** and **12-d-ma** have the same geometry. The resulting ΔG+COSMO data of these complexes is presented in Table SI57, along with the results of the RI-PBE-D3/def2-TZVPPD single points. Additionally, the ΔE+ZPE+COSMO data is included for later comparison of the TS.

Table SI57. ΔG+COSMO values and thermochemical data for complexes **13** and **12** at the various levels of theory; relative to the ISR

complex	RI-PBE-D3/ def2-SVP	RI-PBE-D3/ def2-TZVPPD	B3LYP-D3/ def2-TZVPPD	DLPNO-CCSD(T)/ cc-pVTZ
13j-ma	-140.7	-88.9	-120.5	-105.7
13d-ma	-103.2	-56.1	-62.9	-74.8
13j-mi	-78.6	-41.9	---	---
13d-mi	-129.8	-85.6	---	---
13j-mod-mi	-68.1	-14.3	---	---
12-j-ma	-43.8	-10.0	---	---
12-j-mi	-17.5	5.6	---	---
12-d-mi	-60.3	-28.2	---	---

Table SI58. ΔE+ZPE+COSMO values and thermochemical data for complexes **13** and **12** at the various levels of theory; relative to the ISR

complex	RI-PBE-D3/ def2-SVP	RI-PBE-D3/ def2-TZVPPD	B3LYP-D3/ def2-TZVPPD	DLPNO-CCSD(T)/ cc-pVTZ
13j-ma	-204.1	-152.3	-184.0	-169.1
13d-ma	-166.1	-119.0	-125.8	-137.7
13j-mi	-136.5	-99.8	---	---
13d-mi	-194.1	-149.9	---	---
13j-mod-mi	-135.0	-81.2	---	---
12-j-ma	-102.6	-68.8	---	---
12-j-mi	-67.4	-44.3	---	---
12-d-mi	-116.5	-84.5	---	---

Table SI59. Thermochemical data for complexes **13** and **12**

complex	ZPE	S	G
13j-ma	2695	1.4735	2446.12
13d-ma	2692	1.4791	2442.62
13j-mi	2694	1.4957	2439.61
13d-mi	2692	1.4756	2444.04
13j-mod-mi	2696	1.4564	2450.59
12-j-ma	2739	1.4060	2502.50
12-j-mi	2737	1.4404	2491.61
12-d-mi	2739	1.4150	2500.00

Complexes **13** lie approximately 100 kJ/mol lower in energy than complexes **12** (the difference is reduced a little for the RI-PBE-D3/def2-TZVPPD data, see Table SI57), meaning that the scenario in which the zinc species binds first is thermodynamically favored over the other two alternatives. Therefore, this pathway became the main subject of further investigations.

Association pathways leading from the ISR to complexes **13** and **12** were not studied, as the barriers can be expected to be very small and therefore insignificant.

The starting points for the pathways were constructed in such a way as to arrive to direct, linear trajectories of the approaching substrates. For complexes **12/13** this was done by aligning their structures with complexes **14**, pulling out the aldehyde/lactone-species from the latter in an unhindered direction and then deleting the remainders of the structures **14** (the catalyst and the one substrate which was remained, i.e. the parts which exist in both **14** and **12/13**). Thus, one is left with a complex **12/13** and the approaching substrate further away (at least 7 Å). These geometries were then optimized.

3.9.2.4. Association to complexes 13

For all complexes **13j-ma**, **13d-ma** and **13d-mi** we calculated the pathways leading to the corresponding complexes **14**. Pathways starting from **13j-mi** and **13j-mod-mi** were omitted because of the high energies of these complexes. The pathways start from agglomerate structures where an aldehyde resides in distance to the corresponding complex **13** (at least 7 Å, generated as explained above). The results obtained for the association of the organometallic lactone species are shown in Tables SI58 to SI66. We give here both ΔE+ZPE and ΔG values for the reasons discussed in section 3.9.1, namely the flat hyperplane, resulting in ΔG values that have to be treated carefully and as they are prone to slight deviations (despite all efforts, more than one imaginary frequency remained for all association transition states). It is obvious that the agglomerate ΔG values are considerably shifted to higher energies but the preference for **14j-ma** stemming from the low transition state from **13j-ma** to **14j-ma** remains.

The "agglomerate" geometries in the tables are renamed as follows in section 3.9.1:

- agglomerate for the pathway from **13j-ma** to **14j-ma**: **B1$_{ald}$1**
- agglomerate for the pathway from **13j-ma** to **14d-mi**: **B1$_{ald}$2**
- agglomerate for the pathway from **13j-ma** to **14j-mi**: **B1$_{ald}$3**

Table SI60. ΔE+ZPE+COSMO RI-PBE-D3/def2-SVP data [kJ/mol] for the pathways from complexes **13** to **14**; referenced to **13j-ma**

from:	to:	agglomerate	TS	product (14)
13j-ma	**14j-ma**	0.1	no barrier (14.0)[a]	-68.8
	14d-ma	-1.2	72.5	-51.6
	14j-mi	0.0	98.4	-53.8
	14d-mi	0.1	79.8	-44.4
13d-ma	**14j-ma**	38.1	88.9	-68.8
	14d-ma	38.1	72.6	-51.6
	14j-mi	38.9	115.2	-53.8
	14d-mi	37.9	86.5	-44.4
13d-mi	**14j-ma**	11.1	66.9	-68.8
	14d-ma	10.7	60.2	-51.6
	14j-mi	11.5	79.6	-53.8
	14d-mi	11.2	77.6	-44.4

[a] the woelfling data (ΔE only) are given in brackets

Table SI61. ΔG+COSMO RI-PBE-D3/def2-SVP data [kJ/mol] for the pathways from complexes **13** to **14**; referenced to **13j-ma**

from:	to:	agglomerate	TS	product (14)
13j-ma	**14j-ma**	45.7	49.7	-21.5
	14d-ma	41.8	122.5	-0.7
	14j-mi	32.4	141.2	1.5
	14d-mi	30.3	130.2	-0.7
13d-ma	**14j-ma**	58.4	114.7	-21.5
	14d-ma	83.4	104.0	-0.7
	14j-mi	66.0	166.9	1.5
	14d-mi	67.1	115.8	-0.7
13d-mi	**14j-ma**	33.6	102.5	-21.5
	14d-ma	34.1	106.3	-0.7
	14j-mi	29.6	111.1	1.5
	14d-mi	42.4	114.3	-0.7

Table SI62. ΔE+ZPE+COSMO RI-PBE-D3/def2-SVP data [kJ/mol] for the pathways from complexes **13** to **14**; relative to the ISR

from:	to:	agglomerate	TS	product (14)
13j-ma	**14j-ma**	-204.0	no barrier	-272.8
	14d-ma	-205.3	-131.6	-255.6
	14j-mi	-204.1	-105.6	-257.9
	14d-mi	-203.9	-124.3	-248.5
13d-ma	**14j-ma**	-166.0	-115.2	-272.8
	14d-ma	-166.0	-131.5	-255.6
	14j-mi	-165.2	-88.9	-257.9
	14d-mi	-166.2	-117.5	-248.5
13d-mi	**14j-ma**	-193.0	-137.1	-272.8
	14d-ma	-193.3	-143.9	-255.6
	14j-mi	-192.6	-124.4	-257.9
	14d-mi	-192.9	-126.5	-248.5

Table SI63. ΔG+COSMO RI-PBE-D3/def2-SVP data [kJ/mol] for the pathways from complexes **13** to **14**; relative to the ISR

from:	to:	agglomerate	TS	product (14)
13j-ma	**14j-ma**	-94.9	-91.0	-162.1
	14d-ma	-98.9	-18.2	-141.4
	14j-mi	-108.3	0.6	-139.2
	14d-mi	-110.4	-10.4	-141.4
13d-ma	**14j-ma**	-82.3	-26.0	-162.1
	14d-ma	-57.3	-36.7	-141.4
	14j-mi	-74.6	26.2	-139.2
	14d-mi	-73.6	-24.9	-141.4
13d-mi	**14j-ma**	-107.1	-38.1	-162.1
	14d-ma	-106.6	-34.4	-141.4
	14j-mi	-111.0	-29.6	-139.2
	14d-mi	-98.2	-26.4	-141.4

Table SI64. ΔE+ZPE+COSMO RI-PBE-D3/def2-TZVPPD data [kJ/mol] for the pathways from complexes **13** to **14**; referenced to **13j-ma**

from:	to:	agglomerate	TS	product (14)
13j-ma	**14j-ma**	0.2	no barrier	-55.6
	14d-ma	-1.1	61.6	-38.5
	14j-mi	0.0	73.0	-37.5
	14d-mi	0.0	60.3	-35.2
13d-ma	**14j-ma**	33.8	57.1	-55.6
	14d-ma	33.7	50.4	-38.5
	14j-mi	34.7	105.5	-37.5
	14d-mi	33.2	63.4	-35.2
13d-mi	**14j-ma**	3.7	56.3	-55.6
	14d-ma	3.1	50.7	-38.5
	14j-mi	4.1	60.2	-37.5
	14d-mi	3.8	51.8	-35.2

Table SI65. ΔG+COSMO RI-PBE-D3/def2-TZVPPD data [kJ/mol] for the pathways from complexes **13** to **14**; referenced to **13j-ma**

from:	to:	agglomerate	TS	product (14)
13j-ma	**14j-ma**	45.9	48.9	-8.3
	14d-ma	41.9	111.5	12.4
	14j-mi	32.4	115.8	17.8
	14d-mi	30.1	110.8	8.5
13d-ma	**14j-ma**	54.1	82.9	-8.3
	14d-ma	79.0	81.7	12.4
	14j-mi	61.8	157.2	17.8
	14d-mi	62.5	92.6	8.5
13d-mi	**14j-ma**	26.2	91.9	-8.3
	14d-ma	26.5	96.8	12.4
	14j-mi	22.2	91.7	17.8
	14d-mi	35.0	88.4	8.5

Table SI66. ΔE+ZPE+COSMO and ΔG+COSMO B3LYP-D3/def2-TZVPPD data [kJ/mol]; relative to the ISR for **13j-ma** and referenced to **13j-ma** for the pathways

	13j-ma	agglomerate	TS	product (14)
ΔE+ZPE+COSMO	-184.0	0.2	no barrier	-66.9
ΔG+COSMO	-120.5	45.8	47.1	-19.7

Table SI67. ΔE+ZPE+COSMO and ΔG+COSMO DLPNO-CCSD(T)/cc-pVTZ data [kJ/mol]; relative to the ISR for **13j-ma** and referenced to **13j-ma** for the pathways

	13j-ma	agglomerate	TS	product (14)
ΔE+ZPE+COSMO	-169.1	0.0	no barrier	-62.6
ΔG+COSMO	-105.7	45.7	48.0	-15.3

Table SI68. Thermochemical data ([kJ/mol] or [J/molK]) for the pathways from complexes **13** to **14**

		agglomerate			TS		
from:	to:	ZPE	S	G	ZPE	S	G
13j-ma	**14j-ma**	2981	1.6179	2704.41	2978	1.5927	2707.81
	14d-ma	2980	1.6382	2700.78	2978	1.5945	2705.71
	14j-mi	2981	1.6826	2691.20	2974	1.6169	2694.58
	14d-mi	2981	1.6902	2688.90	2977	1.5944	2705.23
13d-ma	**14j-ma**	2978	1.7295	2676.07	2976	1.7005	2679.56
	14d-ma	2978	1.6224	2701.07	2979	1.6825	2688.13
	14j-mi	2979	1.7020	2683.95	2978	1.5926	2707.46
	14d-mi	2979	1.6942	2686.01	2975	1.6839	2682.00
13d-mi	**14j-ma**	2979	1.7279	2679.25	2976	1.6555	2689.39
	14d-ma	2979	1.7245	2680.16	2977	1.6230	2700.84
	14j-mi	2979	1.7437	2674.96	2977	1.6782	2686.22
	14d-mi	2979	1.6883	2688.00	2977	1.6510	2691.47

3.9.2.5. Interconversion of complexes 13

In order to evaluate the possibility of an interconversion between the pathways leading to the two product enantiomers, the energetic barriers were calculated (Tables SI67 and SI68). They exhibit high barriers, except for the pathway **13j-ma ↔ 13d-mi**. This results in the conversion of any formed **6d-mi** to **14j-ma** via **13j-ma**, since the barriers for the pathways from **13d-mi** to **14** have a higher energy than the interconversion to **13j-ma**.

The Tables contain in the first line the complex **13** (starting point) and from there (to be read in the usual manner; compare to Table SI37 and text above the Table), the remaining pathway until they end at the new complex **13** (right lower corner of each box). The thermochemical data is presented in Table SI69.

Table SI69. ΔE+ZPE+COSMO RI-PBE-D3 data [kJ/mol] for the interconversion pathways of complexes **13**; referenced to **13j-ma**

	def2-SVP		**def2-TZVPPD**	
pathway	**TS**	**ed/int**	**TS**	**ed/int**
13j-ma ↔ 13d-ma		0.0		0.0
	87.2[b]	70.6	62.2[i]	65.0
	73.1	37.9	57.2	33.4
13j-ma ↔ 13d-mi		0.0		0.0
	36.0	10.0	35.8	2.4
13d-ma ↔ 13d-mi		37.9		33.4
	114.4[a,b]	33.8	83.2[a,i]	31.4
	58.0	10.0	56.5	2.4

[a] lower convergence criteria had to be used to be able to converge the TS geometry
[b]More than one imaginary frequency remained from the transition state optimization

Table SI70. ΔG+COSMO RI-PBE-D3 data [kJ/mol] for the interconversion pathways of complexes **13**; referenced to **13j-ma**

	def2-SVP		**def2-TZVPPD**	
pathway	**TS**	**ed/int**	**TS**	**ed/int**
13j-ma ↔13d-ma		0.0		0.0
	90.3[b]	67.4	65.3[i]	61.8
	72.2	37.4	56.2	32.9
13j-ma ↔ 13d-mi		0.0		0.0
	39.8	10.9	39.5	3.3
13d-ma ↔ 13d-mi		37.4		32.9
	116.2[a,b]	31.3	85.0[a,i]	28.9
	57.5	10.9	56.0	3.3

[a] lower convergence criteria had to be used to be able to converge the TS geometry
[b]More than one imaginary frequency remained from the transition state optimization

Table SI71. Thermochemical data ([kJ/mol] or [J/molK]) for the interconversion pathways of complexes **13**

	TS			ed/int		
pathway	**ZPE**	**S**	**G**	**ZPE**	**S**	**G**
13j-ma ↔ 13d-ma [b]				2695	1.4740	2446.12
	2691	1.4488	2445.24	2693	1.4886	2440.97
	2693	1.4730	2443.20	2692	1.4791	2442.62
13j-ma ↔ 13d-mi				2695	1.4740	2446.12
	2693	1.4571	2447.89	2692	1.4756	2444.04
13d-ma ↔ 13d-mi [a,b]				2692	1.4791	2442.62
	2689	1.4564	2441.94	2693	1.4863	2441.62
	2692	1.4724	2442.64	2692	1.4756	2444.04

[a] lower convergence criteria had to be used to be able to converge the TS geometry
[b]More than one imaginary frequency remained from the transition state optimization

3.9.2.6. Association to complexes 12

Additionally, woelfling-calculations were performed for the association to complexes of the type **12** (see Table SI70). Here, only the pathways between complexes of same type were performed – e.g. **12-j-ma** to **14j-ma**. The associations do not proceed barrierless, making this route of association kinetically disfavored. In addition, complexes of the type **13** are thermodynamically more stable.

Table SI72. RI-PBE-D3 woelfling electronic energies [kJ/mol] for the associations to complexes **12**, referenced to **12-d-mi**

basis set:	**pathway from:**	**educt**	**agglomerate**	**TS**	**prod (14)**
def2-SVP	**12-j-ma**	14.0	13.1	46.6	-178.1
	12-d-ma	14.0	13.6	108.1	-160.3
	12-j-mi	53.6	52.6	64.2	-159.5
	12-d-mi	0.0	0.0	71.6	-152.1
def2-TZVPPD	**12-j-ma**	15.4	14.4	31.8	-144.1
	12-d-ma	15.4	15.2	74.5	-127.5
	12-j-mi	44.0	43.0	51.0	-122.8
	12-d-mi	0.0	0.0	48.9	-122.6

3.9.2.7. Interconversion of the educt complexes 14

Interconversion of complexes **14** can proceed via three different "mechanisms" and requires major rearrangements (Figure SI25). The first one is a complete swing of the aldehyde around the lactone (mechanism 1). The second and third proceed via structures that contain a carbon atom which is bound to the two zinc atoms. The two possibilities differ in the orientation of the carbonyl group of the lactone – pointing outside (mechanism 2) or inside (mechanism 3). Examples for mechanisms two and three are illustrated in Figure SI26.

The results of the calculations are listed in Tables SI71 to SI73. The Tables contain in the first line of each double-column the complex **14** (starting point) and from there in the usual manner (see Table SI37 and text above the Table) the rest of the pathway until they end at the new complex **14** (in the right lower corner). "TS" is standing for transition state and "ed/int" refers to "educt complex or intermediate". If no transition state has been located this is marked with "nb." (no barrier). For mechanism three one pathway proved to be impossible as no reasonable reaction coordinate could be located - therefore this pathway is missing in Tables SI71 to SI73.

The two pathways **14j-ma ↔ 14d-ma** and **14j-mi ↔ 14d-mi** are listed together with mechanism one – there is only one possible "mechanism" for them.

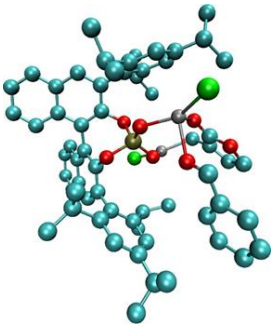

14j-ma

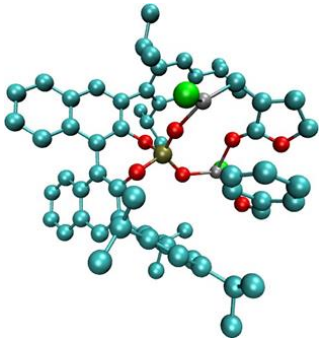

14j-mi

Figure SI25. Strucures of **14j-ma** and **14j-mi**

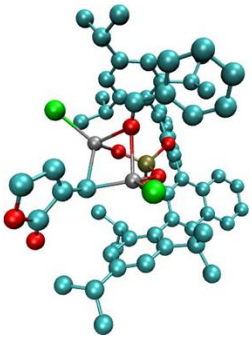

Example TS for mechanism 2

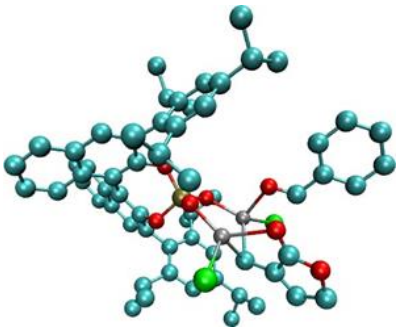

Example TS for mechanism 3

Figure SI26. Examples for transition states of mechanisms two and three

Table SI73. ΔG+COSMO values [kJ/mol] for the interconversion pathways of the four most stable complexes of complexes **14** at the different levels of theory; referenced to **14j-ma**

		RI-PBE-D3/ def2-SVP		RI-PBE-D3/ def2-TZVPPD		B3LYP-D3/ def2-TZVPPD		DLPNO-CCSD(T)/ cc-pVTZ	
	pathway	**TS**	**ed/int**	**TS**	**ed/int**	**TS**	**ed/int**	**TS**	**ed/int**
MECHANISM 1	**14j-ma ↔ 14d-ma**		0.0		0.0		---		---
	[a]	32.1	20.8	23.3	20.7	36.2	---	---	---
	14j-ma ↔ 14j-mi		0.0		0.0		---		---
		93.1	16.7	84.9	13.3	---	---	---	---
		46.2	23.0	42.7	26.2	---	---	---	---
	14j-ma ↔ 14d-mi		0.0		0.0		---		---
		88.7	21.1	74.9	22.2	---	---	---	---
		32.8	20.8	28.2	16.8	---	---	---	---
	14j-mi ↔ 14d-mi		23.0		26.2		---		---
		31.4	20.8	27.3	16.8	34.9	---	---	---
	14d-ma ↔ 14j-mi		20.8		20.7		27.4		26.8
	[a]	55.5	34.8	46.3	20.5	55.7	33.0	---	---
		69.4	19.9	70.2	9.7	85.9	19.5	80.9	---
		31.4	23.0	31.0	26.2	39.4	29.2	---	27.5
	14d-ma ↔ 14d-mi		20.8		20.7		---		---
	[a]	106.7	20.8	95.9	16.8	---	---	---	---
MECHANISM 2	**14j-ma ↔ 14j-mi**		0.0		0.0		---		---
		57.5	55.3	57.3	54.8	---	---	---	---
		96.0	53.1	83.7	55.6	---	---	---	---
		63.0	23.0	68.0	26.2	---	---	---	---
	14j-ma ↔ 14d-mi		0.0		0.0		---		---
		105.8	54.2	83.4	53.4	---	---	---	---
		62.4	20.8	61.8	16.8	---	---	---	---
	14d-ma ↔ 14j-mi		20.8		20.7		27.4		26.8
		37.3	21.3	33.5	26.8	41.5	36.6	---	---
	[a]	nb.	62.1	nb.	64.0	nb.	83.5	---	---
		nb.	74.1	nb.	74.2	nb.	94.1	nb.	80.2
		nb.	57.4	nb.	63.4	nb.	80.1	nb.	---
		59.2	52.9	nb.	53.8	80.6	72.4	---	---
		nb.	22.9	nb.	21.9	nb.	28.9	---	---
		32.7	23.0	32.2	26.2	40.8	29.2	---	27.5
	14d-ma ↔ 14d-mi		20.8		20.7		---		---
	[a]	97.9	34.2	95.7	34.8	---	---	---	---
	[a]	113.7	20.8	99.2	16.8	---	---	---	---
MECHANISM 3	**14j-ma ↔ 14d-mi**		0.0		0.0		---		---
	[a]	95.7	62.2	69.3	64.7	---	---	---	---
		80.0	24.1	75.9	22.9	---	---	---	---
		35.9	30.3	35.3	31.7	---	---	---	---
	[a]	54.9	20.8	51.9	16.8	---	---	---	---
	14d-ma ↔ 14j-mi		20.8		20.7		---		---
		38.3	20.3	34.0	25.8	---	---	---	---
		91.1	80.9	72.9	67.8	---	---	---	---
		nb.	23.0	54.5	26.2	---	---	---	---
	14d-ma ↔ 14d-mi		20.8		20.7		27.4		26.8
		73.9	20.8	82.8	16.8	97.6	22.3	80.6	24.5

Comment marks are always written in the line they refer to.

[a]More than one imaginary frequency remained from the transition state optimization

Table SI74. ΔE+ZPE+COSMO values [kJ/mol] for the interconversion pathways of the four most stable complexes of complexes **14** at the different levels of theory; referenced to **14j-ma**

		RI-PBE-D3/ def2-SVP		RI-PBE-D3/ def2-TZVPPD		B3LYP-D3/ def2-TZVPPD		DLPNO-CCSD(T)/ cc-pVTZ	
	pathway	**TS**	**ed/int**	**TS**	**ed/int**	**TS**	**ed/int**	**TS**	**ed/int**
MECHANISM 1	**14j-ma ↔ 14d-ma**		0.0		0.0		---		---
	[a]	32.9	17.2	24.1	17.1	37.1	---	---	---
	14j-ma ↔ 14j-mi		0.0		0.0		---		---
		94.0	18.0	85.8	14.7	---	---	---	---
		47.2	14.9	43.7	18.1	---	---	---	---
	14j-ma ↔ 14d-mi		0.0		0.0		---		---
		93.8	18.5	80.0	19.7	---	---	---	---
		31.0	24.3	26.3	20.4	---	---	---	---
	14j-mi ↔ 14d-mi		14.9		18.1		---		---
		29.4	24.3	25.3	20.4	32.8	---	---	---
	14d-ma ↔ 14j-mi		17.2		17.1		23.9		23.2
	[a]	47.4	41.1	38.3	26.8	47.7	39.3	---	---
		74.7	20.8	75.5	10.6	91.1	20.4	86.2	---
		28.7	14.9	28.3	18.1	36.7	21.1	---	19.5
	14d-ma ↔ 14d-mi		17.2		17.1		---		---
	[a]	95.1	24.3	84.3	20.4	---	---	---	---
MECHANISM 2	**14j-ma ↔ 14j-mi**		0.0		0.0		---		---
		51.1	51.0	50.9	50.5	---	---	---	---
		98.0	54.5	85.8	57.0	---	---	---	---
		60.2	14.9	65.3	18.1	---	---	---	---
	14j-ma ↔ 14d-mi		0.0		0.0		---		---
		110.7	54.8	88.3	54.0	---	---	---	---
		58.3	24.3	57.6	20.4	---	---	---	---
	14d-ma ↔ 14j-mi		17.2		17.1		23.9		23.2
		33.8	16.8	30.0	22.3	38.0	32.1	---	---
	[a]	nb.	59.7	nb.	61.6	73.4	81.1	---	---
		nb.	66.0	nb.	66.2	nb.	86.1	nb.	72.2
		nb.	55.5	nb.	61.6	86.2	78.2	nb.	---
		57.5	56.0	nb.	56.9	78.8	75.5	---	---
		57.0	22.4	56.9	21.5	nb.	28.5	---	---
		28.8	14.9	28.3	18.1	36.9	21.1	---	19.5
	14d-ma ↔ 14d-mi		17.2		17.1		---		---
	[a]	88.3	33.8	86.0	34.4	---	---	---	---
	[a]	102.9	24.3	88.4	20.4	---	---	---	---
MECHANISM 3	**14j-ma ↔ 14d-mi**		0.0		0.0		---		---
	[a]	92.7	57.2	66.3	59.8	---	---	---	---
		78.1	23.4	74.0	22.1	---	---	---	---
		32.5	30.0	31.8	31.4	---	---	---	---
	[a]	53.3	24.3	50.3	20.4	---	---	---	---
	14d-ma ↔ 14j-mi		17.2		17.1		---		---
		34.4	16.9	30.1	22.3	---	---	---	---
		94.8	88.5	76.6	75.5	---	---	---	---
		nb.	14.9	54.5	18.1	---	---	---	---
	14d-ma ↔ 14d-mi		17.2		17.1		23.9		23.2
		73.0	24.3	81.9	20.4	96.7	25.9	79.8	28.1

Comment marks are always written in the line they refer to.

[a]More than one imaginary frequency remained from the transition state optimization

Table SI75. Thermochemical data ([kJ/mol] or [J/molK]) for the interconversion pathways of the four most stable complexes of complexes **14**

	pathway	TS			ed/int		
		ZPE	S	G	ZPE	S	G
MECHANISM 1	**14j-ma ↔ 14d-ma**				2983	1.6388	2708.08
	[a]	2983	1.6991	2707.23	2984	1.6243	2712.65
	14j-ma ↔ 14j-mi				2983	1.6388	2708.08
		2979	1.6422	2703.17	2982	1.6455	2705.73
		2981	1.6394	2705.06	2983	1.6020	2716.10
	14j-ma ↔ 14d-mi				2983	1.6388	2708.08
		2980	1.6557	2699.97	2984	1.6254	2711.60
		2983	1.6252	2709.95	2982	1.6548	2703.50
	14j-mi ↔ 14d-mi				2983	1.6020	2716.10
		2983	1.6242	2710.10	2982	1.6548	2703.50
	14d-ma ↔ 14j-mi				2984	1.6243	2712.65
	[a]	2981	1.5977	2714.12	2983	1.6626	2701.76
		2980	1.6535	2699.85	2984	1.6421	2708.18
		2982	1.6250	2709.76	2983	1.6020	2716.10
	14d-ma ↔ 14d-mi				2984	1.6243	2712.65
	[a]	2981	1.5706	2717.72	2982	1.6548	2703.50
MECHANISM 2	**14j-ma ↔ 14j-mi**				2983	1.6388	2708.08
		2983	1.6081	2714.48	2984	1.6214	2713.35
		2982	1.6407	2705.04	2982	1.6433	2705.67
		2982	1.6218	2709.84	2983	1.6020	2716.10
	14j-ma ↔ 14d-mi				2983	1.6388	2708.08
		2981	1.6548	2701.20	2981	1.6431	2705.47
		2981	1.6189	2710.25	2982	1.6548	2703.50
	14d-ma ↔ 14j-mi				2984	1.6243	2712.65
		2982	1.6210	2710.56	2985	1.6178	2714.59
	[a]	2982	1.6248	2707.12	2982	1.6236	2709.43
		2981	1.6212	2709.37	2982	1.6006	2715.10
		2981	1.6145	2710.99	2982	1.6321	2708.93
		2982	1.6237	2708.85	2982	1.6498	2703.97
		2983	1.6478	2703.24	2984	1.6376	2709.53
		2982	1.6197	2710.98	2983	1.6020	2716.10
	14d-ma ↔ 14d-mi				2984	1.6243	2712.65
	[a]	2980	1.5862	2714.72	2983	1.6388	2708.46
	[a]	2981	1.5825	2716.86	2982	1.6548	2703.50
MECHANISM 3	**14j-ma ↔ 14d-mi**				2983	1.6388	2708.08
	[a]	2979	1.6135	2707.00	2983	1.6213	2713.04
		2981	1.6249	2708.00	2984	1.6335	2709.86
		2982	1.6197	2710.51	2983	1.6379	2708.40
	[a]	2981	1.6213	2707.67	2982	1.6548	2703.50
	14d-ma ↔ 14j-mi				2984	1.6243	2712.65
		2982	1.6197	2710.98	2985	1.6215	2713.57
		2981	1.6497	2702.37	2981	1.6710	2698.41
		2978	1.6420	2701.79	2983	1.6020	2716.10
	14d-ma ↔ 14d-mi				2984	1.6243	2712.65
		2982	1.6278	2707.94	2982	1.6548	2703.50

Comment marks are always written in the line they refer to.

[a]More than one imaginary frequency remained from the transition state optimization

4. References

(1) Plessow, P., Reaction Path Optimization without NEB Springs or Interpolation Algorithms. *J. Chem. Theory Comput.* **2013**, *9*, 1305-1310.

(2) Fuchs, M.; Schober, M.; Orthaber, A.; Faber, K., Asymmetric Synthesis of β-Substituted α-Methylenebutyrolactones via TRIP-Catalyzed Allylation: Mechanistic Studies and Application to the Synthesis of (S)-(−)-Hydroxymatairesinol. *Adv. Synth. Catal.* **2013**, *355*, 2499-2505.

(3) Grayson, M. N.; Pellegrinet, S. C.; Goodman, J. M., Mechanistic Insights into the BINOL-Derived Phosphoric Acid-Catalyzed Asymmetric Allylboration of Aldehydes. *J. Am. Chem. Soc.* **2012**, *134*, 2716-2722.

(4) Wang, H.; Jain, P.; Antilla, J. C.; Houk, K. N., Origins of Stereoselectivities in Chiral Phosphoric Acid Catalyzed Allylborations and Propargylations of Aldehydes. *J. Org. Chem.* **2013**, *78*, 1208-1215.

(5) *COSMOconf 4.1, COSMOlogic GmbH & Co KG, http://www.cosmologic.de*.

(6) Kozuch, S.; Shaik, S., How to Conceptualize Catalytic Cycles? The Energetic Span Model. *Acc. Chem. Res.* **2011**, *44*, 101-110.

(7) Humphrey, W.; Dalke, A.; Schulten, K., VMD: Visual molecular dynamics. *J. Mol. Graphics* **1996**, *14*, 33-38.